(2)

R85-956328-F

CARS DIAGNOSTICS OF HIGH PRESSURE COMBUSTION – II

MEASUREMENTS OF NO, H_2O AND HIGH PRESSURE FLAMES

Final Report

J.H. Stufflebeam
J.A. Shirley

December, 1985

U.S. Army Research Office
Contract: DAAG29-83-C-0001

UNITED TECHNOLOGIES RESEARCH CENTER
East Hartford, Connecticut 06108

Approved for Public Release;
Distribution Unlimited

83-1-4-1

UNITED TECHNOLOGIES RESEARCH CENTER

UNITED TECHNOLOGIES

East Hartford, Connecticut 06108

R85-956328-F

CARS Diagnostics of High Pressure Combustion - II

Measurements of NO, H_2O and High Pressure Flames

Final Report

J. H. Stufflebeam
J. A. Shirley

December 1985

U. S. Army Research Office
Contract: DAAG29-83-C-0001

United Technologies Research Center
East Hartford, CT 06108

UNCLASSIFIED

SECURITY CLASSIFICATION OF THIS PAGE

AD-A164610

REPORT DOCUMENTATION PAGE

1a. REPORT SECURITY CLASSIFICATION	1b. RESTRICTIVE MARKINGS
2a. SECURITY CLASSIFICATION AUTHORITY: Unclassified	3. DISTRIBUTION/AVAILABILITY OF REPORT: Unlimited
2b. DECLASSIFICATION/DOWNGRADING SCHEDULE	
4. PERFORMING ORGANIZATION REPORT NUMBER(S): R85-956328-F	5. MONITORING ORGANIZATION REPORT NUMBER(S)
6a. NAME OF PERFORMING ORGANIZATION: United Technologies Research Center; 6b. OFFICE SYMBOL (If applicable)	7a. NAME OF MONITORING ORGANIZATION: Department of the Army, U.S. Army Research Office
6c. ADDRESS (City, State and ZIP Code): East Hartford, CT 06108	7b. ADDRESS (City, State and ZIP Code): Research Triangle Park, N.C. 27709-2211
8a. NAME OF FUNDING/SPONSORING ORGANIZATION: Same as Block 7a.; 8b. OFFICE SYMBOL (If applicable)	9. PROCUREMENT INSTRUMENT IDENTIFICATION NUMBER: DAAG29-83-C-0001
8c. ADDRESS (City, State and ZIP Code): Same as Block 7b.	10. SOURCE OF FUNDING NOS: PROGRAM ELEMENT NO. / PROJECT NO. / TASK NO. / WORK UNIT NO.
11. TITLE (Include Security Classification): CARS Diagnostics of High Pressure Combustion II	
12. PERSONAL AUTHOR(S): Stufflebeam, J. H., Shirley, J. A.	
13a. TYPE OF REPORT: Final Technical Report; 13b. TIME COVERED: FROM 10/10/82 TO 12/20/85	14. DATE OF REPORT (Yr., Mo., Day): 85, December; 15. PAGE COUNT
16. SUPPLEMENTARY NOTATION	

17 COSATI CODES		
FIELD	GROUP	SUB. GR.

18. SUBJECT TERMS (Continue on reverse if necessary and identify by block number): CARS, Coherent anti-Stokes Raman Spectroscopy, High Pressure Combustion Diagnostics, Collisional Narrowing, Water Vapor, Nitric Oxide, High Pressure Premixed Flame, Polarization Suppression

19. ABSTRACT (Continue on reverse if necessary and identify by block number)

Under Contract DAAG29-83-C-0001 sponsored by the U.S. Army Research Office, the United Technologies Research Center has conducted spectroscopic investigations into the coherent anti-Stokes Raman spectroscopy (CARS) spectra of NO and H_2O and ~~investigated~~ the capability of CARS for diagnostics of high pressure flames. CARS is a remote laser diagnostic technique for temperature and species measurements in hostile combustion environments. As such it possesses considerable relevance to the Army in the general areas of ballistics and propulsion. This ~~final~~ report describes the results of investigations conducted into the effects of high pressure, specifically the phenomenon of collisional narrowing, on CARS spectra from which temperature and density information derive. Experimental studies of CARS spectra were conducted in NO in a heated, high pressure cell over the range 300K-800K, 1-33 atm, in H_2O from 500K-1000K, 5-30 atm and in a high pressure, premixed CO/air flame (over)

20. DISTRIBUTION/AVAILABILITY OF ABSTRACT: UNCLASSIFIED/UNLIMITED ☐ SAME AS RPT. ☐ DTIC USERS ☐	21. ABSTRACT SECURITY CLASSIFICATION: Unclassified
22a. NAME OF RESPONSIBLE INDIVIDUAL	22b. TELEPHONE NUMBER (Include Area Code); 22c. OFFICE SYMBOL

DD FORM 1473, 83 APR EDITION OF 1 JAN 73 IS OBSOLETE.

UNCLASSIFIED

SECURITY CLASSIFICATION OF THIS PAGE

from 1-15 atm. The CARS spectra obtained were used to evaluate the UTRC CARS computer code. In addition, a new technique, termed dual broadband CARS, was developed which permits the simultaneous detection of a multiplicity of species. This approach removes the nominal limitation on CARS of interrogating just a single constituent at a time. This technique should prove invaluable in the transient environments of combustion processes relevant to the Army.

FOREWORD

This report covers research performed under U. S. Army Research Office Contract DAAG29-83-C-0001 during the period October 10, 1982 to December 20, 1985. The high pressure, high temperature CARS spectra of nitric oxide and water vapor were investigated for the purpose of permitting accurate temperature and concentration measurements of these species in combustion media. This was accomplished by the acquisition of high quality CARS spectra under controlled laboratory conditions of temperature and pressure which were used to refine and verify a theoretical model that predicts the spectra through computer simulation. CARS measurements in high pressure flames were investigated through the acquisition and analysis of CARS spectra from a premixed flame, operated at pressures up to 15 atmospheres.

The personnel involved with this contract have had responsibilities for different phases of the work. John A. Shirley performed the experimental investigations into H_2O CARS spectra and was responsible for their comparison with the theoretical models. Similarly, John H. Stufflebeam did the CARS studies of NO and was also responsible for the high pressure flame measurements, including the analysis of different laser convolution predictions for the CARS spectra. Gregory M. Dobbs provided computer programs based on the Kataoka-Teets laser convolution used for comparison with the experimental data. Alan C. Eckbreth provided the overall direction of the experimental and theoretical aspects of this work and, in addition, supplied specific solutions to experimental problems that were encountered. This contract was monitored by Dr. Robert W. Shaw of the Chemical and Biological Sciences Division, U. S. Army Research Office.

CARS Diagnostics of High Pressure Combustion - II

Measurements of NO, H_2O and High Pressure Flames

TABLE OF CONTENTS

SUMMARY

Under Contract DAAG29-83-C-0001 sponsored by the U.S. Army Research Office, the United Technologies Research Center has conducted spectroscopic investigations into the coherent anti-Stokes Raman spectroscopy (CARS) spectra of NO and H_2O and investigated the capability of CARS for diagnostics of high pressure flames. CARS is a remote laser diagnostic technique for temperature and species measurements in hostile combustion environments. As such it possesses considerable relevance to the Army in the general areas of ballistics and propulsion. This final report describes the results of investigations conducted into the effects of high pressure, specifically the phenomenon of collisional narrowing, on CARS spectra from which temperature and density information derive. Experimental studies of CARS spectra were conducted in NO in a heated, high pressure cell over the range 300 K-800 K, 1-33 atmospheres, in H_2O from 500 K-1000 K, 5-30 atmospheres and in a high pressure, premixed CO/air flame from 1-15 atmospheres. The CARS spectra obtained were used to evaluate the UTRC CARS computer code. In addition, a new technique, termed dual broadband CARS, was developed which permits the simultaneous detection of a multiplicity of species. This approach removes the nominal limitation on CARS of interrogating just a single constituent at a time. This technique should prove invaluable in the transient environments of combustion processes relevant to the Army.

INTRODUCTION

High pressure combustion is extremely important in a variety of practical applications of relevance to the Army such as propulsion and ballistics. Experimental diagnostics of high pressure combustion phenomena are important to gain the understanding required to improve and control these processes. Optical techniques appear ideally suited to diagnosing such phenomena because they are nonintrusive, can be spatially and temporally precise and are not confronted with survival considerations. Many however are inappropriate due to intolerance to interferences. One optical technique, coherent anti-Stokes Raman spectroscopy or CARS, shows considerable promise for diagnosing high pressure combustion phenomena. CARS is spatially and temporally precise and its coherent or beamlike nature is quite amenable to the limited optical apertures typical of high pressure combustion chambers. Furthermore, CARS exhibits a nonlinear dependence on molecular number density and increases rapidly in signal strength as the gas density is elevated. The intensity of CARS, however, is quite linewidth dependent. Collision processes alter the spectra by perturbing the rovibronic linewidth. As the gas density increases, a variety of linewidth phenomena occur such as pressure broadening, shifting, motional or Dicke narrowing, and collisional narrowing which complicate the calculation of the CARS spectrum. For CARS, the collisional narrowing phenomenon is important for pressures above one atmosphere. Collisional narrowing occurs when adjacent Raman transitions have been pressure broadened to the extent that they overlap. The overlap allows communication between lines and they subsequently coalesce or collapse to a narrower bandwidth. Accurate modeling of high pressure, high temperature CARS spectra is necessary to extract temperature and density information and thus, is fundamental to the deployment of the technique as a diagnostic.

Under Army Research Office sponsorship, Contract DAAG29-C-83-0001, UTRC has investigated the phenomenon of pressure-induced, i.e. collisional, narrowing in nitric oxide and water vapor. Well controlled laboratory experiments provided data for comparison with predictions from model calculations. NO CARS spectra have been obtained over the range 1-33 atmospheres, 300-800 K; H_2O CARS spectra from 1-30 atmospheres, 500-1000 K. A computer code was assembled to predict these CARS spectra and comparisons between theory and experiment have been made.

It is also of interest to investigate the capability of CARS for quantitative measurements of the density and temperature of chemical species in high pressure combustion environments. Quantitative measurements were studied in a premixed CO/air flame operated at pressures up to 15 atmospheres.

N_2 and CO CARS spectra were obtained from this flame as well as Raman scattering data for N_2, CO and CO_2. The experimental data were compared to chemical equilibrium code predictions and predictions from the UTRC CARS code for the flame conditions. During the course of this contract, a technical advance in CARS diagnostics was achieved at UTRC through the development of dual broadband CARS. This technique overcomes one of the previous disadvantages of CARS, namely interrogation of one chemical species at a time. With dual broadband CARS a multiplicity of species can be sampled simultaneously, greatly expanding the utility of CARS as a diagnostic.

In the next section of the report, the spectroscopic investigations of H_2O and NO are presented; the succeeding section describes the high pressure flame results and is followed by a section on dual broadband CARS. Finally the references are listed and appendices are attached that list personnel involved in this work, publications/presentations supported under this contract and a reprint of a recent paper on dual broadband CARS.

HIGH PRESSURE CARS SPECTROSCOPY

Introduction

A coherent anti-Stokes Raman vibrational Q-branch spectrum is composed of a large number of transitions which are strongly broadened by collisions and the molecule's dipolar intermolecular potential. At high pressures the closely spaced lines broaden into one another and the spectrum undergoes a transition, referred to as collisional narrowing, in which spectral features appear to coalesce. Under these conditions, the usual calculation of a synthetic spectrum, carried out as if it were composed of isolated lines is no longer appropriate. Beginning in 1979 under ARO sponsorship, UTRC has been studying this phenomenon in a number of molecules of diagnostic relevance to the Army. Under the previous contract, N_2 and CO_2 were investigated (Stufflebeam, et al., 1984; Hall and Stufflebeam, 1984) and under the current effort such studies have been extended to H_2O and NO. CO was studied under an investigation supported by the Air Force Rocket Propulsion Laboratory (Stufflebeam, et al., 1983).

In the earlier contract, Hall et al. (1980) developed the exact CARS spectral intensity expression in the collisional narrowing regime within the impact approximation. This description requires a knowledge of state-to-state relaxation rates and inversion of the G-matrix at every point in frequency space. The technique of Gordon and McGinnis (1968), requiring just a single matrix diagonalization and inversion per spectrum, was only very recently applied by Koszykowski et al. (1985) to nitrogen CARS calculations. Thus, this approach was not available during the present investigations. The algorithm represents a significant computational economy and will be implemented into the UTRC CARS codes in the near future.

Because of the large number of transitions possible in water vapor, calculations within this G-matrix framework are prohibitive even on a fast minicomputer, and therefore approximate formulations have been sought. Hall and Greenhalgh (1982) extended Gordon's rotational diffusion concept to describe collisional narrowing in N_2 CARS spectra and compared the model with measurements in pure water vapor at pressures up to 16 atmospheres (Greenhalgh, et al., 1984). These measurements have been extended in this report to include nitrogen broadening, typical of actual combustion situations. The CARS spectrum of water vapor has been studied in flames by Hall et al. (1979), at lower temperatures in a heated cell with a number of collision partners at UTRC (Hall and Shirley, 1983) and at elevated pressures at AERE Harwell (Greenhalgh, et al., 1984). The measurements reported here

were undertaken to test calculations at elevated temperatures typical of practical devices with air-fed combustion. In such devices the water mole fraction can vary from a fraction of a percent to 15-20 percent. The measurements undertaken simulate these conditions in a closed cell with a nitrogen collision partner, at temperatures from 500 to 1000 K. These measurements therefore complement the Harwell investigations and, in addition, the spectral resolution in the reported measurements is higher, posing a more critical test of theoretical calculations.

The CARS spectrum of NO has been studied up to 2 atmospheres by Laane and Kiefer (1980) and at lower pressure by Lempert, et al. (1984). This report contains measurements of the CARS spectrum of NO at pressures up to 33 atmospheres, nearer the practical combustion environments typical of propellants where this molecule is an important intermediate product that may control energy release mechanisms.

In this section the treatment of CARS calculations at high pressure is described, followed by a brief description of pertinent aspects of H_2O and NO spectroscopy, linewidth measurements and the linewidth models used to provide the input for computer calculations. The experiments are then discussed and comparisons are made with theoretical predictions. Finally the conclusions of these studies and directions for future investigations are discussed.

Theoretical Description of CARS at High Pressure

The theoretical basis for the calculation of CARS spectra in the pressure narrowing regime is well described in the literature (Hall, et al., 1980; Hall and Greenhalgh, 1982; Hall and Eckbreth, 1984; Koszykowski, et al., 1985). The purpose of this section is to give a physical picture of narrowing and to present the various CARS models developed, so their differences can be understood.

The frequencies of rotational components of the vibrational Q-branch, for which there is no change in rotational quantum number during the transition, differ because of the effect of rotation on the vibrational frequency, i.e. vibrational-rotational interaction. Therefore, depending upon rotational state, molecules radiate at slightly different vibrational frequencies, leading to a simple broadening of components of the Q-branch. When the collision frequency, which leads to individual line broadening, is small compared to the vibration-rotation frequency shift, the Q-branch is well resolved. If the molecular density is increased, and therefore collisions occur more rapidly, a point is reached when the collision frequency is

comparable to the frequency shift due to the vibration-rotation interaction. The Q components then overlap and rotationally-inelastic collisions cause transitions so quickly that it is possible to speak only of the aggregate of molecules in an average J state. As a result the band collapses to a position determined by the most probable rotational state. Note that broadening can still occur through vibrationally-inelastic and dephasing collisions.

The isolated lines approximation is valid at low pressures. The CARS susceptibility expression then is just the result of simple summation of individual transitions:

$$\chi^{(3)} = \frac{2N}{\hbar} \sum_{if} \frac{\alpha_{if}^2 \Delta\rho_{if}^{(0)}}{2(\omega_{if} - \omega_1 + \omega_2) - i\Gamma_{if}} + \chi^{nr} = \sum_j (\chi_j' + i\chi_j'') + \chi^{nr} \quad (1)$$

where N is the molecular number density, α_{if} is the matrix element of the polarizability, ρ_{if} is the density matrix element, ω_{if} is the Raman transition frequency, Γ_{if} is the Raman linewidth and ω_1 and ω_2 are the CARS pump and probe frequencies, respectively. χ^{nr} is the nonresonant susceptibility. Given linewidths, this expression is straightforward to evaluate.

When the collision frequency is high, the susceptibility must be evaluated from the expression derived from the polarizability and impact approximations (Hall et al., 1980; Gordon, 1966b).

$$\chi^{(3)}(\omega) = \frac{iN}{\hbar} \sum_r \alpha_r \sum_s [G]_{rs}^{-1} \Delta\rho_s^{(0)} \alpha_s \quad (2)$$

where the elements of the G-matrix are given by

$$G_{rs} = i(\omega_1 - \omega_2 - \omega_r)\delta_{rs} + [(\Gamma_r/2) - i\Delta_r]\delta_{rs} + \gamma_{rs}(1 - \delta_{rs}) \quad (3)$$

Here the α_r are the components of the matrix elements of the polarizability, Δ_r is the frequency shift with pressure, δ_{rs} is the Kronecker delta and the γ_{rs} are the off-diagnonal linewidth parameters, describing the rate of collisional energy transfer between states. Calculation of CARS spectra involves inversion of the G-matrix at each frequency, ω, a cumbersome and time consuming chore for molecules with many transitions, like water. The Gordon-McGinnis technique is attractive because it is exact and only one matrix diagonalization and inversion is required per spectrum however it was unavailable during this study.

An approximate approach, based on Gordon's (1966a) J-diffusion model results in a simpler expression to evaluate:

$$\chi^{(3)}_{v,v+1} = \frac{2N}{\hbar}\alpha^2_{v,v+1}\frac{\sum_j \Delta\rho^{(0)}_{jj}/(2\Delta\omega_j - i\Gamma_j)}{1 + i\sum_j (1-\phi_j)\Gamma_j\rho^{(0)}_{jj}/(2\Delta\omega_j - i\Gamma_j)} \qquad (4)$$

where ϕ_j represents the fractional contribution of pure dephasing processes to the linewidth of the transition and $\Delta\omega_j$ is the detuning frequency factor seen in parentheses in the denominator of the first expression of the right hand side of Eqn. (1). The advantage of this expression is that it requires little more time to evaluate than the isolated lines expression.

For moderate pressures, where the effects of overlap are small G^{-1} can be expanded to first order in density to give the first order perturbation approximation:

$$\chi^{(3)} = \frac{2N}{\hbar}\left[\sum_r \frac{\alpha_r^2\Delta\rho_r^{(0)}}{2\Delta\omega_r - i\Gamma_r} + 2i\sum_r \frac{\alpha_r}{2\Delta\omega_r - \Gamma_r}\sum_s \frac{\gamma_{rs}\alpha_s\Delta\rho_s^{(0)}}{2\Delta\omega_s - \Gamma_s}\right] \qquad (5)$$

Note that overlap effects appear as a correction to the isolated lines approximation.

In calculating the CARS spectrum of molecules from these formulae, two things are needed: (1) knowledge of the spectroscopy and (2) linewidths (or equivalently the energy transfer rates). The spectroscopy affects energy levels, transition frequencies and polarizability matrix elements (selection rules). This is very briefly discussed in the next section.

Water Vapor

Spectroscopy of Water Vapor

The water molecule is an asymmetric top. It has three fundamental vibrational modes corresponding to symmetric stretching, bending and asymmetric stretching motions; denoted respectively by vibrational quantum numbers v_1 v_2 v_3. All modes are Raman-active but the v_1 mode at a Raman shift of 3657 cm^{-1} is by far the strongest. At low temperatures only the ground state is significantly populated, and Raman transitions belonging to the 000 → 100 band are most important. The first level in the bending mode has an energy of 1597 cm^{-1}, so the vibrational hot band, 010 → 110, and others become important as the temperature increases.

The rotational substructure is not amenable to representation by an explicit expression. The structure is represented by the rotational quantum number J and pseudo quantum number τ. τ takes on values in the range $-J<\tau<J$. Rotational energies in the 2J+1 sub-levels increase as τ increases from -J to +J.

Modeling the transitions present in the CARS spectrum of H_2O has been described in many papers (Hall and Shirley, 1983; Greenhalgh, et al., 1984; Gordon, 1966b). The same prescription has been followed here. The energy level data compiled by Bribes et al. (1976) and supplied by R. L. St. Peters has been used. The Raman cross section for water is subject to uncertainty (Greenhalgh, et al., 1984). A value of $1.4 \times 10^{-30} cm^2/sr$ has been used here. Likewise the nonresonant susceptibility of water is not well known, a value 2.0 times that of nitrogen was used (Hall and Shirley, 1983).

Water Linewidths

Modeling of linewidths is crucial in the formulation of CARS spectroscopy of H_2O at high pressures (Greenhalgh, et al., 1984). In the pressure broadened regime the linewidth is governed by inelastic lifetime-limiting collisions and by elastic collisions which dephase the vibrational and rotational motions. Inelastic collisions in which a change occurs in vibrational or rotational energy can both contribute. Water has a strong dipole moment so rotationally inelastic collisions would be expected to be important. Hall and Eckbreth (1984) have pointed out that when lifetime-limiting rotationally inelastic collisions predominate, the linewidths should not have a significant dependence on the radiative vibrational and rotational selection rules. Therefore the widths for microwave, infrared and vibrational Raman transitions are expected all to be roughly the same. This is fortunate because the linewidths of microwave (Benedict and Kaplan, 1959; 1964) and infrared transitions have been the subject of investigations (Mandin, et al., 1982).

Benedict and Kaplan computed linewidths of water microwave transitions within the Anderson theory framework, which models collisions of molecules as following straight line paths under the influence of an attractive potential. The short range repulsion is handled with a 'catch-all' distance of closest approach parameter. The transfer of rotational energy is controlled, like many energy transfer processes, by the resonance energy concept, which considers the energy defect in the collision and radiative process. The energy defect must be made up by translational energy, the availability of which, is of course determined by the temperature.

Benedict and Kaplan (1964) modeled water-water broadening with a solely dipole-dipole attractive potential. The broadest lines they calculated were

transitions involving small J and τ. Over the range 300< T <360 K, the dependence of average linewidth on temperature went as T^{-n}, where n = 0.9. They noted that extrapolation of the widths to higher temperatures encountered in flames and exhaust was not warranted for individual lines, but presumed that the average n for entire bands will approach n = 1.0, expected for resonant dipole collisions. The agreement with microwave data for linewidths at a particular J averaged over τ is fairly good.

Benedict and Kaplan (1959) also reported calculations of nitrogen broadened microwave widths. A dipole-quadrupole attractive potential was used. Calculated widths varied from 0.2 to 0.06 cm^{-1} at 300 K, with the broader widths occurring for smaller J and τ. Over the limited temperature range from 220 to 300 K the temperature exponent varied widely among lines, with n = 0.8, being typical. At higher temperatures, however no such simple variation was found due to the fact that at higher temperatures all lines show a degree of resonance.

More recently, the self broadened widths of infrared water transitions have been reported by Mandin et al. (1982). They calculated widths taking into account dipole-dipole, dipole-quadrupole, quadrupole-dipole and quadrupole-quadrupole intermolecular interactions within the theory of Anderson-Tsao-Curnutte (Tsao and Curnutte, 1962). For broadening of the v_1 transitions these and the Benedict-Kaplan calculations are comparable.

The greatest impediment to H_2O CARS modeling may be that linewidth data at high temperature is lacking. In order to model broadening of transitions at high temperatures, the exponential gap model of Polyani and Woodall (1972) was adopted. In this concept, explicit selection rules governing the change of rotational quantum number, ΔJ, are suppressed, but the rate is taken to depend exponentially on the energy defect. This approach has the advantage of simplicity while retaining a phenomenologically correct character. The linewidth is given by:

$$\frac{1}{2}\Gamma_{J\tau} = p\alpha_o(T)\sum_{J'\tau'}\rho^{(0)}_{J'\tau'}exp\left(-c|\Delta E_{J\tau,J'\tau'}|/kT\right) \qquad (6)$$

where p is the pressure, α_o a parameter corresponding to the broadening coefficient at zero-energy defect, $\Delta E_{J\tau,J'\tau'}$ is the energy defect in the transition and c is a fitting parameter. The parameter α_o is taken to be a function of temperature, of the form T^{-n}. The n's for water and nitrogen broadening are taken from the sensitivity calculations of Benedict and Kaplan. The other parameters have been found by fitting linewidths in the exponential gap model to the measurements of Mandin et al. (1982) for H_2O-H_2O, and

Benedict and Kaplan's (1959) calculations for H_2O-N_2. The agreement is shown in Fig. 1. The linewidths shown for a particular J have been averaged over all τ. While the agreement for average width is good for both water and nitrogen broadened widths, if individual transitions are considered, it is seen that the Benedict-Kaplan calculations tend to predict a broader width for small $|\tau|$, and a more narrow width for larger $|\tau|$. This could be an important discrepancy because, many of the peaks observed in H_2O CARS spectra correspond to the overlap of the more highly populated $|\tau| \approx J$ transitions. The parameters assumed for the calculations shown are summarized in Table 1.

Table 1.

Exponential Gap Linewidth Model Parameters

	H_2O-H_2O	H_2O-N_2
α_o	1.025	0.20
n	1.0	0.8
c	0.08	0.25

Nitric Oxide

Spectroscopy of NO

The electronic structure of the NO molecule, more fully discussed in Lempert et al. (1984), is complicated by ground state splitting that results in the overlap of two Q-branch series in the CARS spectrum. The two series are separated by approximately 0.2 cm^{-1} and the two series are not resolved by the equipment used in the current measurements (0.5 cm^{-1}). Collisional coupling between the rotational levels of the two states has initially been ignored in the computer model but may be incorporated in a later revision, if needed.

NO Linewidths

The linewidths used in the NO CARS code are the recent measurements of Lempert, et al. (1984). For NO, the number of rotational transitions is tractable and use of the full matrix inversion, Eqns. (2) and (3), is preferable to the Gordon model of rotational diffusion because it was shown to be more accurate in N_2 and CO (Stufflebeam, et al., 1983; Stufflebeam, et

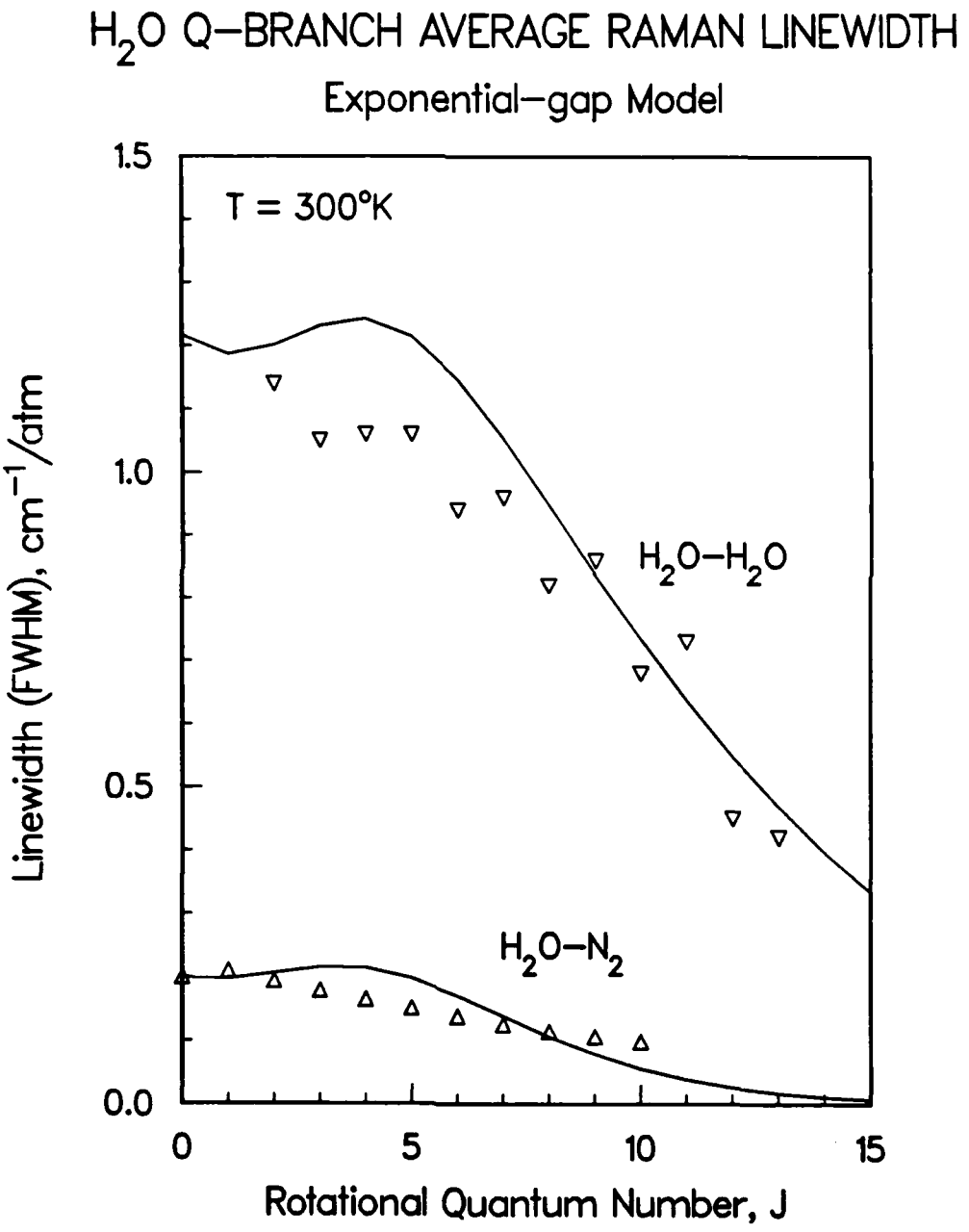
H_2O Q-BRANCH AVERAGE RAMAN LINEWIDTH
Exponential-gap Model
T = 300°K
H_2O-H_2O
H_2O-N_2
Linewidth (FWHM), cm^{-1}/atm
Rotational Quantum Number, J
1.5
1.0
0.5
0.0
0
5
10
15

al., 1984; Koszykowski, et al., 1985). The pressure broadening of the lines is modeled by a form of the inverse power law, previously used successfully in N_2. The inverse power law is employed to model the off diagonal matrix elements γ_{rs}:

$$\gamma_{rs} = -K_0 \rho_{rr}^{(0)} |\Delta E_{rs}|^{-a} \tag{7}$$

These are related to the theoretical linewidths through detailed balance and conservation of probability.

$$\frac{1}{2}\Gamma_r = -\sum_{r \neq s} \gamma_{rs} \tag{8}$$

The theoretical linewidths are then least-squares fit to the experimental ones to determine the fitting parameters K_o, a.

$$\frac{\partial}{\partial K_0}, \frac{\partial}{\partial \gamma} \sum_r \left(\Gamma_r^{(exp)} - \Gamma_r^{(th)}\right)^2 = 0 \tag{9}$$

This procedure produces the fit (lines) to experimental widths shown in Fig. 2. The inverse power law model does not fit the measured linewidths very accurately. The discrepancy is largest at low J for the Ω = 3/2 state. It is expected from previous work in CO at this laboratory (Stufflebeam, et al., 1983) that another rate model originally proposed by Dexheimer, et al. (1982)

$$\gamma_{rs} = -K_0(2r+1)e^{(\Delta E_{rs}/2kT)} |\Delta E_{rs}|^{-a} e^{-b|\Delta E_{rs}|/kT} \tag{10}$$

or the exponential gap model, Eqns. 6 and 7, will fit the experimental linewidths more closely. Evaluation of these models in the NO CARS code will be the next step in evaluation of the code.

FIG. 2

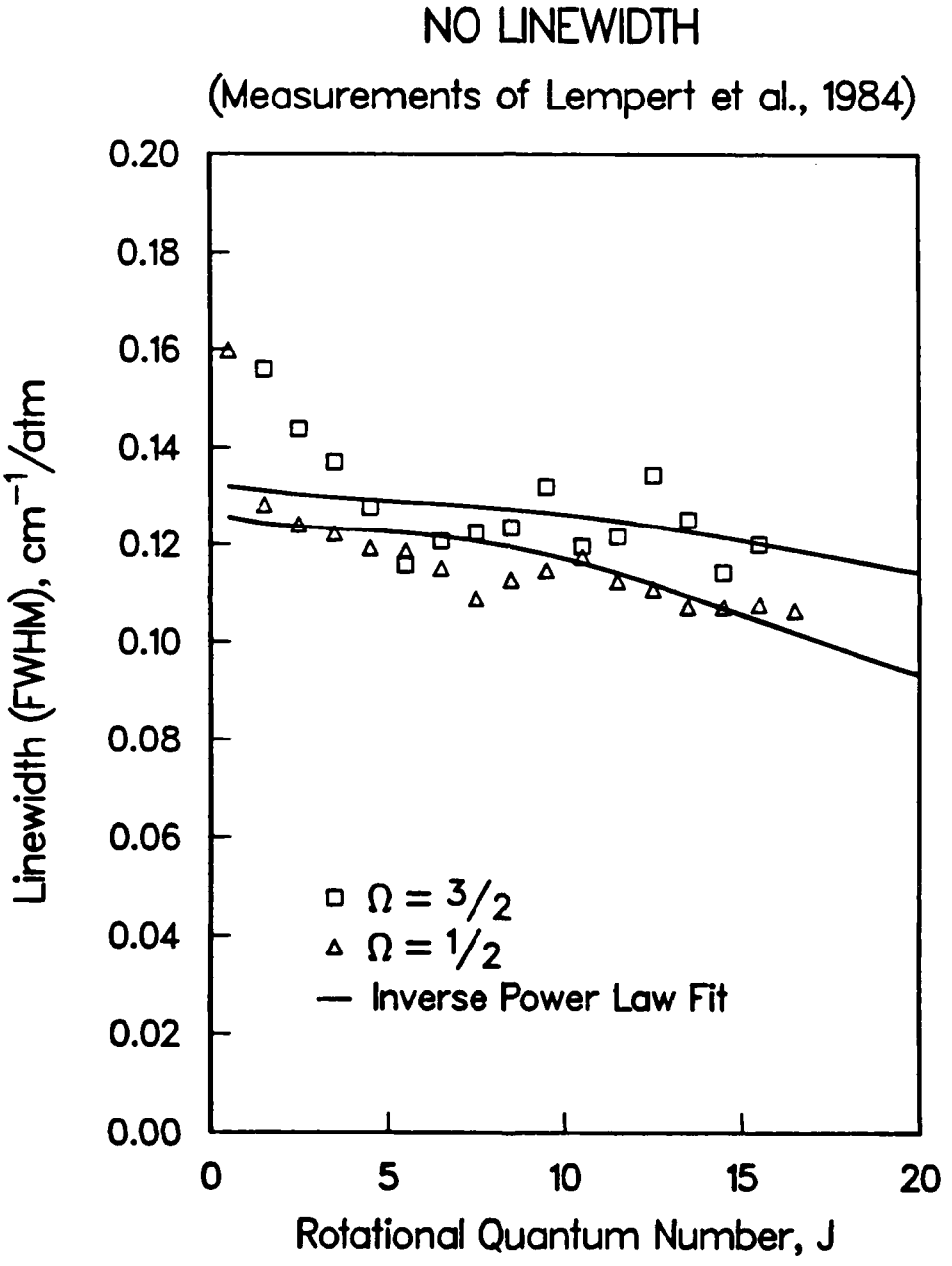
NO LINEWIDTH
(Measurements of Lempert et al., 1984)
Linewidth (FWHM), cm^{-1}/atm
0.20
0.18
0.16
0.14
0.12
0.10
0.08
0.06
0.04
0.02
0.00
0
5
10
15
20
Rotational Quantum Number, J
□ Ω = 3/2
△ Ω = 1/2
— Inverse Power Law Fit

H_2O Experimental Measurements

Experimental Apparatus

The CARS apparatus used in these experiments has been described previously (Hall and Shirley, 1983). The laser beams focus through the water vapor in a collinear CARS arrangement. The Stokes wave is provided by a broadband dye laser operated with either LD-690 dissolved in methyl alcohol or DCM dissolved in dimethyl sulfoxide (DMSO), (Eckbreth and Anderson, 1985). The DCM mixture was centered better with respect to the Stokes band and had higher output power.

The high pressure cell used in these experiments is shown in Fig. 3. It is made up of heated cell within an outer, pressure-containing cell. The outer cell has been hydrostatically tested to 2200 psi, but is not meant to withstand high temperatures. The water vapor is mostly contained within the inner cell which is sealed off, except for the connection to the water reservoir. The inner cell, therefore is pressurized by nitrogen through the reservoir. A small diameter vent tube prevents water from being forced out of the reservoir as the pressure rises in the inner cell due to heating. The temperatures of the reservoir and inner cell are controlled separately. In operation, the temperature of the inner cell is brought up to the desired operating point and the temperature in the reservoir is slowly raised, varying the water concentration within the inner cell. To prevent condensation on the outer cell windows, the area surrounding the reservoir is filled with molecular sieves.

From a knowledge of the reservoir temperature, the concentration of water vapor in the inner cell can be calculated in theory from water p-V-T data. It appears, however, because the cell is not in equilibrium, that this approach is not reliable. The concentration of water vapor in the inner cell is not well known, therefore. There are no instruments capable of measuring water vapor concentrations, or relative humidity in the extreme environment of the cell.

It was also found that the laser flux through the inner windows had to be limited to prevent optical damage, because the windows were so close to the focal point. Sapphire windows, expected to have superior chemical inertness with respect to the high temperature, high pressure water vapor, could not withstand as high a laser flux as quartz (probably due to lower quality surface finish on the sapphire). To obtain the highest quality spectra, quartz windows were used. Degradation was not a serious problem for the limited time which the windows were exposed.

HIGH PRESSURE WATER VAPOR APPARATUS

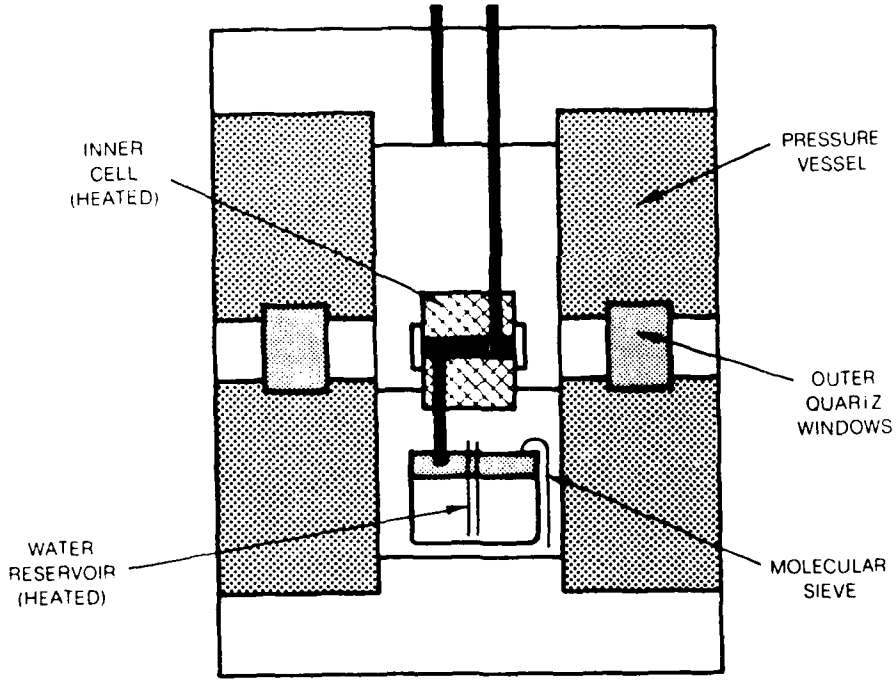

85-12-29-1

H_2O CARS Experiments

Measurements were undertaken in a matrix of pressure and temperature combinations. The intended measurements ranged over the limits of normal operating pressures in combustion devices, and temperatures attainable in the heated cell. Measurements were made at 500, 750 and 1000 K at pressures of 5, 10, and 20 atmospheres. The initial pressure in the cell was set to these values and was permitted to rise as the sealed off cell was heated. Once the cell test temperature was reached, spectra were recorded as the reservoir temperature was raised, increasing the concentration of water in the inner cell.

Figures 4 and 5 show CARS spectra of water vapor measured at 500 K for several different total pressures. Figure 4 is spectra of low water vapor concentration and Fig. 5 is of high concentration spectra. The experimental spectral resolution is about 2 cm^{-1} for these data. The spectra are shown displaced vertically by 0.2 units for clarity. The modulation due to the nonresonant background is clearly apparent in Fig. 4. Features are more sharply defined in the low pressure spectrum as expected. This is true in the high concentration spectra as well, (Fig. 5). The estimated concentration in Fig. 5 is 15-20%, while in Fig. 4 the concentration is probably about 5%.

CARS spectra of high water vapor concentrations, measured at 750 and 1000 K, are shown in Figs. 6 and 7, for successively higher pressures. At the lowest pressure and 750 K the spectral atures are quite distinct, but lose contrast at the higher pressures. The same is true at 1000 K. Note that whereas some of the features of the band closest to the bandhead are somewhat resolved at 500 K at the highest pressure, at the higher temperatures the same band is totally unresolved at high pressure. At the highest pressures the cell heater was unable to attain 1000 K. Consequently the actual measured temperature at 29 atmospheres was 931 K and at 12 atmospheres it was 985 K.

Results and Discussion

Model calculations have been prepared, guided by the results of the experiments. Calculations with full matrix inversion have not been done, because of the prohibitive time required for calculations with the full set of energy levels (831) on a VAX/750 with a floating point accelerator. On the other hand, it was found that the rotational diffusion and perturbation models gave similar results when similar linewidth parameters were used.

The isolated lines and rotational diffusion calculations at 500 K showed no discernable difference at 6 atmospheres. At 13 atmospheres the

FIG. 4

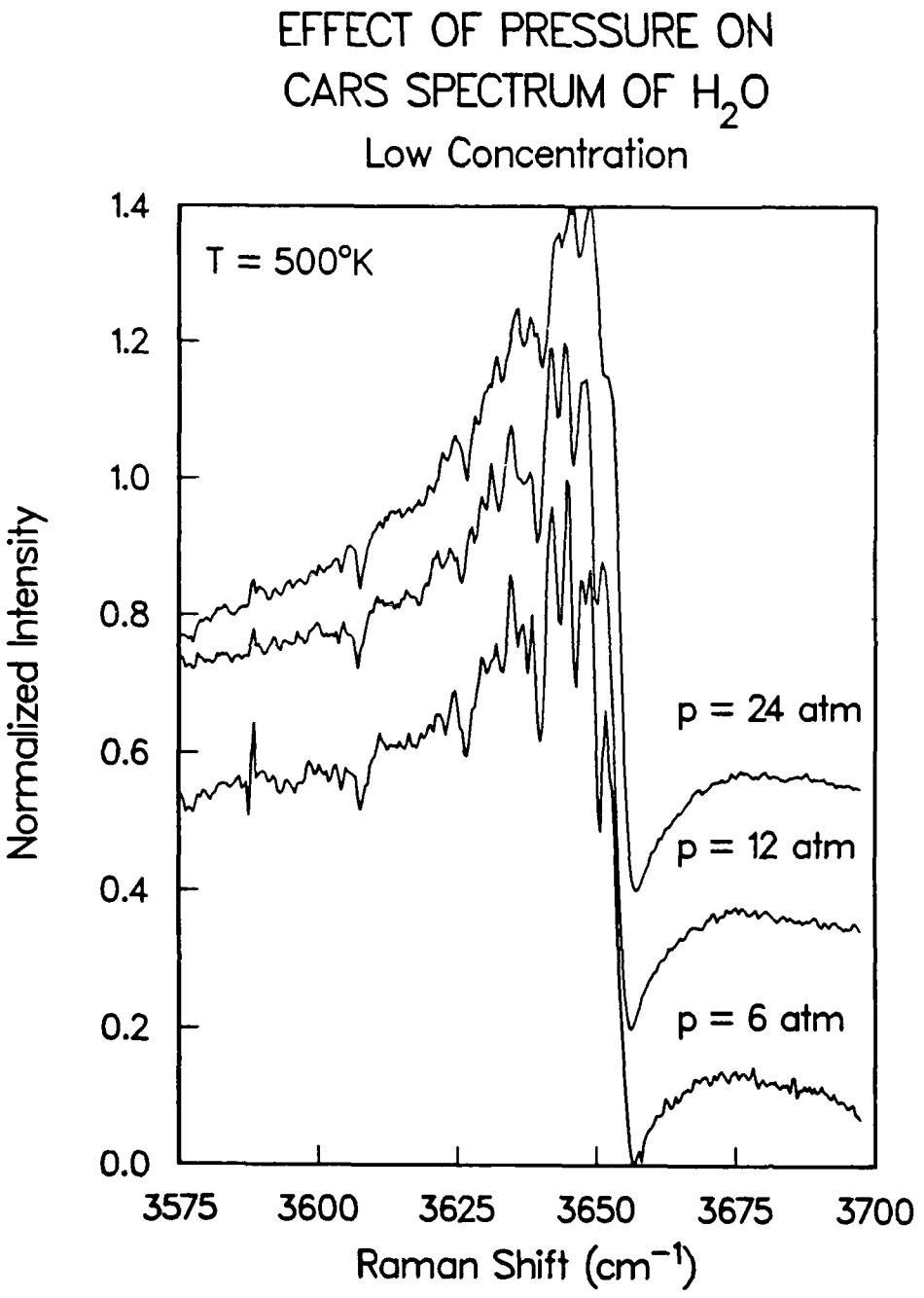
EFFECT OF PRESSURE ON
CARS SPECTRUM OF H_2O
Low Concentration
T = 500°K
p = 24 atm
p = 12 atm
p = 6 atm
Normalized Intensity
1.4
1.2
1.0
0.8
0.6
0.4
0.2
0.0
3575
3600
3625
3650
3675
3700
Raman Shift (cm^{-1})

FIG. 5

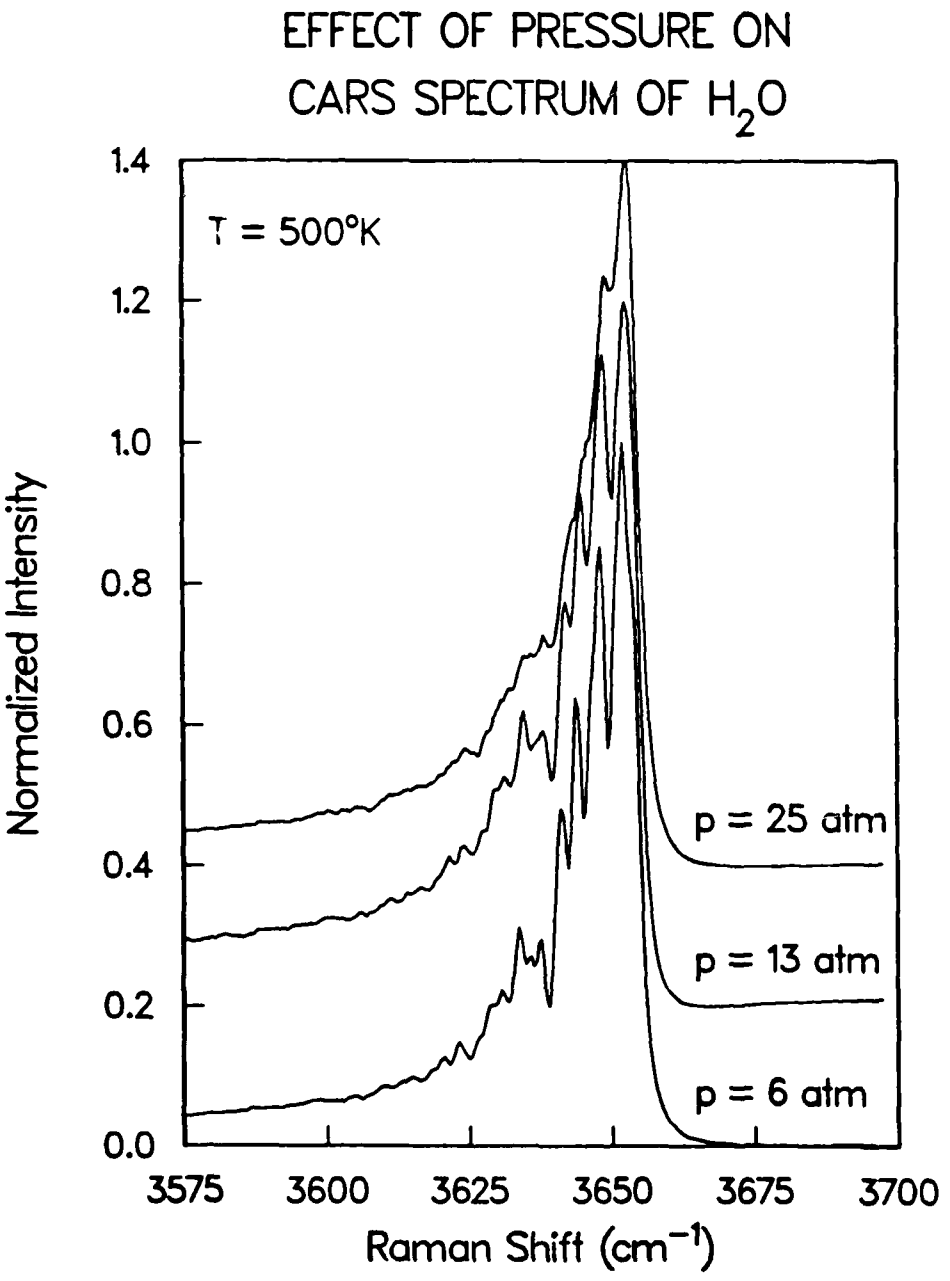
EFFECT OF PRESSURE ON
CARS SPECTRUM OF H_2O
T = 500°K
p = 25 atm
p = 13 atm
p = 6 atm
Normalized Intensity
1.4
1.2
1.0
0.8
0.6
0.4
0.2
0.0
3575
3600
3625
3650
3675
3700
Raman Shift (cm^{-1})

FIG. 6

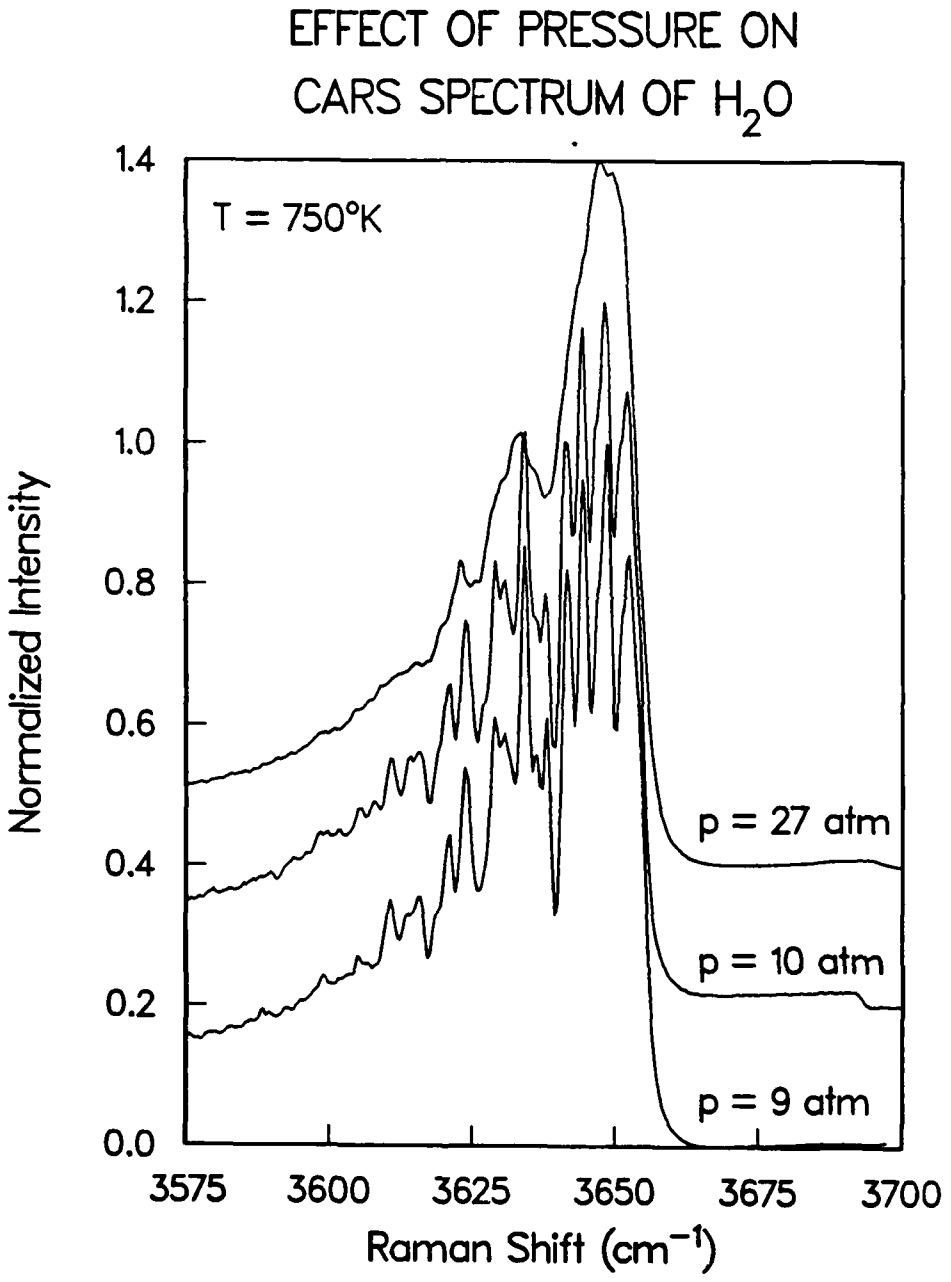
EFFECT OF PRESSURE ON
CARS SPECTRUM OF H_2O
T = 750°K
p = 27 atm
p = 10 atm
p = 9 atm
Normalized Intensity
Raman Shift (cm^{-1})
0.0
0.2
0.4
0.6
0.8
1.0
1.2
1.4
3575
3600
3625
3650
3675
3700

FIG. 7

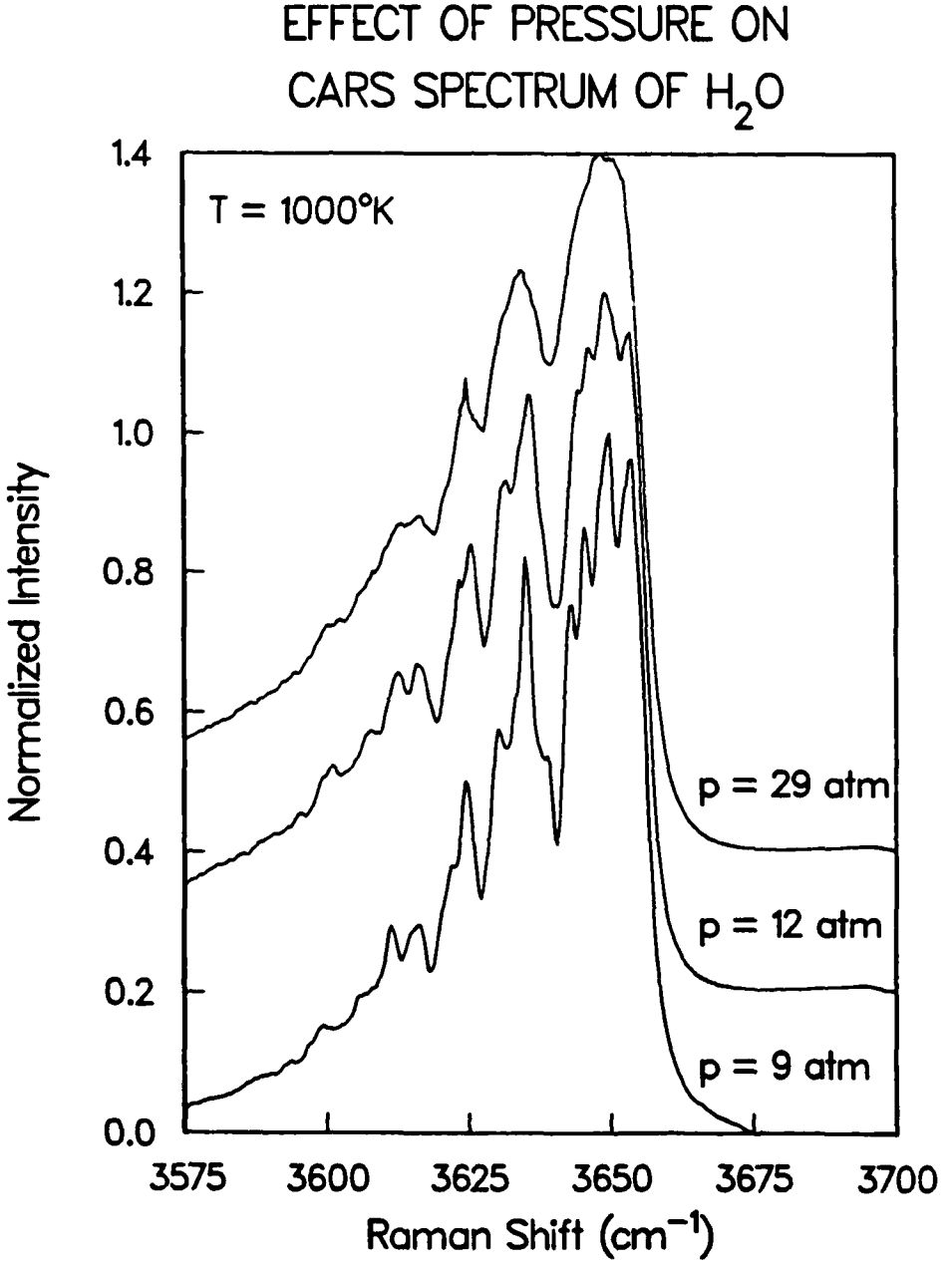
EFFECT OF PRESSURE ON
CARS SPECTRUM OF H_2O
T = 1000°K
p = 29 atm
p = 12 atm
p = 9 atm
Normalized Intensity
0.0
0.2
0.4
0.6
0.8
1.0
1.2
1.4
3575
3600
3625
3650
3675
3700
Raman Shift (cm^{-1})

features remained more distinct in the rotational diffusion model, for the same assumed concentration. The diffusion model agreed with experiments, in showing a rapid fall in intensity away from the bandhead on the low energy side, in contrast to isolated lines model calculations. At 25 atmospheres the low energy tail was about 50% higher for isolated lines. This difference could cause a considerable error in concentration measurements.

The experimental trends, illustrated in Figs. 4-7, have been examined with the rotational diffusion model. Calculations at temperatures and pressures comparable to the experiments are shown in Figs. 8-10. The general trends are certainly predicted by the calculations, which used the linewidth parameters in Table 1, with no contribution for dephasing collisions. Clearly however, at lower pressures spectral features are more distinct in the experiments than the calculations show. Reducing the parameter α_0 to one-half of the Mandin et al. (1982) and Benedict-Kaplan (1964) values resulted in sharper features at 500 K, but at 1000 K such rates show the spectral features as remaining distinct, in disagreement with the measurements. Adding a dephasing contribution may affect this, but there has been no corroborating evidence for such a scheme.

Figure 11 shows a direct comparison of model calculations and an experiment in the middle of the experimental range. The experimental data are shown as points and the full line gives the calculation. The assumed water concentration has been adjusted to fit the band head and the tail region. The experimental spectral features are more distinct than the calculation. The spectral bandwidth used in the calculations has also been adjusted to fit the experiment, but it is found that unreasonable values are required with the linewidth parameter set in Table 1 to obtain a fit to the experiments.

If one examines the transitions which cause the appearance of the spectrum an interesting observation is revealed. First consider the grouping of features in the spectrum. The first four features arise from the fundamental band 000 → 100. The contribution of these levels is falling rapidly, when at about 3640 cm^{-1}, the first hot band, 010 → 110, arises. The next major group is the second hot band, 020 → 120. Looking closely at transitions within these groups, they appear to correspond in many cases to the overlap of transitions arising with $|\tau| = J$. These are the transitions that have larger widths in the exponential gap model than appear reasonable from Mandin et al. and Benedict-Kaplan's calculations. Smaller linewidths would sharpen these features, to give the higher contrast present in the experimental spectra.

FIG. 8

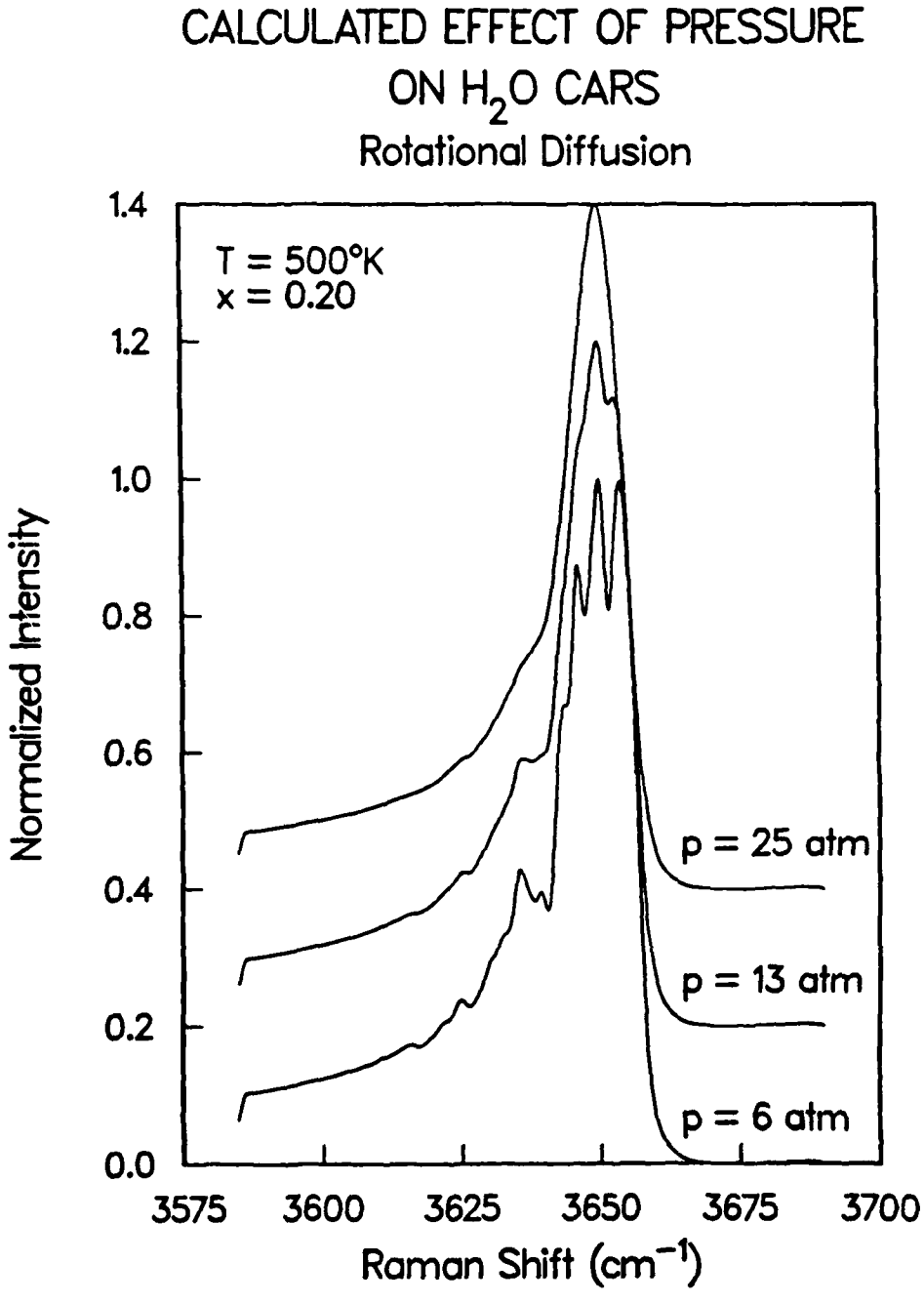
CALCULATED EFFECT OF PRESSURE
ON H_2O CARS
Rotational Diffusion
T = 500°K
x = 0.20
p = 25 atm
p = 13 atm
p = 6 atm
Normalized Intensity
1.4
1.2
1.0
0.8
0.6
0.4
0.2
0.0
3575
3600
3625
3650
3675
3700
Raman Shift (cm^{-1})

FIG. 9

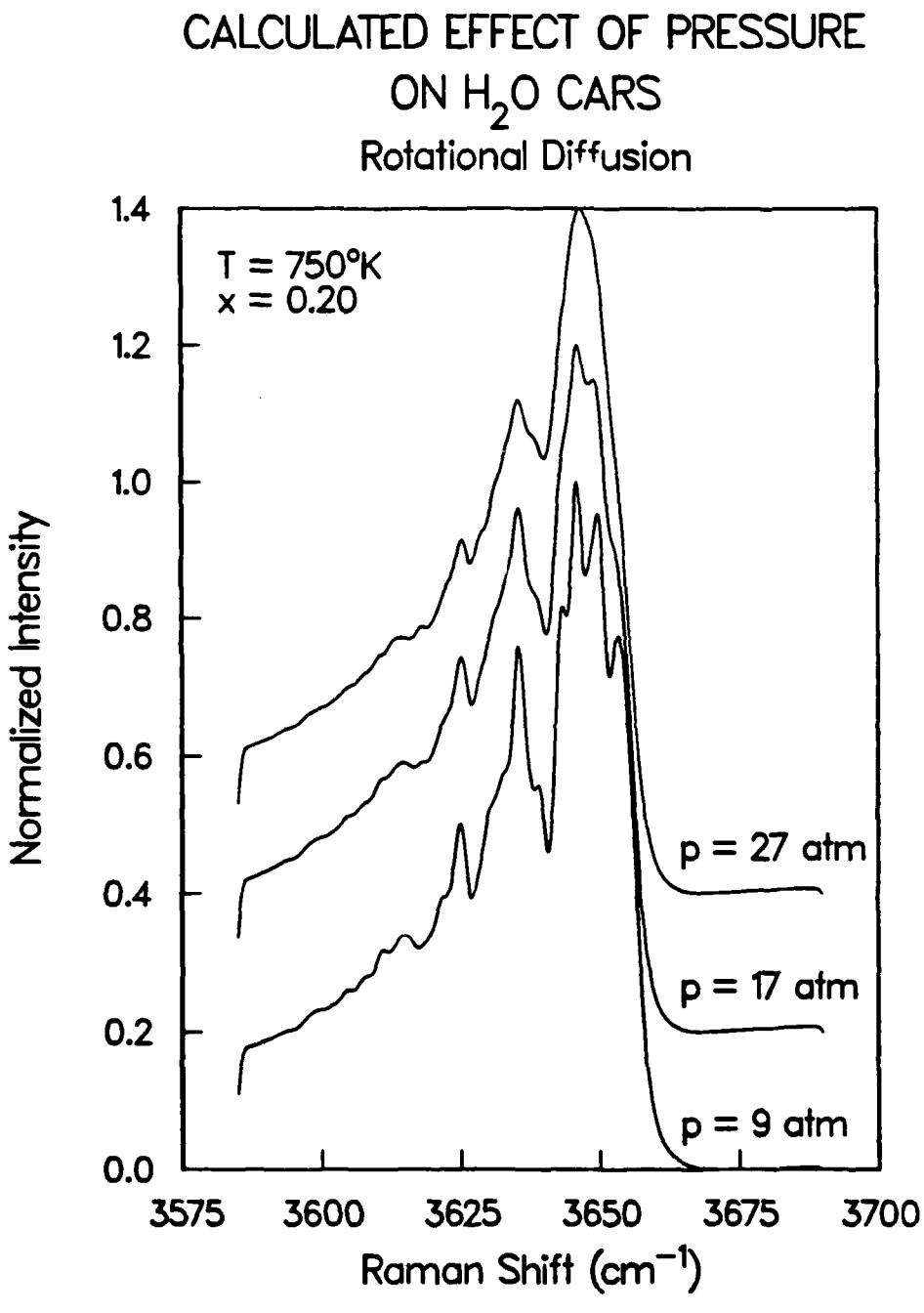
CALCULATED EFFECT OF PRESSURE
ON H_2O CARS
Rotational Diffusion
T = 750°K
x = 0.20
p = 27 atm
p = 17 atm
p = 9 atm
Normalized Intensity
1.4
1.2
1.0
0.8
0.6
0.4
0.2
0.0
3575
3600
3625
3650
3675
3700
Raman Shift (cm^{-1})

FIG. 10

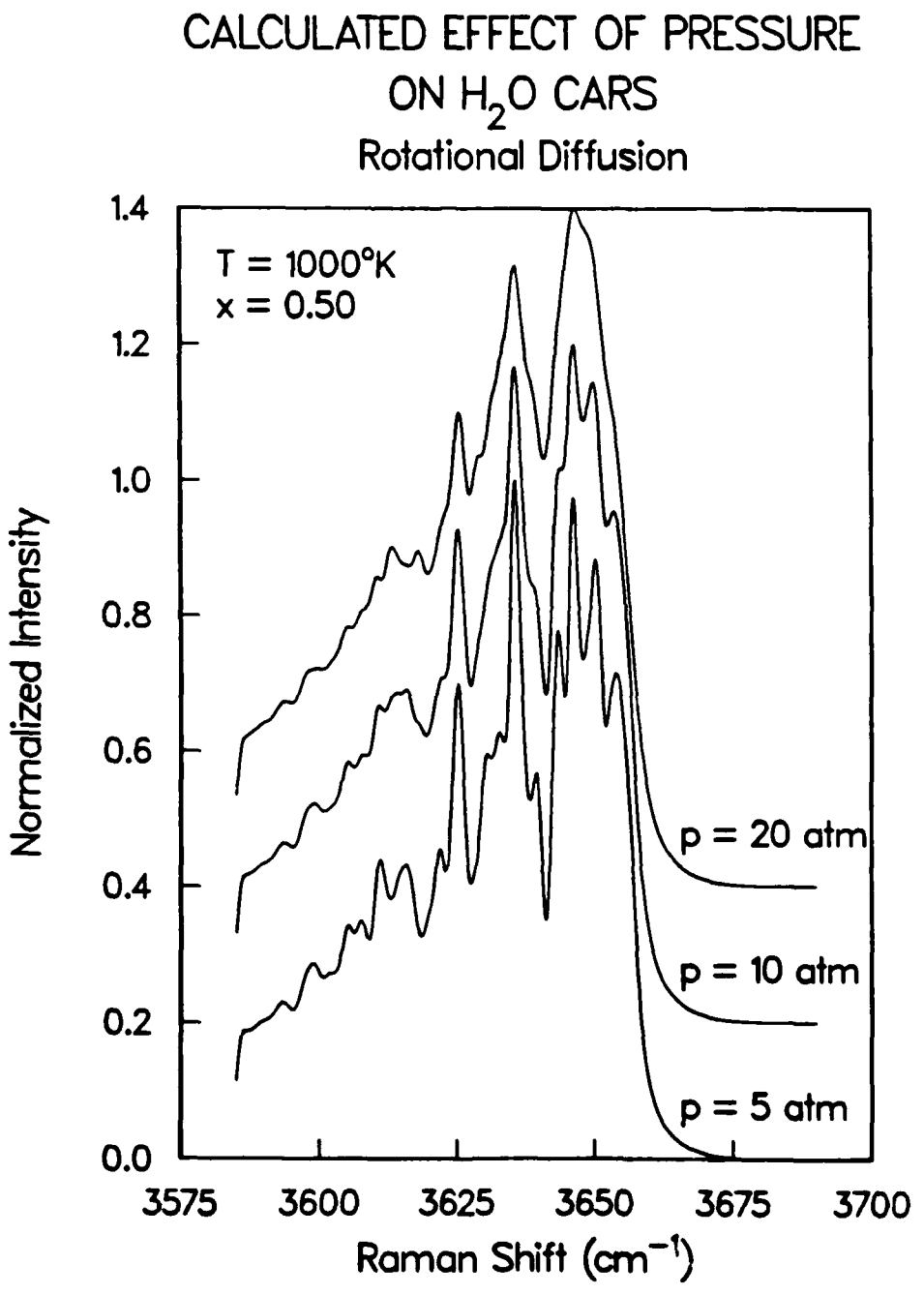
CALCULATED EFFECT OF PRESSURE
ON H_2O CARS
Rotational Diffusion
T = 1000°K
x = 0.50
p = 20 atm
p = 10 atm
p = 5 atm
Normalized Intensity
1.4
1.2
1.0
0.8
0.6
0.4
0.2
0.0
3575
3600
3625
3650
3675
3700
Raman Shift (cm^{-1})

FIG. 11

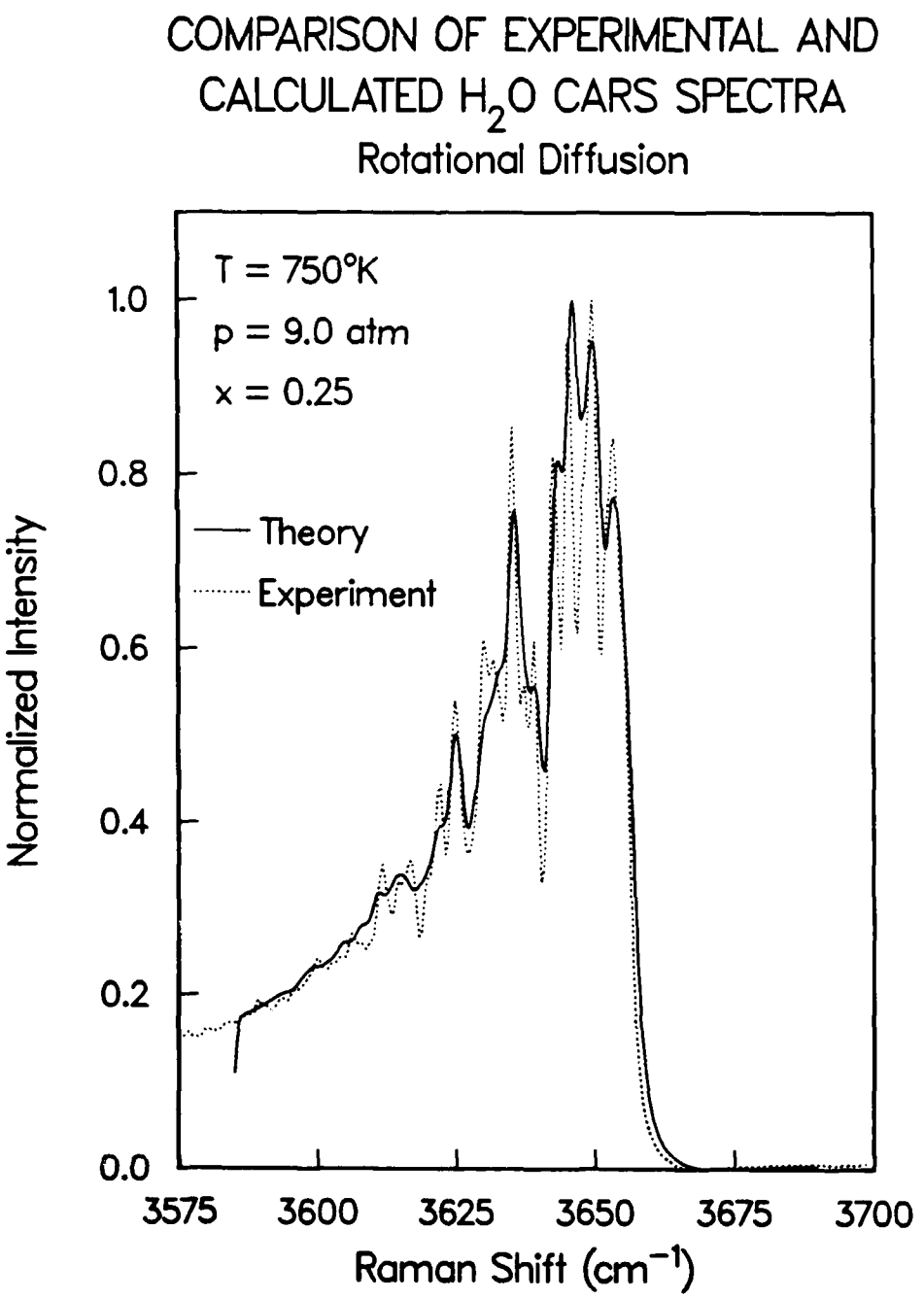
COMPARISON OF EXPERIMENTAL AND CALCULATED H_2O CARS SPECTRA
Rotational Diffusion
T = 750°K
p = 9.0 atm
x = 0.25
Theory
Experiment
Normalized Intensity
1.0
0.8
0.6
0.4
0.2
0.0
3575
3600
3625
3650
3675
3700
Raman Shift (cm^{-1})

Conclusions and Recommendations

It appears at present that the collision narrowing models used in CARS calculations are not the prime limitation to water vapor calculations. Rather it seems to be more the case that the deficiency is in the detailed behavior of the linewidths. Before progress can be made, an independent means of determining the concentration is necessary. Unfortunately no known instrumentation exists which is suitable for application in the relevant parameter range. The best approach may be to measure absorption on a well resolved infrared transition with a tunable diode laser. A fruitful avenue of research may be that of incorporating linewidth calculations into the CARS code.

Measurements of widths, with high resolution inverse Raman, for example, would be very useful. Calculations show important differences among transitions, including alternating widths. It is expected however that it would not be possible to resolve all important lines, because of the combined width and proximity of lines with large $|\tau|$.

Future improvements include use of the Kataoka et al. (1982) and Teets (1984) convolution, which is more appropriate for measurements with current laser sources. It is is expected that these calculations would improve the fit of spectra near the bandhead. Recently Koszykowski et al. (1985) reported the use of the Gordon and McGinnis (1968) technique with CARS calculations to eliminate repeated matrix inversions needed to calculate a complete spectrum. With this simplification a matrix needs to be inverted only once.

It is clear that further work is necessary before CARS can be used for concentration determinations of water in high pressure combustion situations.

NO Experimental Measurements

NO CARS spectra have been obtained over the range 1-33 atmospheres, 300-800 K. Specific combinations of these parameters were selected for the acquisition of CARS spectra as indicated in Fig. 12. A computer code was assembled to predict the NO CARS spectra and comparisons between theory and experiment have been made

Experimental Apparatus

To provide well controlled conditions of temperature and pressure for the acquisition of NO CARS spectra, the high pressure vessel described in Stufflebeam, et al. (1984) was utilized. It is a static, internally heated

FIG. 12

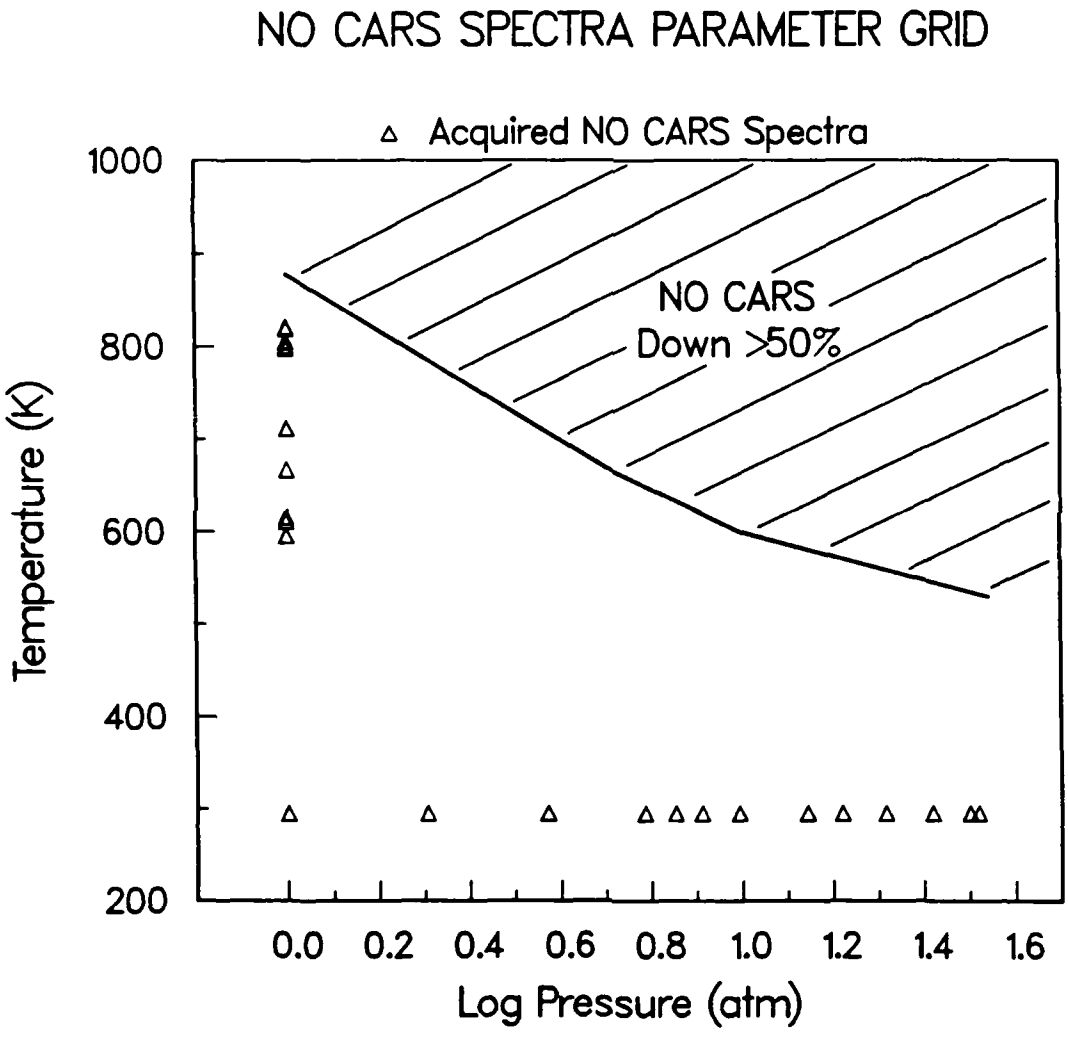
NO CARS SPECTRA PARAMETER GRID
Acquired NO CARS Spectra
NO CARS
Down >50%
Temperature (K)
1000
800
600
400
200
0.0
0.2
0.4
0.6
0.8
1.0
1.2
1.4
1.6
Log Pressure (atm)

cell that is rated for temperatures to 1750 K and pressures to 5000 psig. It is equipped with a pressure gauge, type S thermocouples, and an optical pyrometer to measure the pressure and temperature of the sample. Only the central 15 cm is heated and sapphire rods extend into the heated region to reduce thermally-induced density gradient effects in the gas. The limited optical access provided by the test cell dictates either collinear alignment of the pump and Stokes lasers used to generate CARS or a tightly packed BOXCARS arrangement. A folded BOXCARS phase matching geometry was employed for the NO measurements with an axial resolution of approximately 4 mm to avoid any problems from axial temperature gradients in the cell. The UTRC High Pressure CARS Facility provided the hardware for these measurements and is fully described in the experimental apparatus section of the high pressure flame measurements of this report.

NO Experiments

A problem was encountered during the NO investigations that prohibited acquisition of NO spectra at all potential conditions of interest (see Fig. 12). NO is highly susceptible to catalytic reactions for temperatures below 1000 K and this presented a problem for acquisition of CARS spectra from the high pressure cell. As mentioned in Stufflebeam, et al. (1984) the cell contains many refractory oxide materials such as alumina and zirconia and its heater is pure platinum. All these surfaces are highly reactive with NO as investigated many years ago by Wise and Frech (1955), Fraser and Daniels (1958), Yuan, et al. (1959), among others. The catalytic reaction converts the NO to NO_2 which is highly absorbing for visible wavelengths. Calculations indicate only 0.5% NO_2 at 1 atmosphere pressure will produce a 50% reduction in the expected CARS signal. The reduction accounts for absorption of the pump laser in addition to the absorption of the CARS frequency. Tests of this effect were performed by loading the heated cell with 100% NO and monitoring the absorption of the ω_1 beam that was propagated through the gas. At 1 atmosphere pressure, the NO would allow transmission of the pump beam and remain optically clear for more than one and one-half hours up to a temperature of 800 K. At 300 K the cell remained optically clear to the highest available pressure of 33 atmospheres for extended periods also. The CARS data acquisition mode utilized for the NO spectra employs broadband generation and scanned, narrowband detection. Since the scanning CARS technique requires up to 40 minutes to obtain the CARS spectrum, and time is required for thermal equilibrium after filling the cell with NO, it was judged that any observable NO_2 generation in less than one hour would jeopardize the experiment. Our absorption tests indicated this was possible at 1 atmosphere from 300-800 K and at 300 K from 1-33 atmospheres (Fig. 12). For pressures above 1 atmosphere the usable temperature range was so limited, up to about 450 K, as to preclude useful information to be gained for this

investigation. The above limits were also confirmed through an analysis using the CHEMKIN chemical kinetics code to predict NO_2 production using activation energies and frequency factors for the heterogeneous reaction published by Wise and Frech (1955) with additional reactions published by McCullough, et al. (1977). There was insufficient time to design and fabricate a new high pressure cell with materials that would not react with NO, so only those spectra indicated in Fig. 12 were acquired.

CARS spectra of NO were acquired at 295 K over the pressure range 1-33 atmospheres and the bandwidths (FWHM) measured from the experimental data. These data are presented in Fig. 13, where the different symbols represent data acquired on different days. As with other molecules studied at UTRC, there is little change in bandwidth as the pressure is varied and it is obvious the collisional narrowing process is operative over this pressure range.

The experimental spectra acquired at 1 atmosphere, 616 and 801 K are presented in Figs. 14 and 15. The abrupt discontinuity in these spectra in the region of 20,620 cm^{-1} is artificially produced during the scan to check the zero signal level. It is observed that even the 616 K spectrum exhibits a hot band and that both spectra show significant modulation of the nonresonant background in the vicinity of the fundamental bandhead. The nonresonant background susceptibility of NO is 3 times that of N_2 so modulation is expected at these temperatures even for high concentration of the active molecule. Computer predictions are in progress for these experimental conditions.

Results and Discussion

Shown in Fig. 16 is the experimental CARS spectrum of NO at 295 K, 1 atmosphere (dots) together with the prediction of the NO CARS code for the same conditions. The computer prediction used the measured NO linewidths of Lempert et al (1984) and the inverse power law model to determine the off-diagonal linewidth elements of the G matrix (Stufflebeam, et al, 1984). Other models such as isolated lines or the Gordon model of rotational relaxation also predict this case well, but the inverse power law reproduces the spectra most closely over the whole pressure range. Figure 17 is the same as Fig. 16 except the pressure is 20 atmospheres. The fit is again very good and for this case the other models of linewidth do not compare as favorably with the experiment.

FIG. 13

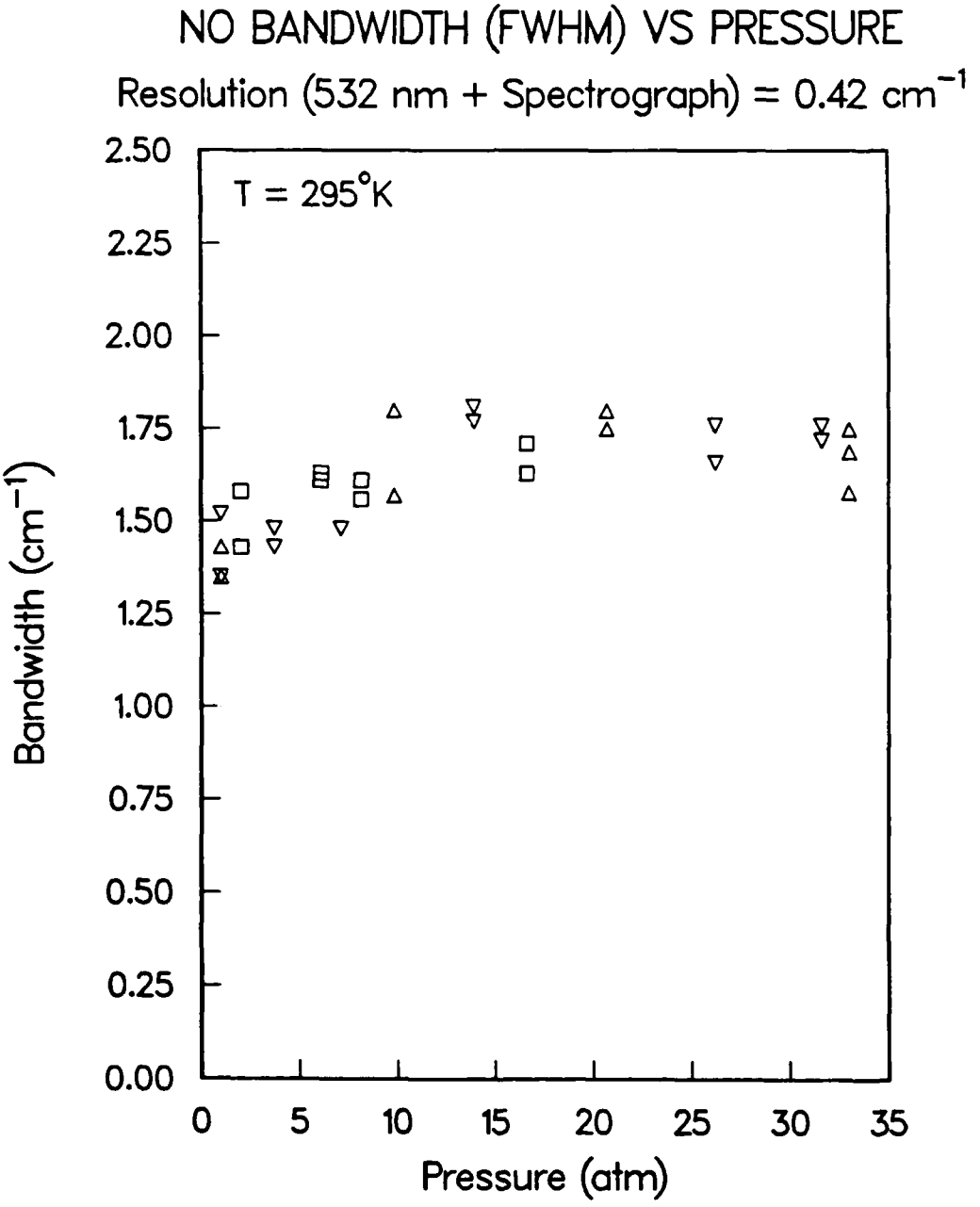
NO BANDWIDTH (FWHM) VS PRESSURE
Resolution (532 nm + Spectrograph) = 0.42 cm^{-1}
T = 295°K
Bandwidth (cm^{-1})
2.50
2.25
2.00
1.75
1.50
1.25
1.00
0.75
0.50
0.25
0.00
0
5
10
15
20
25
30
35
Pressure (atm)

FIG. 14

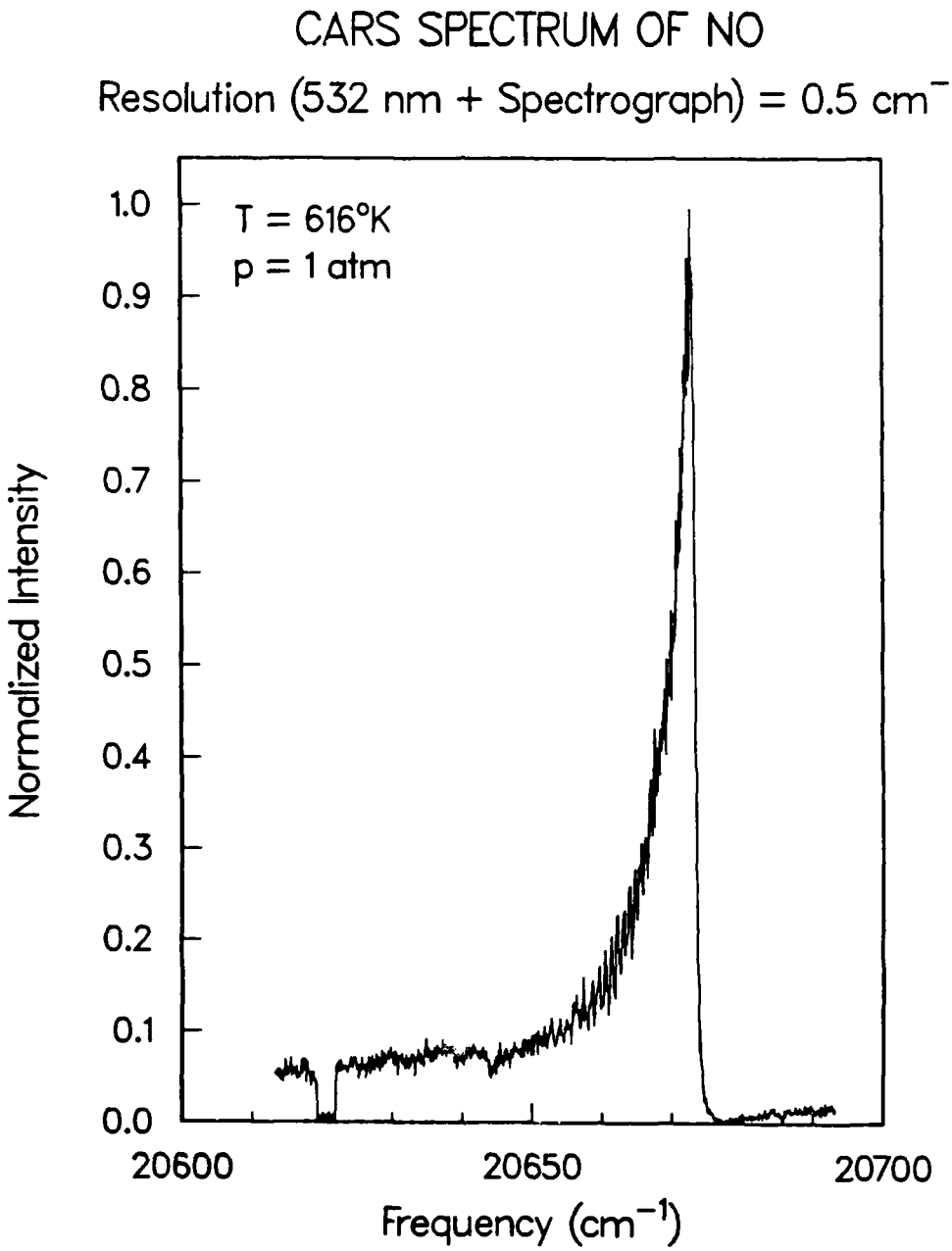
CARS SPECTRUM OF NO
Resolution (532 nm + Spectrograph) = 0.5 cm^{-1}
T = 616°K
p = 1 atm
Normalized Intensity
1.0
0.9
0.8
0.7
0.6
0.5
0.4
0.3
0.2
0.1
0.0
20600
20650
20700
Frequency (cm^{-1})

FIG. 15

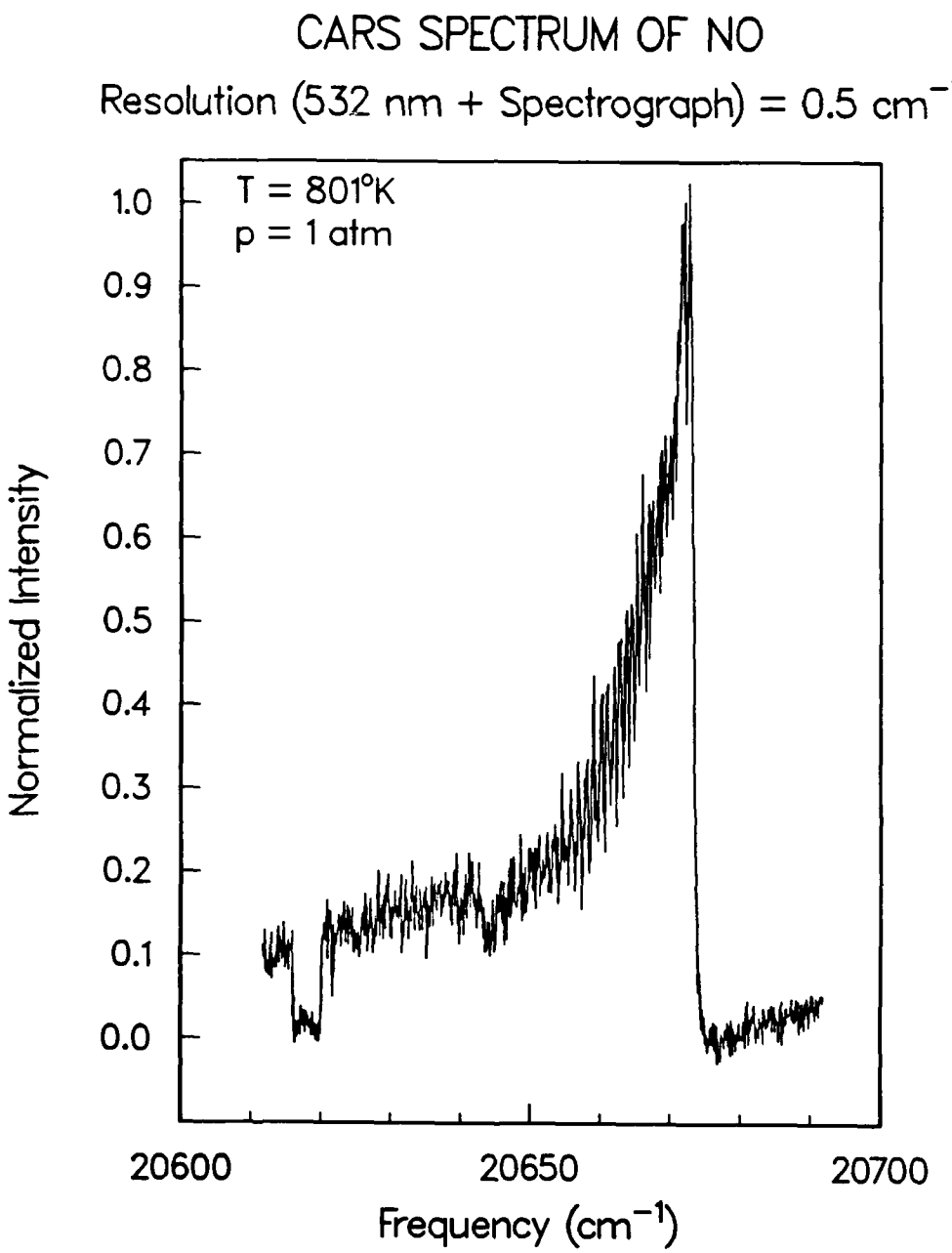
CARS SPECTRUM OF NO
Resolution (532 nm + Spectrograph) = 0.5 cm^{-1}
T = 801°K
p = 1 atm
Normalized Intensity
1.0
0.9
0.8
0.7
0.6
0.5
0.4
0.3
0.2
0.1
0.0
20600
20650
20700
Frequency (cm^{-1})

FIG. 16

CARS SPECTRUM OF NO

Comparison of Inverse Power Law and Experiment

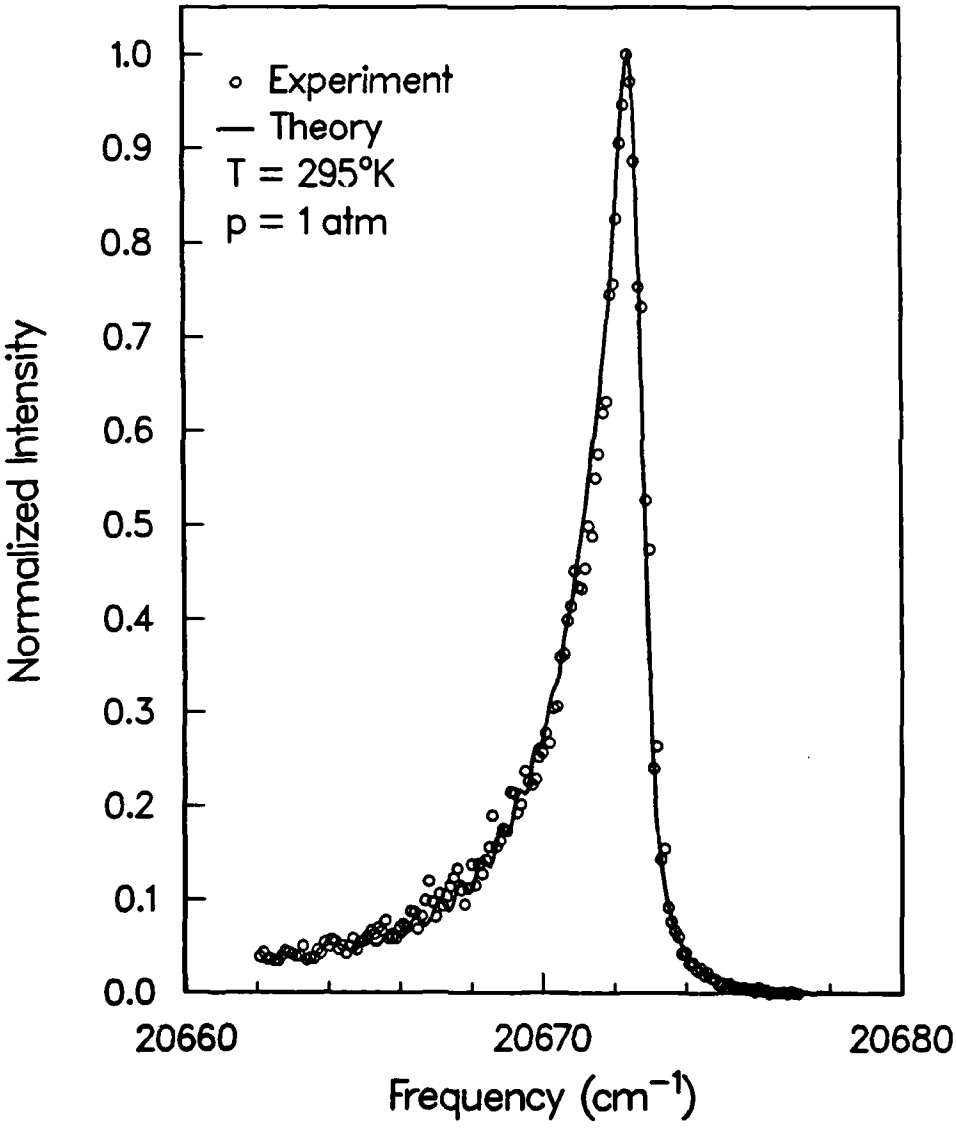

FIG. 17

CARS SPECTRUM OF NO

Comparison of Inverse Power Law and Experiment

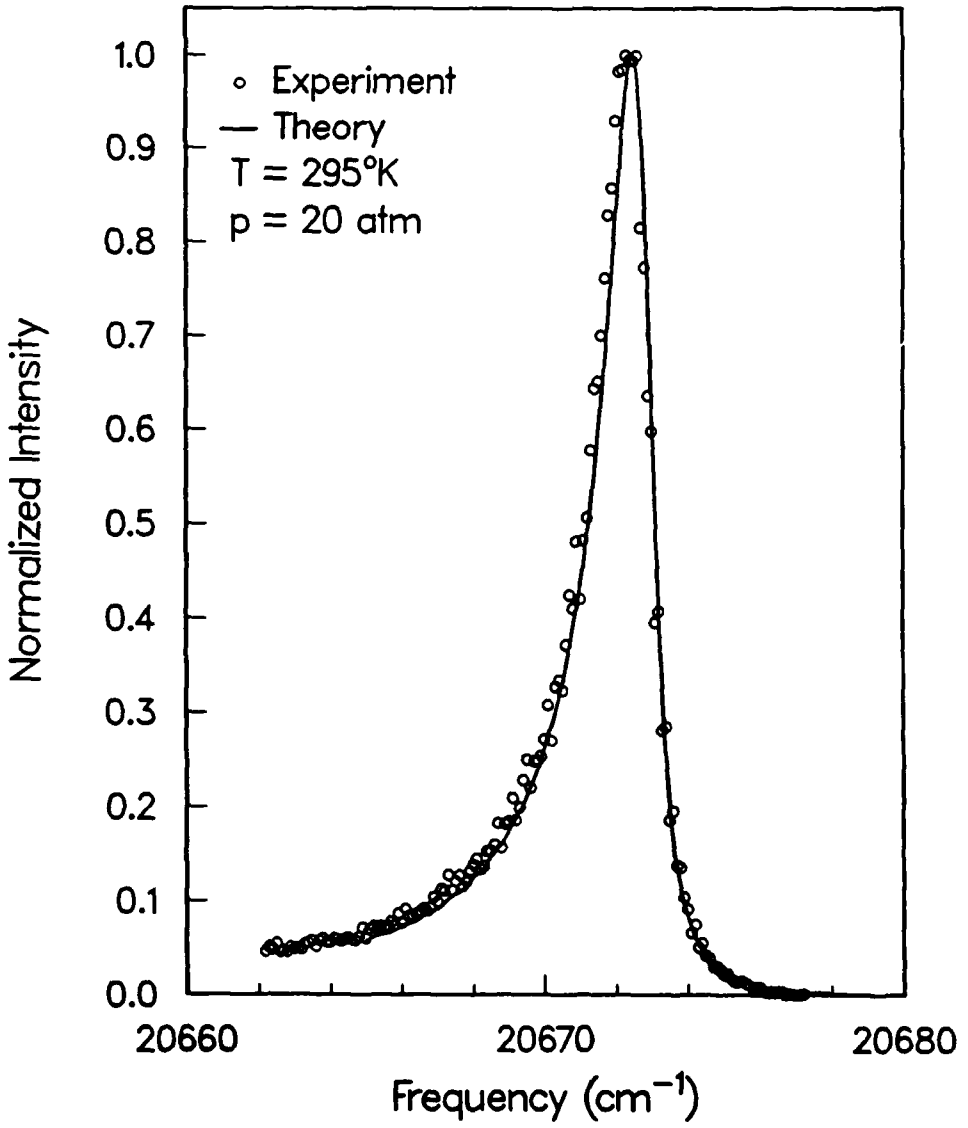

Recommendations

The basis for the NO predictive CARS code is the laser bandwidth convolution proposed by Yuratich (1979) to model the effect of finite bandwidth pump lasers on the predicted CARS spectrum. In recent years this approach has been questioned by researchers in Japan (Kataoka, et al., 1982) and in the U.S. (Teets, 1984). They proposed a new convolution that has been shown, through rigorous comparisons, to give better agreement with experimental data. It is known as the Kataoka-Teets (K-T) convolution and is discussed more fully in connection with high pressure flame measurements later in this report. The improvements are most pronounced for spectra of resonant species in low concentration and when the ratio of pump laser width to Raman linewidth, $\Delta\omega/\Gamma$, is large. It is not expected to have a large effect for the current studies because they deal with high concentration of the active molecule and the parameter $\Delta\omega/\Gamma$ gets smaller at high pressure. It would appear necessary, however, to convert the current NO CARS code to one based on the K-T convolution for predictions of NO spectra at low concentration and low pressure and this effort is currently in progress.

Future directions of this work involve implementation of the Dexheimer power law (Eqn. 10) and exponential gap (Eqn. 6) models of rotational relaxation in the NO CARS code as well as to fit the 1 atmosphere high temperature data. It is expected from previous results (Stufflebeam, et al., 1983) that the Dexheimer power law will predict the NO CARS spectrum more closely over the entire range of temperature and pressure studied. It will also be interesting to compare calculations using the exponential gap model to the results, as Koszykowski, et al. (1985) achieved good comparisons with this model for N_2 CARS spectra up to 10 atmospheres. To decide on which of these models is best, comparisons are needed with high pressure, hot spectra. These studies will be difficult unless special cells are built to prevent the NO NO_2 conversion problem encountered here.

HIGH PRESSURE FLAME MEASUREMENTS

Introduction

As part of the current contract, UTRC extended the previous studies of high pressure CARS spectra of various molecules to the regime of high pressure flames. For these studies a CO/air premixed flame was chosen because of the relatively simple chemistry involved. Furthermore there are no hydrocarbons or soot formed which can complicate interpretation of temperature and concentration measurements from the CARS spectra (Dobbs et al., 1985). A premixed flame was chosen to avoid the complication of having to account for diffusion effects in the flame. The products of the flame chemistry and their relative concentrations form a useful base for CARS measurements. Nitrogen is the major species and is used for thermometry. CO is present in low enough concentration to demonstrate concentration measurements by spectral shape. Also as will be shown, both spectra can be obtained simultaneously with the apparatus employed for this work. This turns out to be advantageous for temperature and concentration measurements as will become clear in later sections of this report.

The next section describes the high pressure flame facility developed for this contract. Then the CARS and Raman-scattering apparatus are described. Finally, the results of the CARS and Raman studies of the high pressure flame are presented and discussed; directions for future work are also indicated.

Experimental Apparatus

High Pressure Flame Facility

The premixed flame was chosen to operate in non-sooting fashion and with a fairly simple chemical system. Consequently, the simple fuel CO, was selected. The choice of CO as the fuel gave a very simple product gas composition (CO, CO_2, N_2, and possibly O_2) to expedite atom balance closure for quantitative CARS evaluation. This avoided complicating the CARS measurements with the inclusion of H_2, H_2O, and other hydrogenic species. The oxidation of CO to CO_2 involves an intermediate reaction with an OH radical. It was necessary to include a trace amount of a gas that would promote the ignition and reaction of CO with air. Consequently, ultra pure CO is used as the fuel and a trace amount of C_2H_4 is introduced into the fuel stream as a source of the OH intermediate. This allowed the flame to be well controlled

over the entire range of operating pressure. It also allowed some control over the flame speed.

A high pressure test cell, designed and constructed earlier was employed to house the burner. The vessel is a heavy wall cylinder with top and bottom flanges sealed with O-rings. Optical access is provided by four large aperture (2.5 cm) quartz windows at 90 degrees, thus permitting CARS, LIF or Raman measurements to be made. Provision has also been made for thermocouples, pressure transducers, gas supply, ignition, and exhaust. The flameholder, designed for flexibility of application, is replaceable and can be changed by removing the bottom flange. The inside surface of the quartz windows are located about 6 cm from the centerline of the test cell to prevent damaging the windows by the incident high energy laser beams.

A premixed flame burner was designed, constructed, and employed to investigate quantitative CARS measurements in a high pressure CO/air flame. The burner design uses a 1.3 cm diameter fuel tube capped with a brass tip that has 37 drilled holes (1.0 mm diameter) in a closely-packed hexagonal pattern. Figure 18 illustrates the burner design and shows the details of the brass burner tip. The flame was operated with the cavity beneath the burner tip filled with No. 12 grade, HP copper shot, 0.15 cm in diameter. The feed tube is surrounded by a 3.8 cm o.d. (0.09 cm wall) stainless tube that provides the secondary shroud flow, generally nitrogen. There was no observable difference in the premixed flame whether or not the shroud flow was used. Consequently, the shroud flow was not used in the CARS experiments. The flame is ignited at atmospheric pressure with a spark from a removable wire centered over the burner tip and driven by a commercial Tesla coil. The ignitor wire is positioned over the center of the premixed burner so that a spark of about 4-5 mm in length is obtained.

Provision was made to have five gases available to the burner; carbon dioxide, nitrogen, air, carbon monoxide, and ethylene. Standard gas cylinders are connected to Hastings mass flowmeters and then to needle valves which provide the flow control. The flowmeters were calibrated with a wet test meter. The two fuel lines, CO and C_2H_4, and the air line are connected to a mixing chamber, thence to the fuel tube of the burner. The mixing chamber cavity is filled with No. 9 lead shot which distributes and mixes the flow.

The pressure in the high pressure test cell is controlled by regulating the exhaust flow out of the cell through a needle valve. The flow rates are adjusted to maintain a stable flame at the desired stoichiometry and as the cell is pressurized, the exhaust needle valve is adjusted to maintain the test cell pressure. Once stable conditions have been reached, the cell operates for hours without any apparent change in burner characteristics or operating pressure.

HIGH PRESSURE PREMIXED BURNER

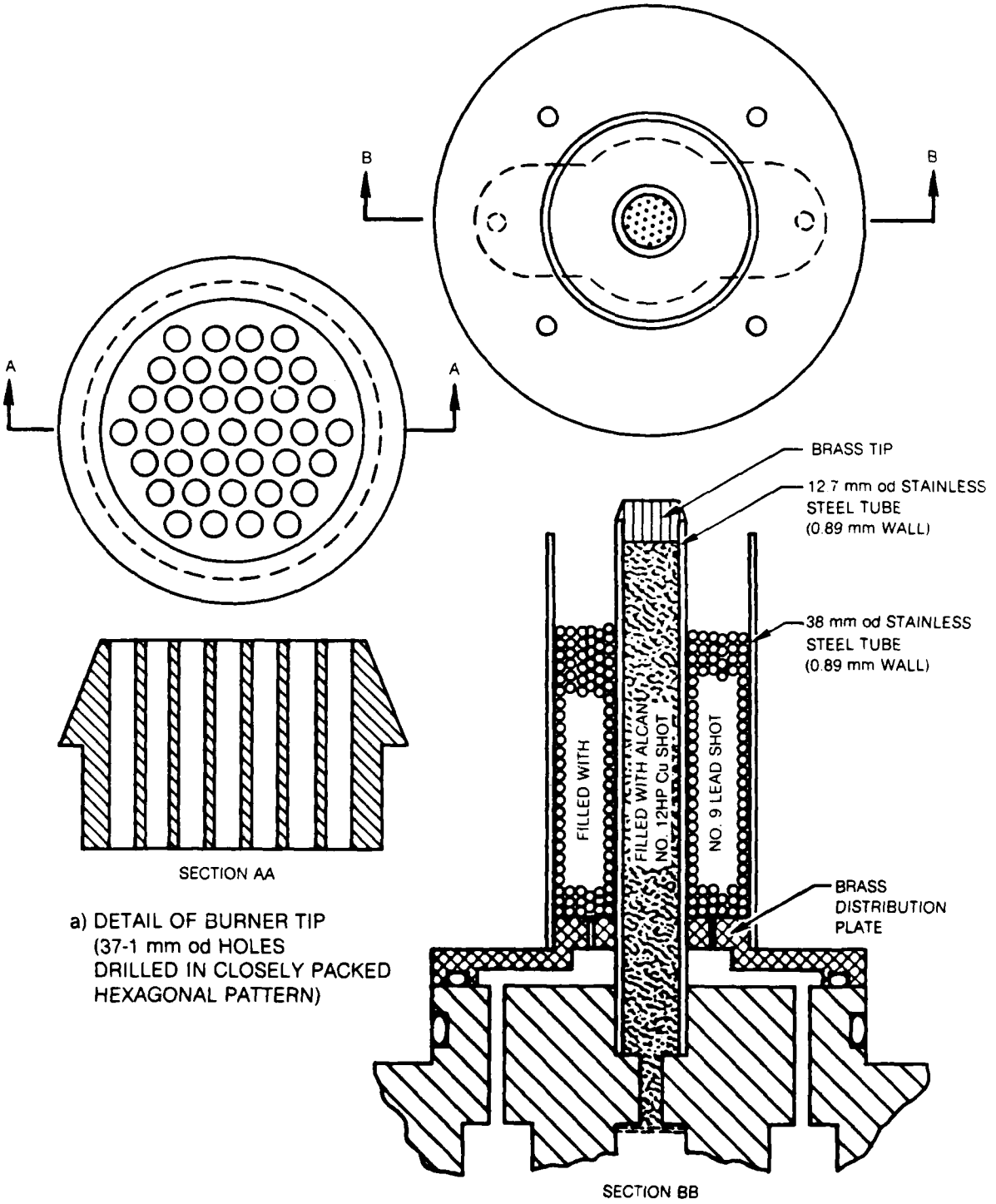

a) DETAIL OF BURNER TIP (37-1 mm od HOLES DRILLED IN CLOSELY PACKED HEXAGONAL PATTERN)

b) DETAIL OF ASSEMBLED BURNER

85-11-92-2

The brass tip with the small holes stabilizes the flame front about 1 mm above the surface. The premixed flame burner was operated successfully at pressures up to about 15 atmospheres, providing a flat premixed flame about 1 cm in diameter at atmospheric pressure and a slightly reduced diameter at elevated pressure as shown in Fig. 19. It was necessary to increase the flow rate of fuel and air to the burner at elevated pressure to prevent quenching of the flame on the burner surface. It was also possible to blow the flame off the burner if the feed rate was too high.

Experiments were performed to determine the practical operating envelope of the burner at various flow rates, air/CO ratios, and pressure levels (Hedman, et al., 1986). A set of "design" gas flow rates was selected for CARS measurements at each operating pressure. The design air/CO ratio selected is about 1.6, chosen to reside well within the stable operating envelope. Based on adiabatic chemical equilibrium calculations (Gordon and McBride, 1976), these operating conditions give the product gas distribution and adiabatic flame temperature listed in Table 2.

Table 2

Gordon-McBride Predictions of CO/air Premixed Flame

Pressure	% CO	% CO_2	% N_2	AFT
1 atm	18.5	26.1	53.4	2295 K
5	16.9	27.2	54.2	2334
10	16.3	28.0	54.4	2352

CARS Apparatus

The experiments were carried out in the UTRC High Pressure CARS Facility shown schematically in Fig. 20. The output of a Quanta-Ray Nd:YAG laser is frequency doubled to generate a horizontally polarized, "primary" pump beam at 532 nm (ω_1). The 10 Hz laser has an average output of 2.2 Watts at 532 nm with a pulse duration of 7 nanoseconds. A beamsplitter separates 30% from ω_1 to pump the broadband Stokes dye laser oscillator and amplifier. The primary pump is subsequently passed through a polarizer then divided into two pump beams for the folded BOXCARS phase-matching geometry (Shirley, et al., 1980) by a beamsplitter/mirror combination. The polarization of each beam is independently controlled by half-wave plates. An optical delay line is inserted in one of the ω_1 legs to establish the degree of correlation desired for the two pump beams. An optical flat is inserted after the Stokes beam amplifier to displace ω_2 out of the plane of the two primary pumps.

1 atm

5 atm

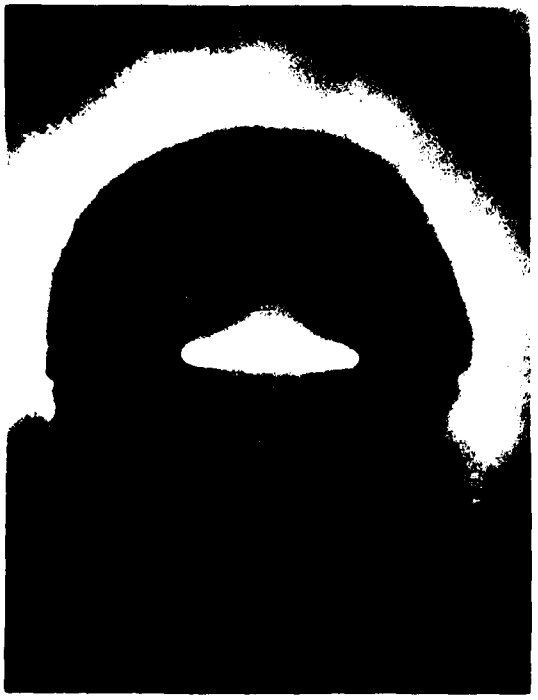

10 atm

15 atm

85 490-C

85-11-92-12

HIGH PRESSURE, HIGH TEMPERATURE CARS FACILITY

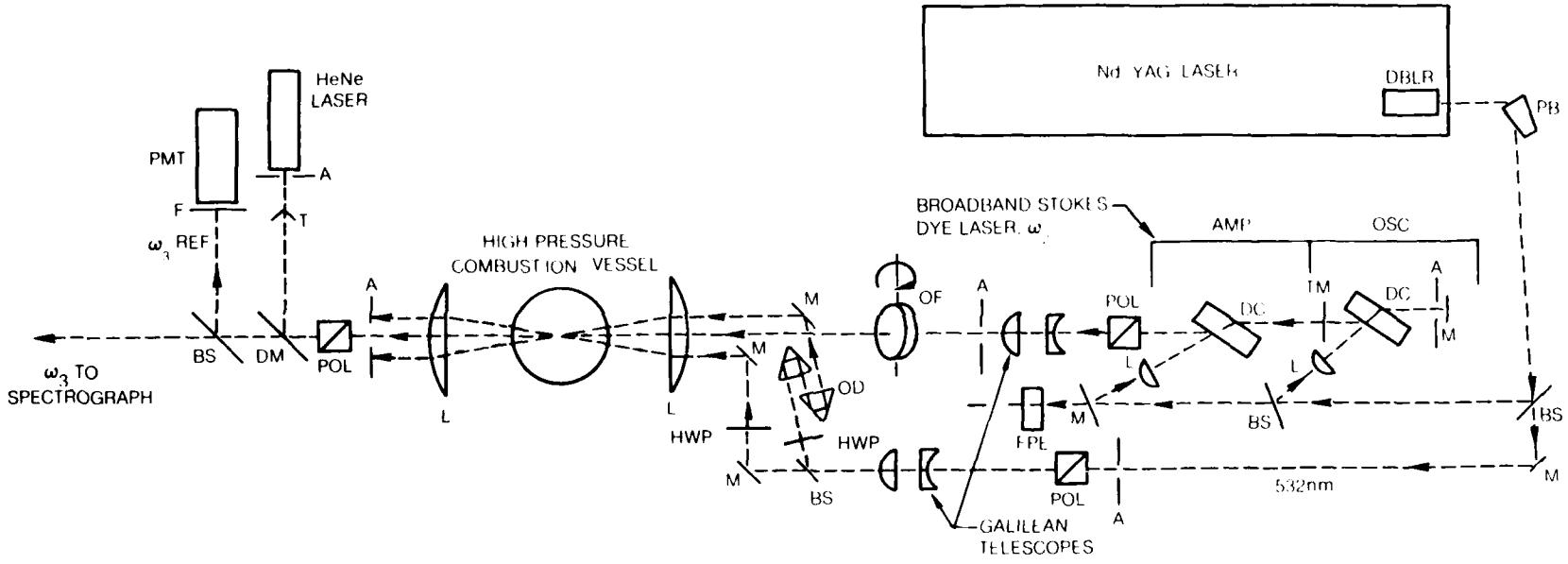

A — APERTURE
M — MIRROR
DM — DICHROIC MIRROR
TM — PARTIALLY TRANSMITTING MIRROR
BS — BEAM SPLITTER
L — LENS
P — PRISM
PB — PELLIN-BROCA PRISM
POL — POLARIZING CUBE

F — FILTER
DBLR — FREQUENCY DOUBLER
FPE — FABRY-PEROT ETALON
DC — DYE CELL
PMT — PHOTOMULTIPLIER TUBE
OF — OPTICAL FLAT
T — TRAP
OD — VARIABLE OPTICAL DELAY
HWP — HALF WAVE PLATE

84-6-85-1

FIG 20

Galilean telescopes are provided to control beam waists and the focal zone locations of ω_2 and the ω_1's. CARS, at ω_3, is generated in the focal volume, and all three frequencies (ω_1, ω_2, ω_3) are recollimated after exiting the cell. The CARS beam is separated from the pump beams by a spatial filter then passed through a broadband polarization analyzer, for the background suppression experiments (Eckbreth and Hall, 1981), before the signal is incident on the slit of a 0.5 m spectrograph. A He-Ne laser is shown whose output is coincident with the ω_2 path and used for optical alignment. A beamsplitter in the ω_3 leg provides a reference signal to a photomultiplier which is used to monitor the spectrally-integrated CARS signal strength. A broadband diode array detector is mounted on the spectrograph. It is a 1000 channel, intensified array that allows acquisition of very broad CARS spectra (~ 600 cm^{-1}). Use of the vidicon greatly expedites signal collection and reduces measurement times considerably. The data (spectra) from the diode array are sent to the computer for spectral processing and archival storage.

Raman Apparatus

To complement CARS measurements in the high pressure, premixed, CO/air flame, a Raman scattering diagnostic capability was designed and assembled for the UTRC High Pressure CARS Facility. The Raman diagnostic system shown in Fig. 21, consists of two photomultiplier tube detectors, monitored through gated integrators for single laser pulse temporal response. Their output is recorded by A/D converters in a laboratory computer. One tube detects Stokes-shifted Raman scattering from the 532 nm pump laser and the other tube detects anti-Stokes shifted photons from the same laser pulse. The laser polarization was rotated to vertical for the Raman measurements. Several narrowband interference filters were designed and obtained so that various flame species (CO, CO_2, N_2) could be monitored. The Raman scattered radiation was imaged on an aperture to control the size of the observed experimental volume. Additional shields and absorbing glass filters were employed to reduce interference from scattered radiation at 532 nm. The system was calibrated for each filter by Raman scattering from a gas at known conditions (i.e. N_2 at NTP). Data from the flame then yielded the number density (Stokes shifted scattering) of the observed gas species in the combustion environment. Similarly, the anti-Stokes radiation was calibrated by a tungsten lamp at known temperature and the experimental data was recorded. The ratio of anti-Stokes to Stokes scattering gives an estimate of the gas temperature (Eckbreth, at al., 1979).

Photographs of the experimental apparatus are shown in Figs. 22 and 23. The high pressure combustion vessel and Raman apparatus are evident in Fig. 22; the pump laser and beam manipulation optics used to generate the folded BOXCARS phase matching geometry are shown in Fig. 23.

FIG. 21

RAMAN SCATTERING EXPERIMENT

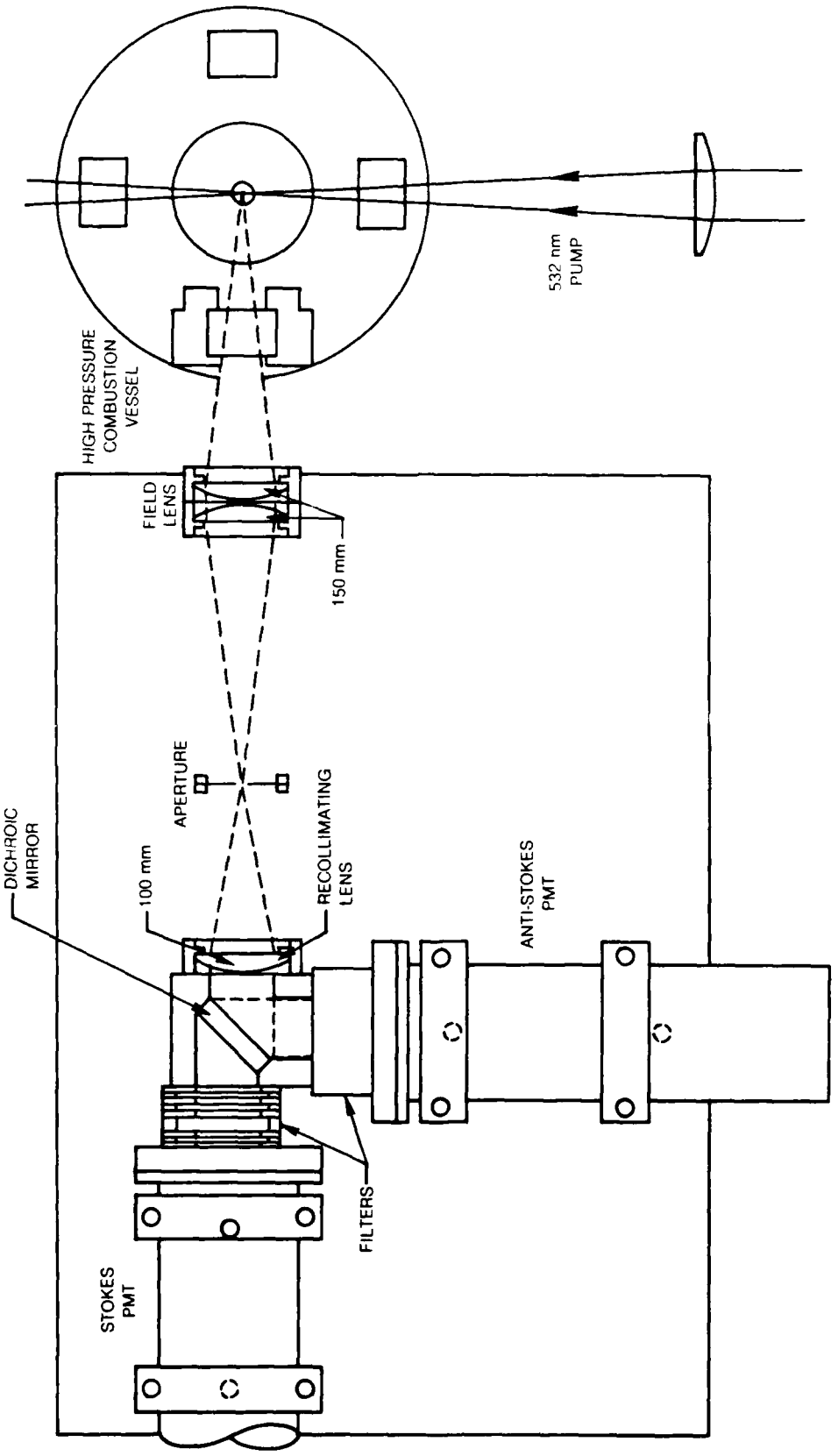

85 490 83

HIGH PRESSURE FLAME FACILITY

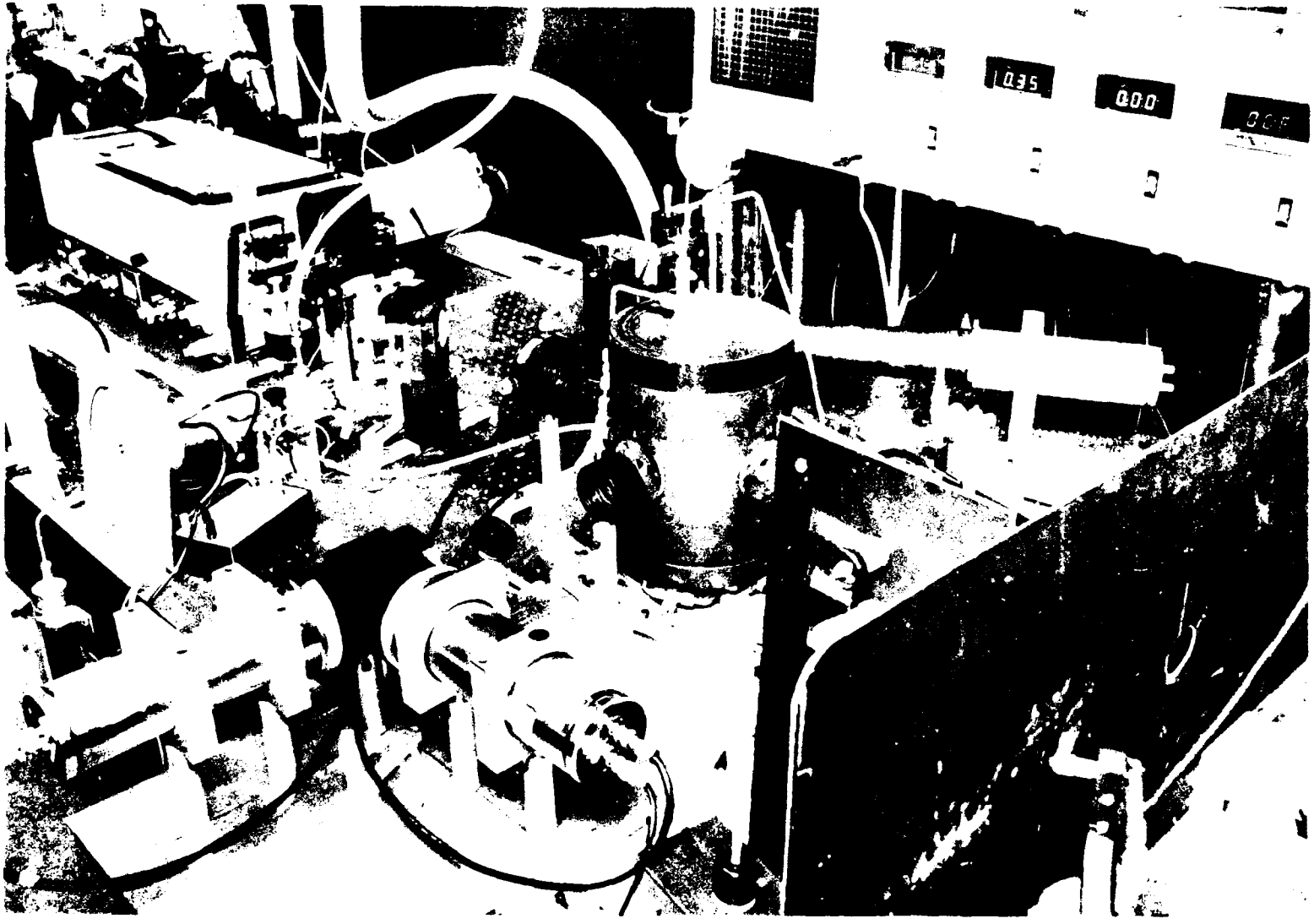

85-11 92-13

FIG. 23

CARS APPARATUS FOR HIGH PRESSURE INVESTIGATIONS

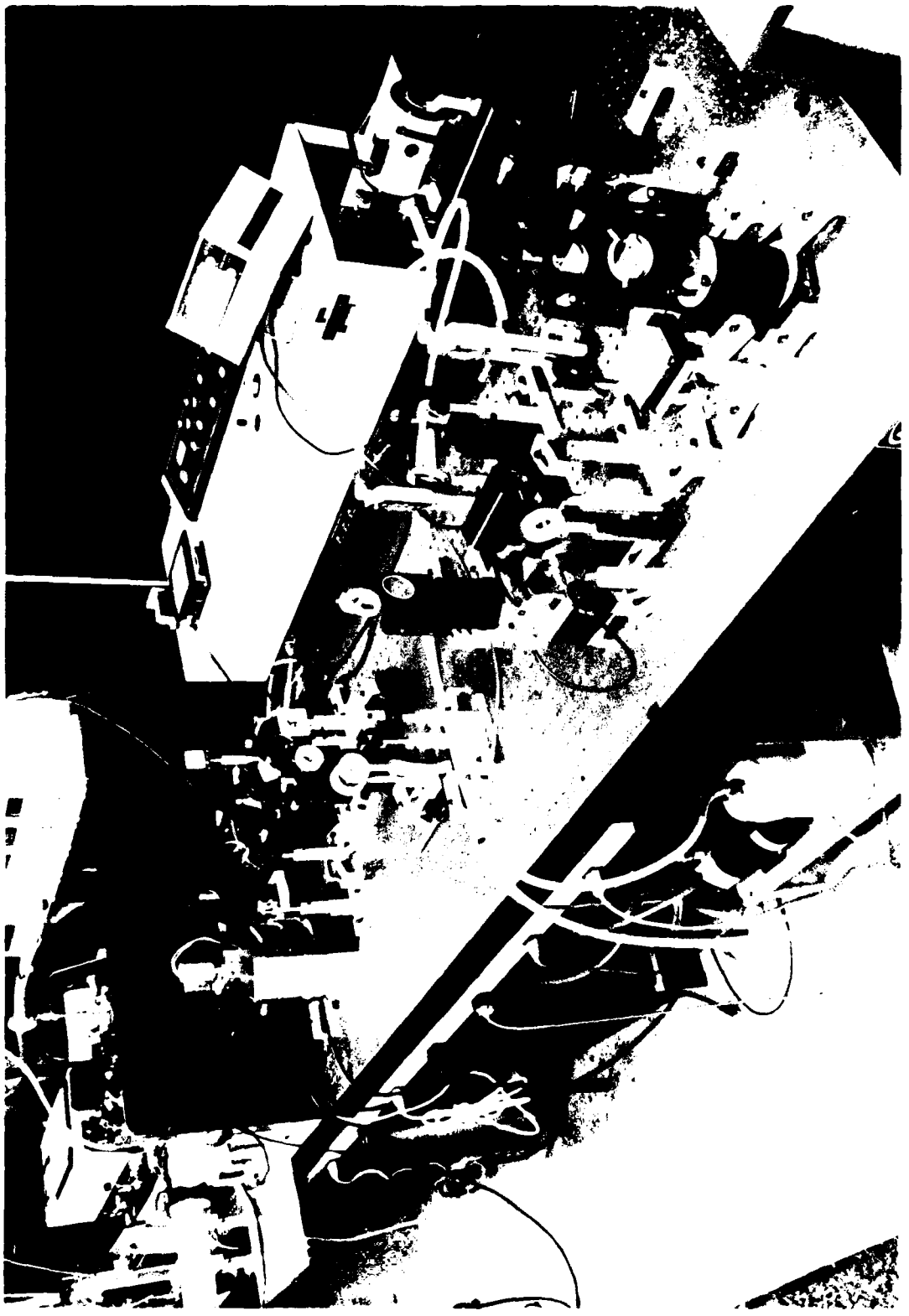

85-490-B7

85-11-92-11

Experimental Measurements

Raman Measurements

Using the previously described Raman apparatus, measurements of product gas relative concentration were taken. The flame was stabilized at each operating pressure and the output of the gated integrator that monitors the Stokes Raman PMT was sampled by an A/D converter. Five hundred, single-pulse datapoints were obtained for each gas species of interest. Different gases were measured by changing the narrow band (~ 40 cm^{-1} FWHM) interference filter in front of the PMT. Each filter was designed to minimize its temperature sensitivity vis-a vis the number of resonant species photons collected (Eckbreth, at al., 1979). In this way the collected signal is proportional to the number density of the scattering species and independent of the temperature. Each filter combination was calibrated at room temperature with the cell filled with 100% of the respective gas that was being measured. The calibrations then are used to relate measured signals to gas number density and relative concentrations. The gas temperatures can be inferred through Raman measurements described in Eckbreth et al. (1979). The basic technique is to measure the ratio of anti-Stokes to Stokes scattering for the same molecule, in this case nitrogen. The Raman apparatus was designed to obtain this measurement and the data were acquired for each operating pressure of the flame. At this time the temperature data have not been fully analyzed; however, the analysis is ongoing and results are expected in the near future. The Raman measurements of relative species concentrations in the premixed flame are presented in Fig. 24. The symbols indicate experimental measurements and the lines are the predictions from the Gordon-McBride computer code. The agreement for N_2 and CO_2 is within 7% and quite good. The comparisons for CO are less favorable (20%) and indicate a need for further analysis. Since the experimental data are uniformly higher than the computer prediction, a recalibration of the CO Stokes detector may be necessary.

CARS Measurements

The UTRC high pressure flame facility provided the medium to obtain CARS spectra from the high pressure premixed flame. The CARS spatial resolution was measured as a .16 mm dia. x 3.5 mm long cylinder which is adequate to probe the 1 cm dia. high pressure flame. The pump beams were crossed in the folded BOXCARS phase matching geometry approximately 2 mm above the burner surface. This is above the reaction zone so that only flame products were measured. Examples of CARS spectra from various operating pressures of the flame are shown in Figs. 25-28. All of these data are from the $CO-N_2$

FIG. 24

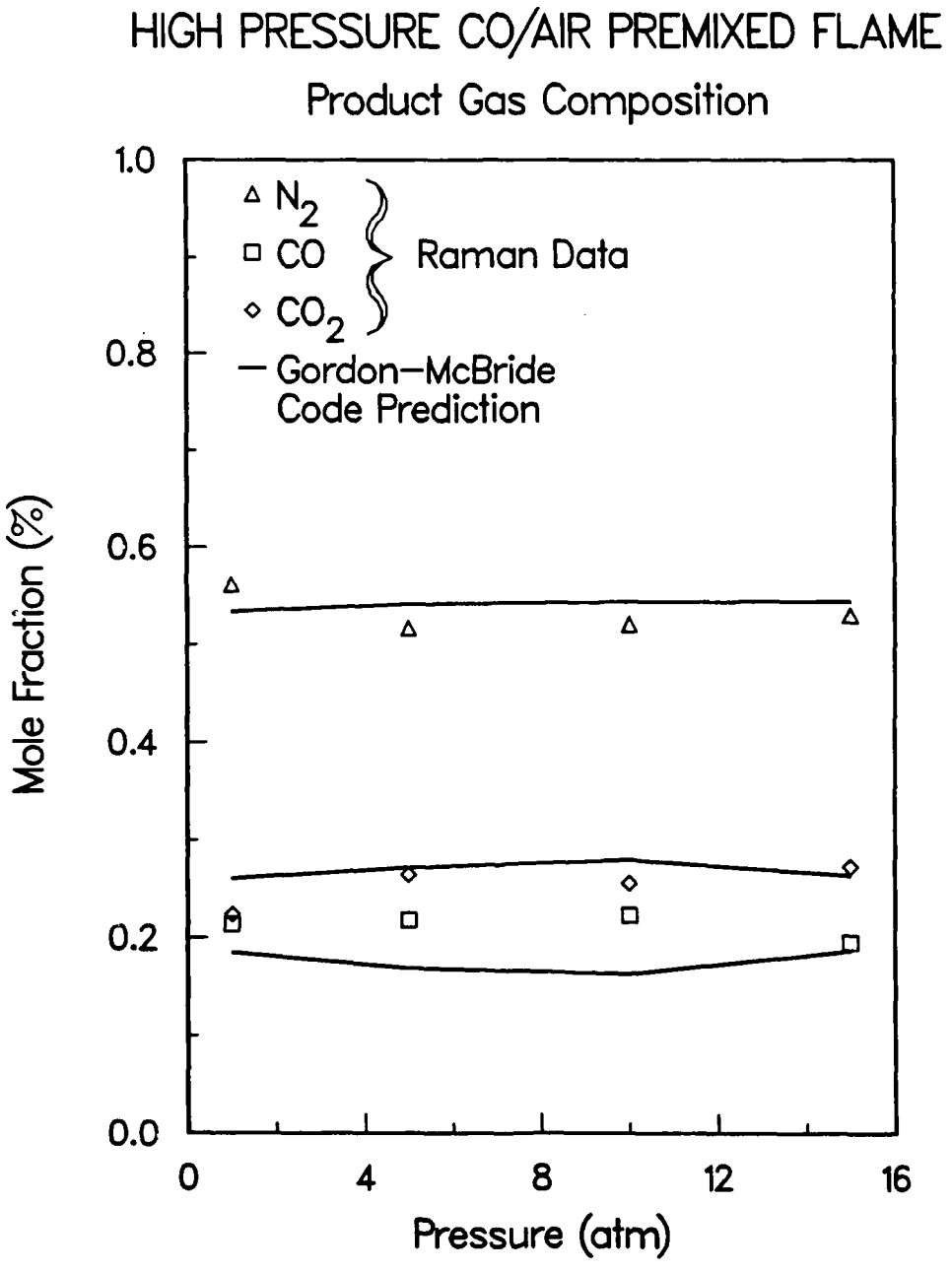
HIGH PRESSURE CO/AIR PREMIXED FLAME
Product Gas Composition
1.0
0.8
0.6
0.4
0.2
0.0
Mole Fraction (%)
△ N_2
□ CO
◇ CO_2
Raman Data
— Gordon–McBride Code Prediction
0
4
8
12
16
Pressure (atm)

FIG. 25

CARS SPECTRUM FROM CO/AIR PREMIXED FLAME

100 Pulse Avg., 2.5 cm^{-1} Resolution

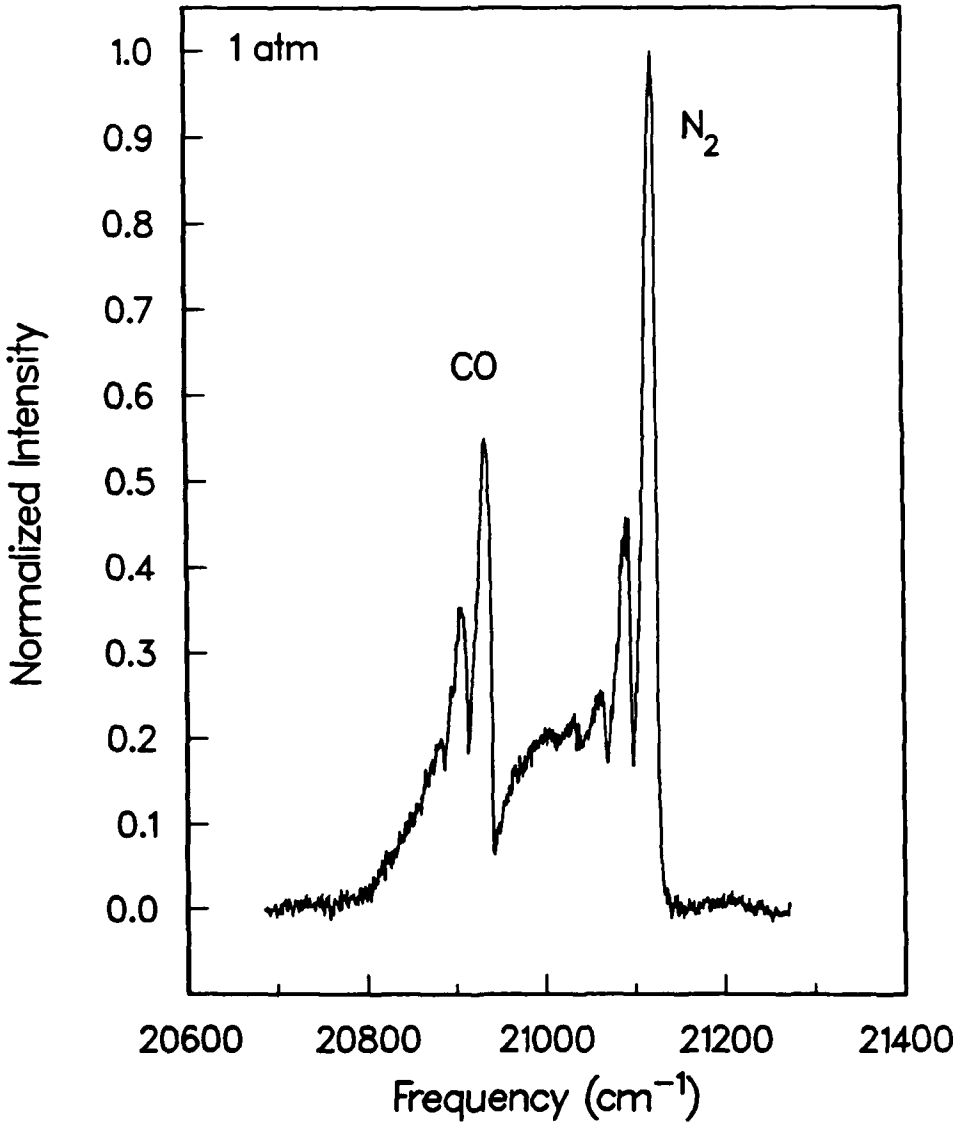

FIG. 26

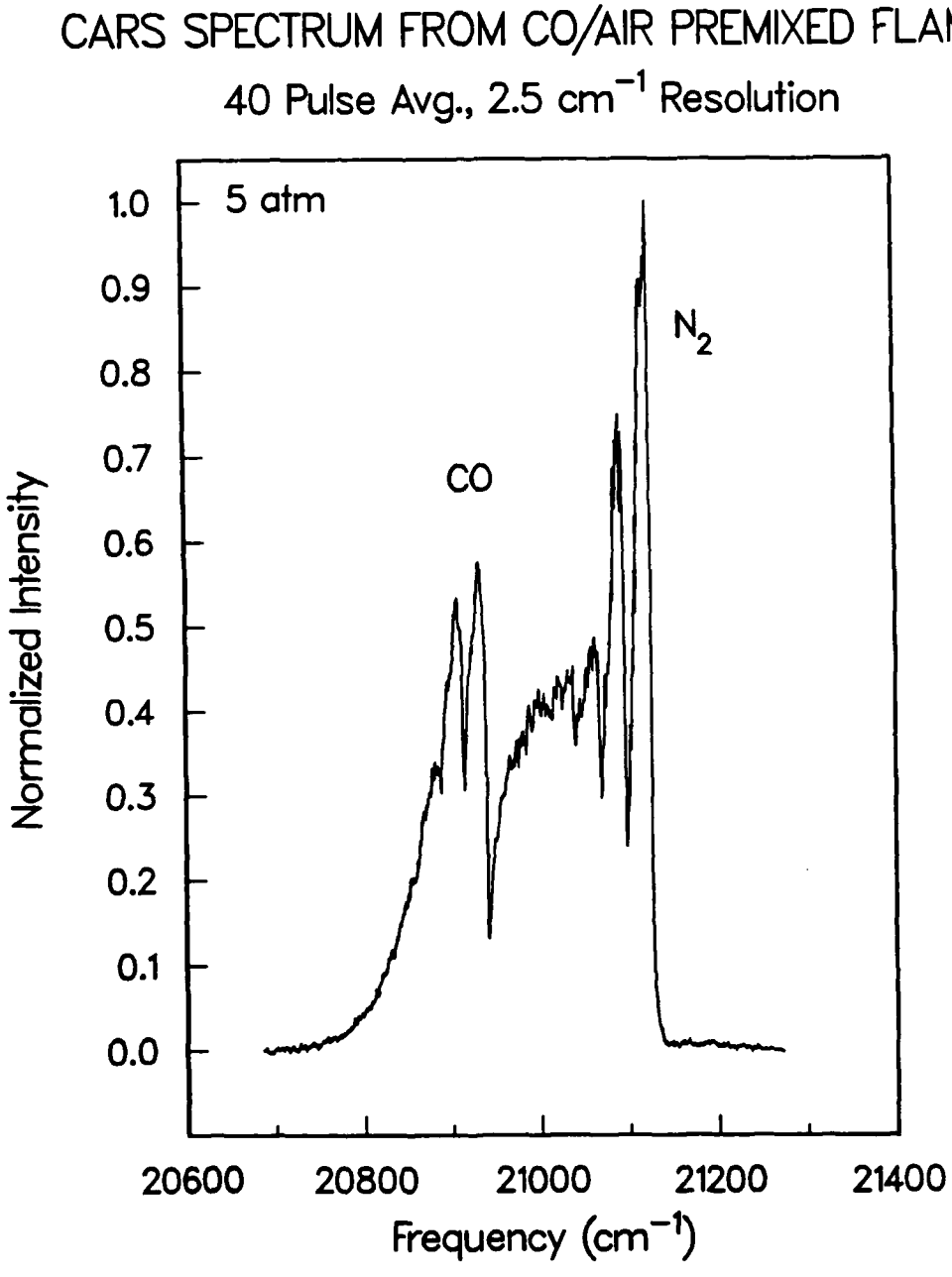
CARS SPECTRUM FROM CO/AIR PREMIXED FLAME
40 Pulse Avg., 2.5 cm^{-1} Resolution
5 atm
CO
N_2
Normalized Intensity
1.0
0.9
0.8
0.7
0.6
0.5
0.4
0.3
0.2
0.1
0.0
20600
20800
21000
21200
21400
Frequency (cm^{-1})

CARS SPECTRUM FROM CO/AIR PREMIXED FLAME

20 Pulse Avg., 2.5 cm^{-1} Resolution

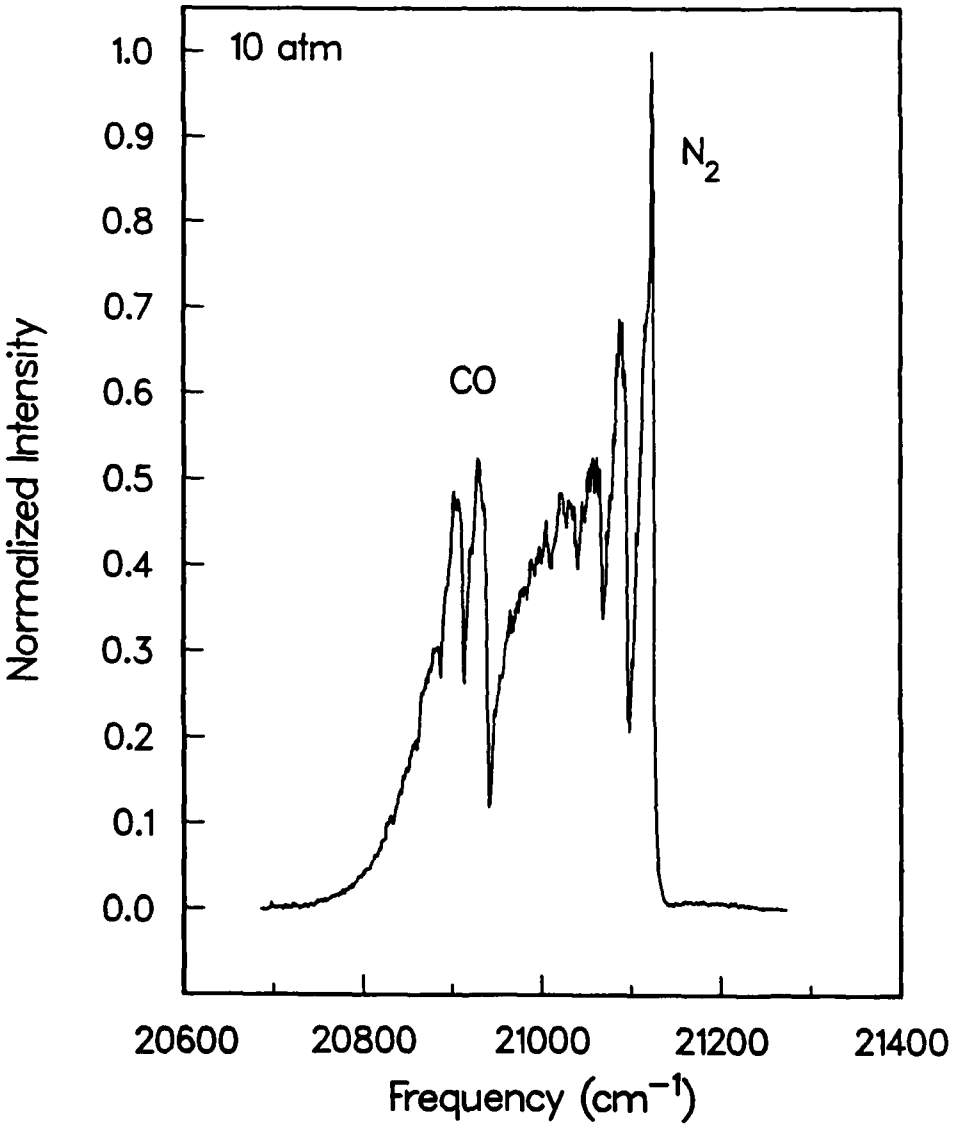

FIG. 28

CARS SPECTRUM FROM CO/AIR PREMIXED FLAME

80 Pulse Avg., 2.5 cm^{-1} Resolution

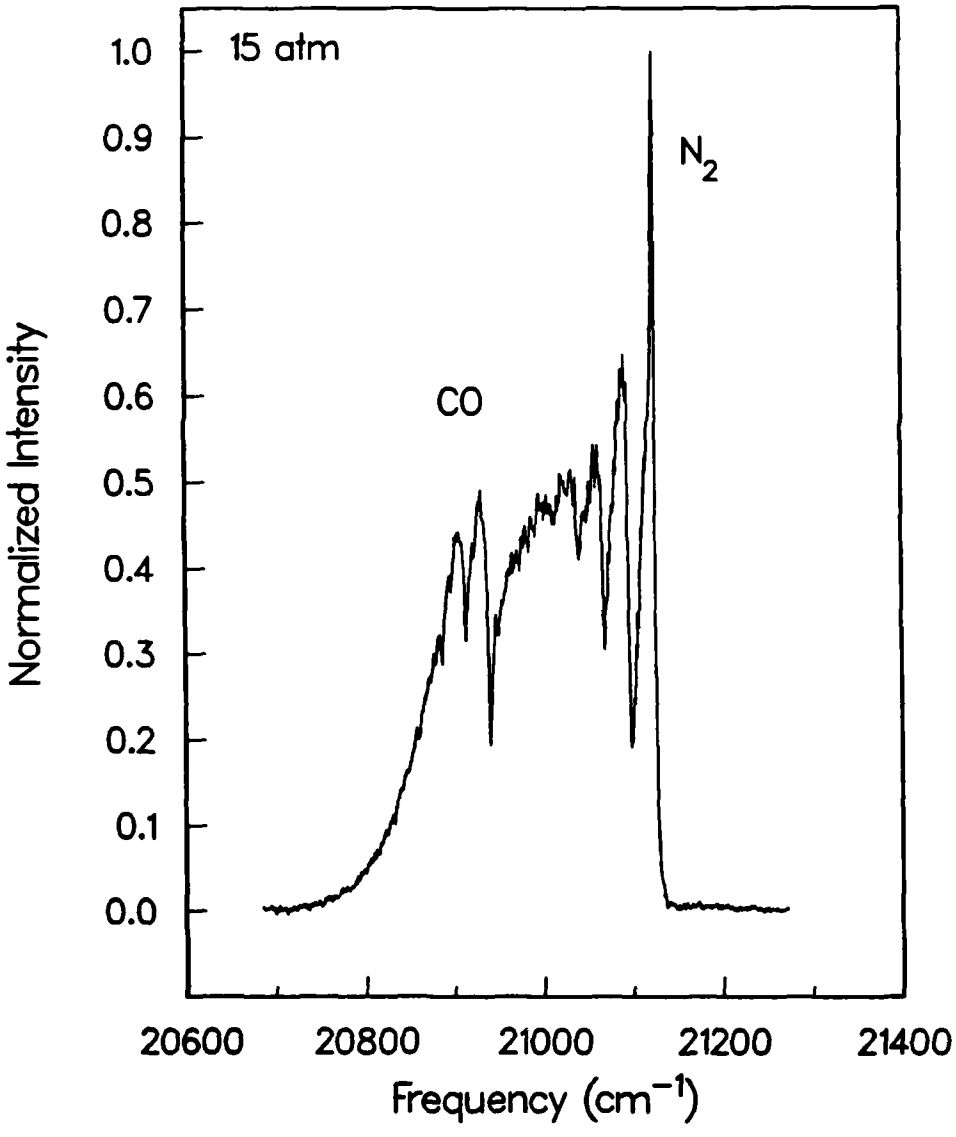

Raman-resonant region and effects of pressure are most noticeable as the narrowing and sharpening of the fundamental bandhead of the CARS signatures. Previous work supported by ARO (Contract DAAG29-79-C-0008) has shown that collisional narrowing is the dominant mechanism operational in this pressure range. The operating pressure limit of the current premixed flame is obviously adequate to produce the collisional narrowing phenomenon in the CARS signatures so that higher operating pressures were not sought.

Results and Discussion

The approach to CARS measurements in the high pressure flame involves analyzing the CARS spectral distribution (i.e. intensity variation with frequency) and is fully described in Hall and Eckbreth (1984). A CARS spectrum such as Fig. 25 is composed of resonant and nonresonant contributions. The resonant parts (i.e. CO and N_2) are functions of the resonant molecule number density, temperature, resonant molecular constants, and pressure, through the rovibrational linewidths of the molecule. The nonresonant contribution is dispersionless, a function of total gas density and implicitly temperature, through the ideal gas law. Assuming the pressure is independently measured and accurate values of molecular constants are available, data such as Fig. 25 contain information on the concentrations of CO, N_2, the total gas density, and the gas temperature. The difficulty in extracting the information lies in separating the various functional dependencies to yield estimates of the experimental parameters. In general, any point of the intensity distribution of Fig. 25 is dependent to some degree on all the above parameters. In mathematical terms the data is represented by the squared modulus of the third order, nonlinear susceptibility (Eqn. 1),

$$|\chi|^2 = \chi'^2 + 2\chi'\chi^{nr} + \chi^{nr2} + \chi''^2 \qquad (11)$$

where χ' and χ'' are the real and imaginary parts of the resonant susceptibility and χ^{nr} is the nonresonant part. Examination of Eqn. (11) can guide data analysis. For instance, it is clear that even when there is no resonant response in the sampled frequency interval i.e. χ', $\chi'' = 0$, there is still a CARS signal represented by χ^{nr} which is proportional to total gas density and, by invoking the ideal gas law, temperature. If a molecule has a resonance in the frequency window but is in low concentration such that $(\chi^{resonant})^2 \ll (\chi^{nr})^2$, a modulation of the nonresonant spectrum is predicted through the $2\chi^{nr}\chi'$ term. For this low density region, the spectral shape is density and temperature dependent and potentially useful for

measurements of these parameters. CARS is a unique spectroscopy in this regard, concentration can be measured from spectral shape in certain density ranges. The technique is limited to relatively low concentration, say less than 30%, and yields only a relative concentration to the total density represented by the nonresonant part. For higher concentration of a resonant species the spectral shape concentration sensitivity is lost and concentration measurements must rely on an absolute measurement. For molecules in very high concentration, the background (nonresonant) signal is lost and the pure resonant response is most evident. This response is very sensitive to frequency and temperature, and of course the integrated resonant response is proportional to concentration of the resonant molecule squared, although the frequency distribution of the resonant part is not as concentration sensitive at this high level. This region of high density is generally utilized for thermometry because the CARS intensity distribution with frequency is largely just a function of temperature if the resonant gas concentration is high.

The foregoing ideas have been incorporated in computer models that predict CARS spectra given the total gas temperature and density and the concentration of the resonant species. By comparing an experimental spectrum against a library of computed predictions, a CARS signature can be 'least squares' fit for temperature and species concentration; the reliability of the estimates depends on the concentration range of the data. Generally temperature is most reliable from the CARS spectrum of a species in high concentration and this is why N_2 thermometry is usually employed. Estimates of the concentration from spectral fits are most reliable for concentrations in the range 1-30%.

UTRC has developed CARS predictive codes and fitting routines based on equations published by Yuratich (1979). The equations account for the convolution of pump laser linewidth and resonant Raman linewidth to produce the observed CARS frequency distribution. In general the solutions are very complex but have been solved for some cases of practical interest. The solution employed here assumes Gaussian laser statistics. Measurements were conducted using the Quanta Ray DCR-1A laser of the UTRC high pressure CARS facility to investigate the mode statistics of the pump laser in a manner similar to the experiments of Rahn et al. (1984). Using the folded BOXCARS phase matching geometry, an optical delay was introduced in one leg of the primary pump. With the laser operating at a linewidth of ~ 0.8 cm^{-1}, the correlation length of the optical pulse is ~ 1.2 cm. The spectrally integrated CARS signal generated in both a nonresonant gas and resonant N_2 in air at 295 K were monitored on a photomultiplier/gated integrator detector. The two signals and their ratio, as a function of the optical delay, are presented in Fig. 29. Following the analysis of Rahn et al. (1983), the data

FIG. 29

PUMP MODE CORRELATION EFFECTS IN UTRC HIGH PRESSURE CARS FACILITY

(LASER: QUANTA-RAY 2 × Nd: YAG DCR-1A)

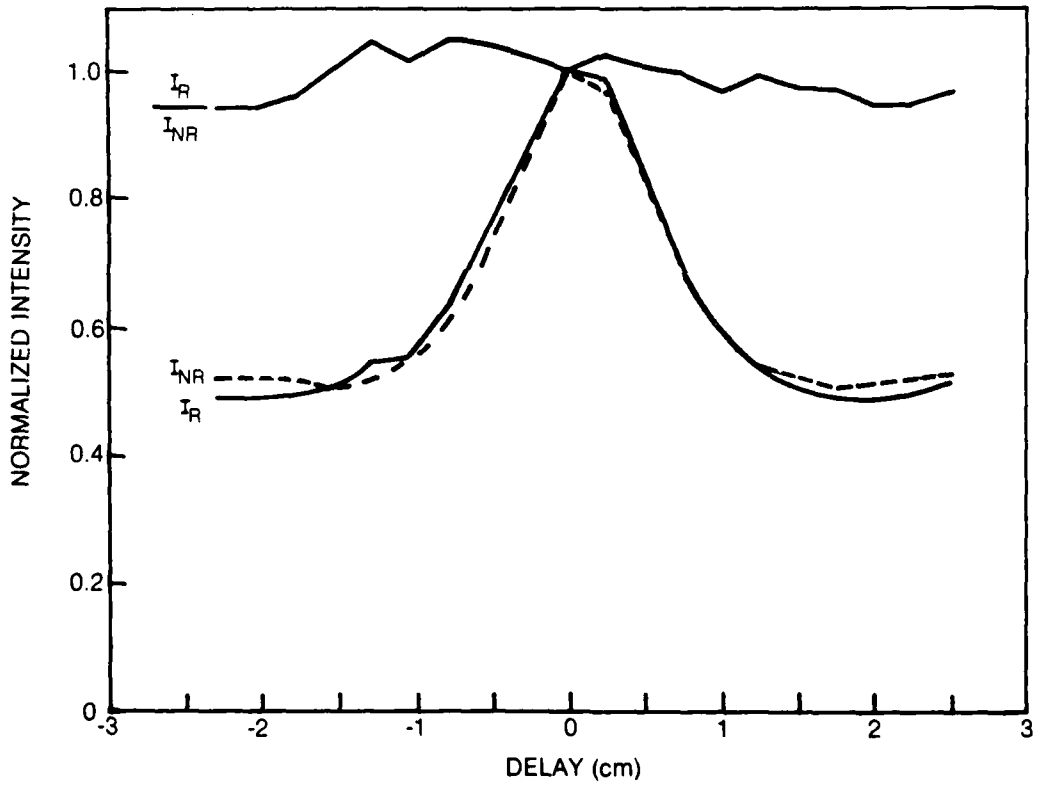

84-10-54-1

describe a laser with Gaussian mode statistics. Of significance for our CARS experiments and in contrast to the Sandia experiments is that the ratio of resonant to nonresonant signals is independent of the pump beam correlation. It is an advantage to operate at full correlation (0 delay) since the signal strengths are highest and the signal to noise ratio is maximized.

Using the UTRC fitting code, which utilizes the Yuratich convolution the data of Fig. 25 were analyzed for temperature and concentration by spectral shapes. A comparison of experimental data (dots) and computer fit (line) is presented in Fig. 30. The match between theory and experiment is excellent for a theoretical temperature of 1922 K and concentration of 38% N_2. The concentration measurement is below that predicted by the Gordon-McBride equilibrium calculation and the Raman scattering measurements and may be a result of the insensitivity to concentration of spectral shape measurements in this concentration region. The predicted temperature is reasonable since the adiabatic flame temperature is 2295 K and we expect radiation losses and conduction losses to the metal burner. Using the same code, the CO portion of Fig. 25 can also be fit for temperature and resonant species concentration and those results are presented in Fig. 31. The fit again appears to be excellent and this time the estimated concentration (17.2%) is closer to the equilibrium calculation of 18.5%. However the predicted temperature is not the same as that predicted for the N_2-resonant segment of the same spectrum and moreover, is very near the adiabatic flame temperature which is physically unrealistic. Resolution of this dilemma resides in the laser convolution used to predict CARS spectra for the fitting routine.

During the period of this contract several researchers (Kataoka, et. al., 1982; Teets, 1984) have questioned the validity of the Yuratich laser convolution calculations. Kataoka and later Teets presented alternate solutions of the convolution equations that they showed to be more accurate for certain experimental conditions. Farrow and Rahn, (1985) also presented data to verify the new, (K-T), convolution. When the pump laser linewidth is very narrow with respect to the Raman transition linewidth of interest, the Yuratich solution is valid. For the case where the pump laser linewidth is larger than the Raman linewidth, additional terms have to be included in the equation. The Quanta Ray laser has a linewidth of ~ 0.3 cm^{-1} at 532 mm when used with the optional intra cavity etalon and a linewidth of ~ 0.8 cm^{-1} when the etalon is not used. Either condition is larger than typical Raman linewidths in atmospheric flames (~ 0.03 cm^{-1}). Greg Dobbs of our group has programmed a CARS predictive code based on the K-T convolution. A comparison of this computer prediction with the data of Fig. 25 is shown in Fig. 32. A rigorous, least squares fit was not possible for this case as the K-T predictive code is undergoing evaluation and has not yet been incorporated in the CARS fitting routine. The results of Teets' work, confirmed by Farrow and Rahn, indicate the major impact of the K-T convolution is for spectra of low

FIG. 30

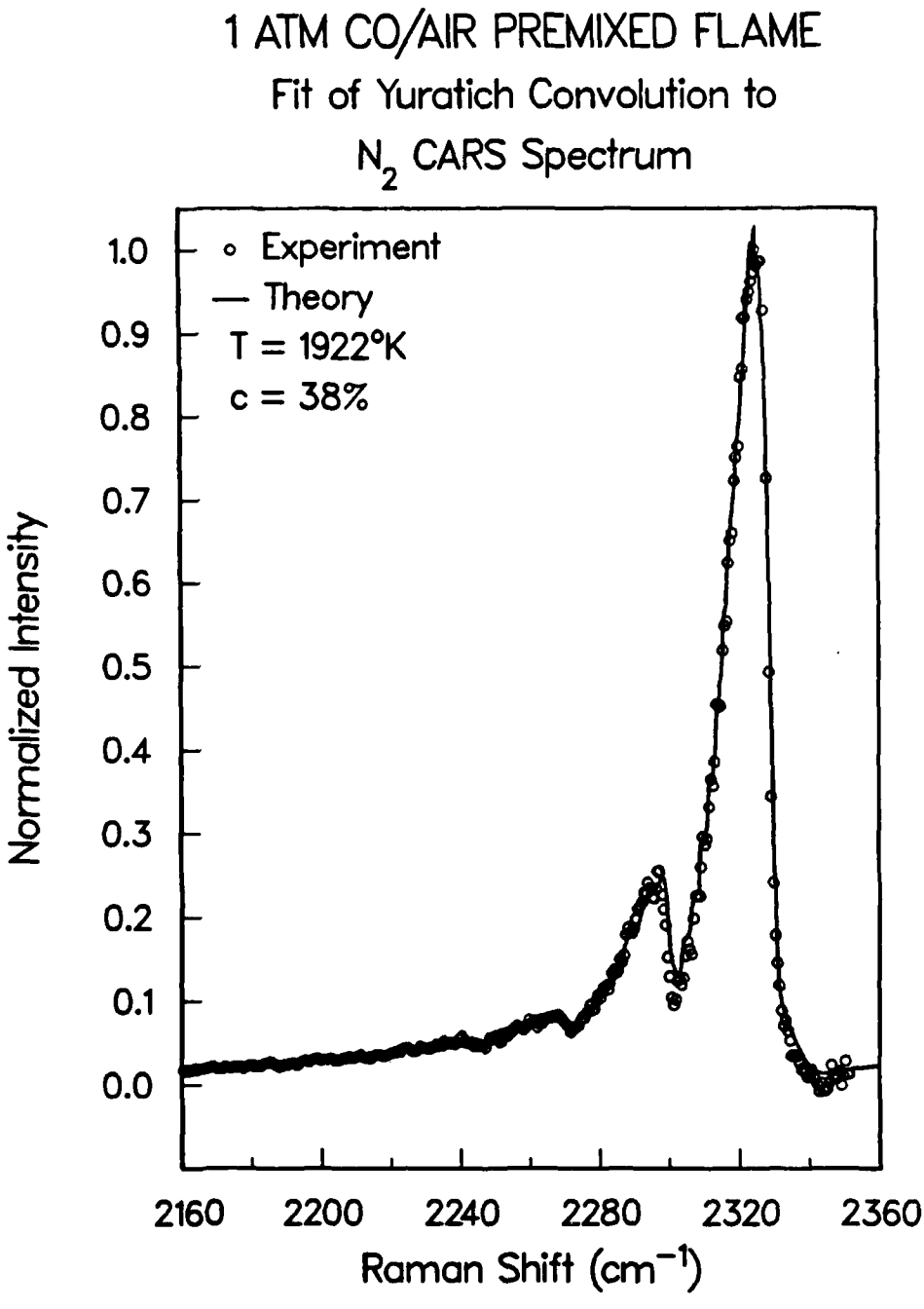
1 ATM CO/AIR PREMIXED FLAME
Fit of Yuratich Convolution to
N2 CARS Spectrum
Experiment
Theory
T = 1922°K
c = 38%
Normalized Intensity
1.0
0.9
0.8
0.7
0.6
0.5
0.4
0.3
0.2
0.1
0.0
2160
2200
2240
2280
2320
2360
Raman Shift (cm-1)

FIG. 31

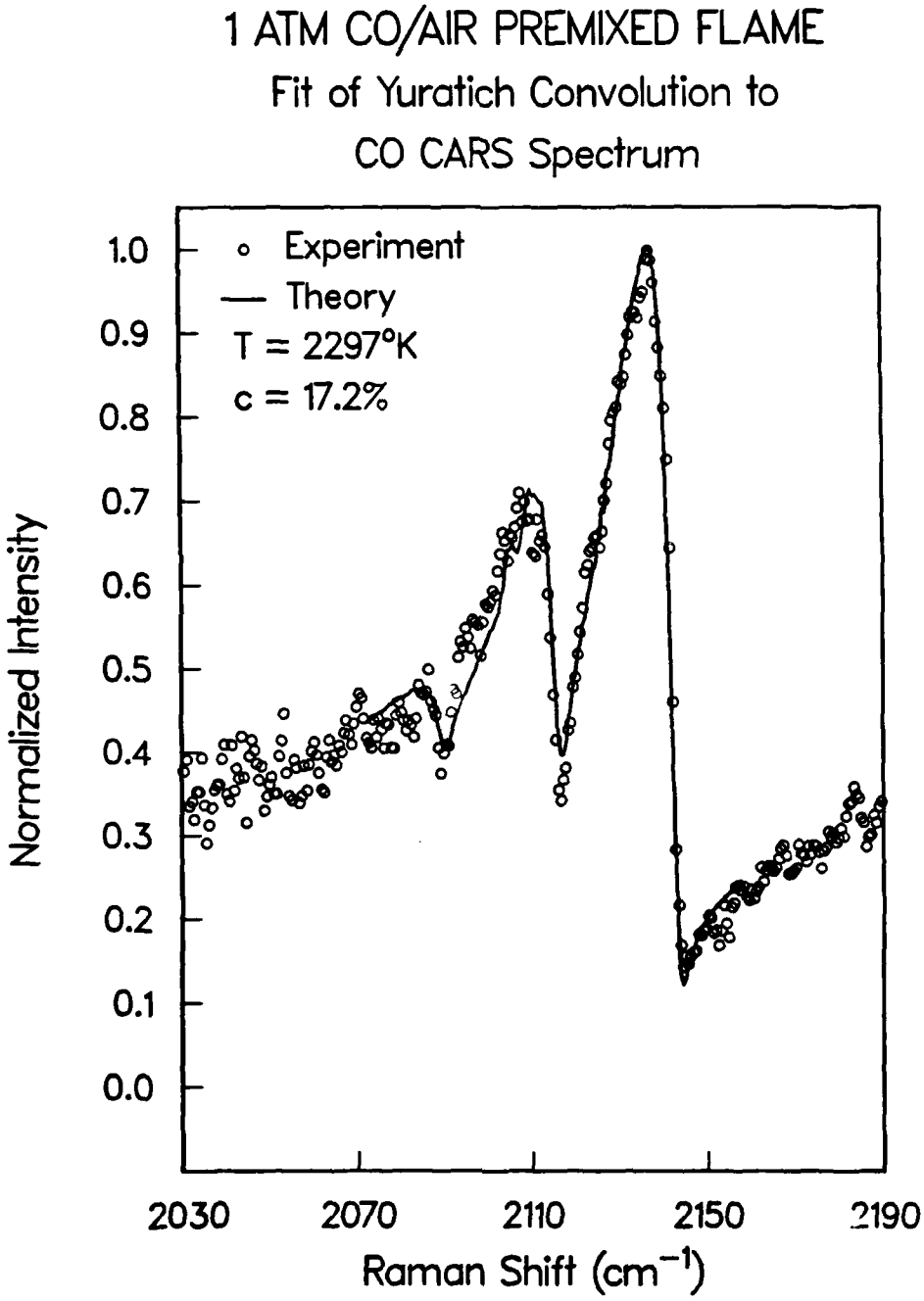
1 ATM CO/AIR PREMIXED FLAME
Fit of Yuratich Convolution to
CO CARS Spectrum
Experiment
Theory
T = 2297°K
c = 17.2%
Normalized Intensity
1.0
0.9
0.8
0.7
0.6
0.5
0.4
0.3
0.2
0.1
0.0
2030
2070
2110
2150
2190
Raman Shift (cm⁻¹)

FIG. 32

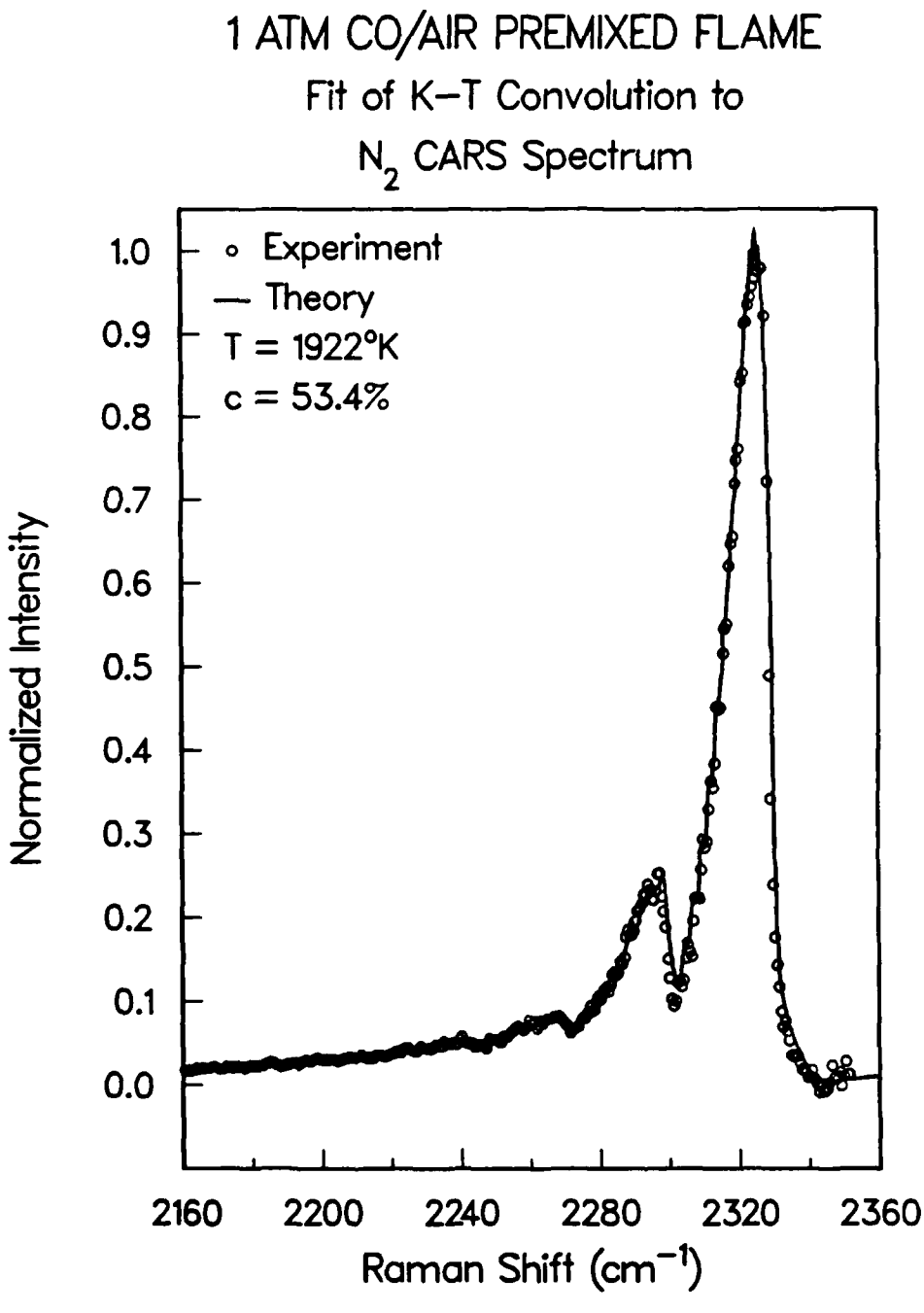
1 ATM CO/AIR PREMIXED FLAME
Fit of K–T Convolution to
N_2 CARS Spectrum
o Experiment
— Theory
T = 1922°K
c = 53.4%
Normalized Intensity
1.0
0.9
0.8
0.7
0.6
0.5
0.4
0.3
0.2
0.1
0.0
2160
2200
2240
2280
2320
2360
Raman Shift (cm^{-1})

concentration gases, and that temperature predictions based on the K-T convolution for majority species will not be very different from that predicted by the Yuratich convolution for the same majority species. Starting from the assumption then, that the predicted N_2 temperature from Fig. 30 is nearly correct, a series of visual fits were prepared for the data that represents the resonant nitrogen part of the experimental spectrum. This analysis showed (Fig. 32) that the concentration predicted by the chemical equilibrium code and as measured by the Raman scattering data fit the experimental data closely. Also, variations in predicted temperatures were evaluated and the 1922 K estimate, based on the Yuratich result was best. The estimated temperature and concentration were 1922 $\pm$ 25 K and 53 $\pm$ 5%, based on this visual fitting. Figure 33 presents a similar visual fit of the resonant CO portion of the same experimental data (Fig. 25). The starting assumption for this visual fit was that the CO temperature should be the same as the N_2 temperature. This assumption was borne out in the fitting procedure, with the additional result that the predicted concentration is in agreement with the Gordon-McBride and Raman scattering data.

It is satisfying to achieve the foregoing consistent set of data and computer predictions. It appears clear from this work that the K-T convolution needs to be incorporated in the CARS spectral fitting routines. A theoretical aspect still needs to be addressed however; the K-T convolution has not been rigorously proven applicable to an experimental situation with correlated pump lasers. In the work at Sandia (Farrow and Rahn, 1985), where the lasers apparently exhibited non-Gaussian statistics, decorrelation of the pump beams was necessary to obtain spectral agreement with the K-T theory. With the apparent Gaussian statistics here, good agreement was obtained with correlated pump beams. Further investigation is necessary in this area.

Measurements from the CARS spectra at high pressure are more cumbersome than the 1 atmosphere case. The primary reason for this is that the UTRC high pressure CARS code is predictive at this time and not incorporated into a computer fitting routine. Thus visual overlays are required to obtain estimates of temperature and concentration. Based on the previous results of the 1 atmosphere case, the K-T convolution will be required at high pressure. Although the ratio of laser linewidth to Raman linewidth is smaller at high pressure, the ratio should still be in the region where K-T is required i.e. $\Delta\omega/\Gamma > 1$. The K-T convolution has not yet been implemented for the high pressure case at UTRC so concentration measurements from spectral shapes of high pressure CARS spectra such as Figs. 26-28 could not be performed. The resonant nitrogen portion of the spectrum should still yield reliable temperature measurements through analysis with the Yuratich laser convolution, however. It was shown in previous work at UTRC, (Stufflebeam, et al., 1983; 1984) that high pressure CARS spectra are most accurately predicted by a full

FIG. 33

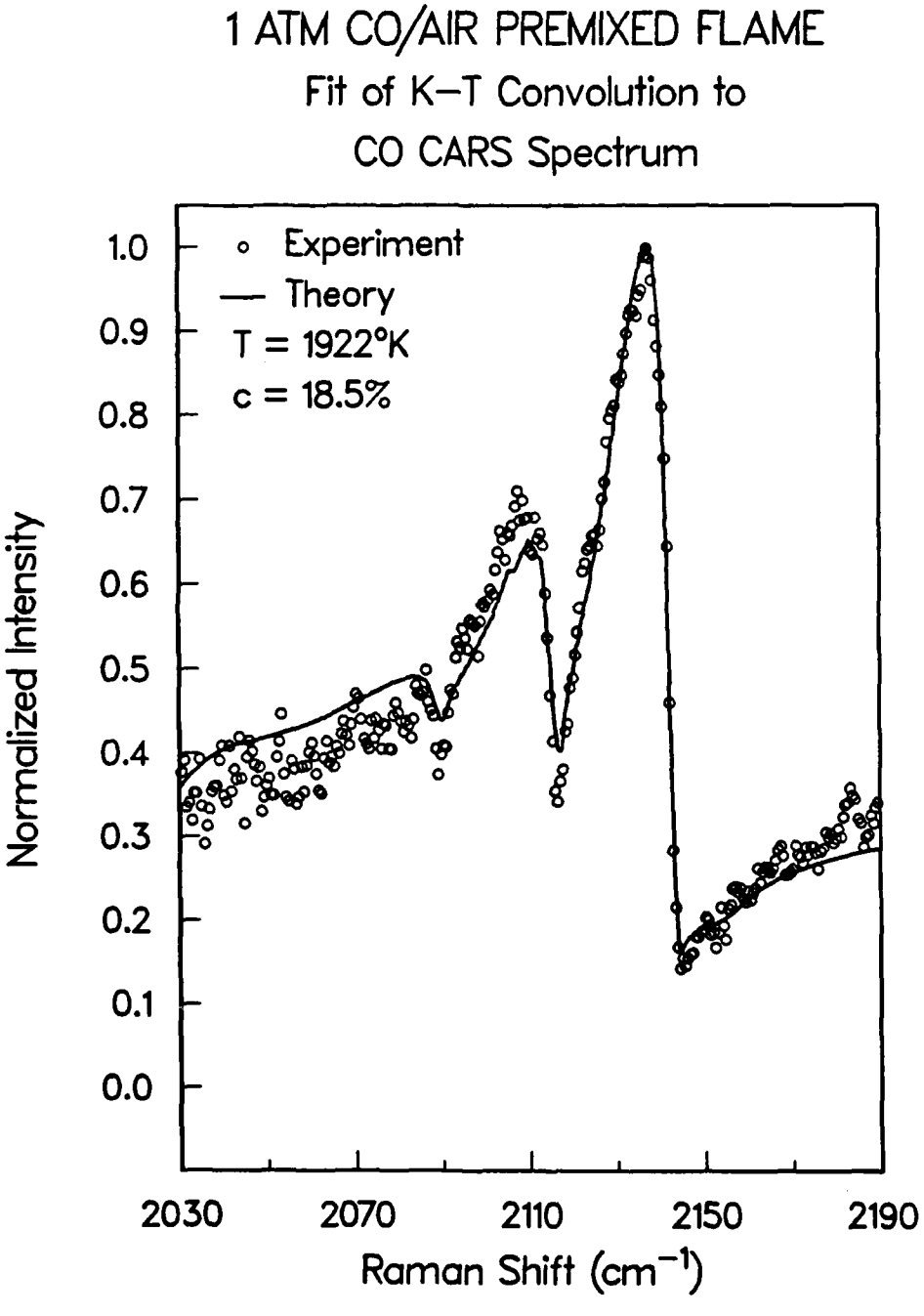
1 ATM CO/AIR PREMIXED FLAME
Fit of K–T Convolution to
CO CARS Spectrum
Experiment
Theory
T = 1922°K
c = 18.5%
Normalized Intensity
1.0
0.9
0.8
0.7
0.6
0.5
0.4
0.3
0.2
0.1
0.0
2030
2070
2110
2150
2190
Raman Shift (cm⁻¹)

matrix inversion model of the resonant signature. Simpler, faster models such as isolated lines, perturbation expansion or the Gordon model of rotational relaxation were inadequate for the pressures encountered in these experiments. The need to revert to matrix inversion slows the analysis immensely. Twenty-four hours of CPU time on a VAX 750 are required to produce one CARS spectrum from the high pressure predictive code using matrix inversion with the inverse power law model used to predict the off diagonal matrix elements. The algorithm of Gordon and McGinnis, (1968), not yet incorporated in the UTRC codes, should help this situation. The Gordon model is applicable to high pressure and much faster ($\sim$ 3 min. of CPU time) although less accurate. It was used to narrow the temperature range of analysis and then a full matrix spectrum was generated for confirmation with the experimental data. The result for the 10 atmosphere case (Fig. 27) is shown in Fig. 34. The temperature predicted by the visual fitting is 2150 K and seems physically resonable based on the adiabatic flame temperature of 2352 K. The 'best fit' concentration was 80% which seems clearly in error and reinforces the need for K-T convolutions at high pressures. Based on the extensive computer time required for these fits and the suspicious concentration estimates and overpredictions of temperature derived from Yuratich convolutions of low concentration spectra, an attempt was not made to analyze the CO portion of the experimental data at 10 atmospheres (Fig. 27).

Additional techniques can be used to measure resonant species concentration from CARS data. These are appropriate when the density is high enough to invalidate spectral shape fitting. The techniques involve absolute intensity measurements and must be calibrated to a known set of conditions of density and temperature. They require monitoring the resonant species signal intensity, integrated over all transition frequencies of the molecule, and have to be normalized to the pump laser intensities $I_1^2 I_2$.

As mentioned previously the CARS spectrum generally contains contributions from a resonant species and the dispersionless, nonresonant background. When the resonant species signal strength is much greater than the nonresonant contribution, an absolute intensity measurement merely requires splitting off a portion of the total CARS signal to a photomultiplier and calibrating the signal to a known standard gas, in effect the nonresonant signal is swamped by the resonant signal and neglected. Pump laser normalization could be achieved by directly measuring the intensities on a photodiode but this ignores space and time effects of the intensity in the experimental volume and can be dangerous for all but the most benign combustion environments. It is preferable to generate a nonresonant signal in an exterior cell of known gas concentration and temperature. The resultant calibration signal from the nonresonant cell would also be proportional to $I_1^2 I_2$ and could be used for normalization.

FIG. 34

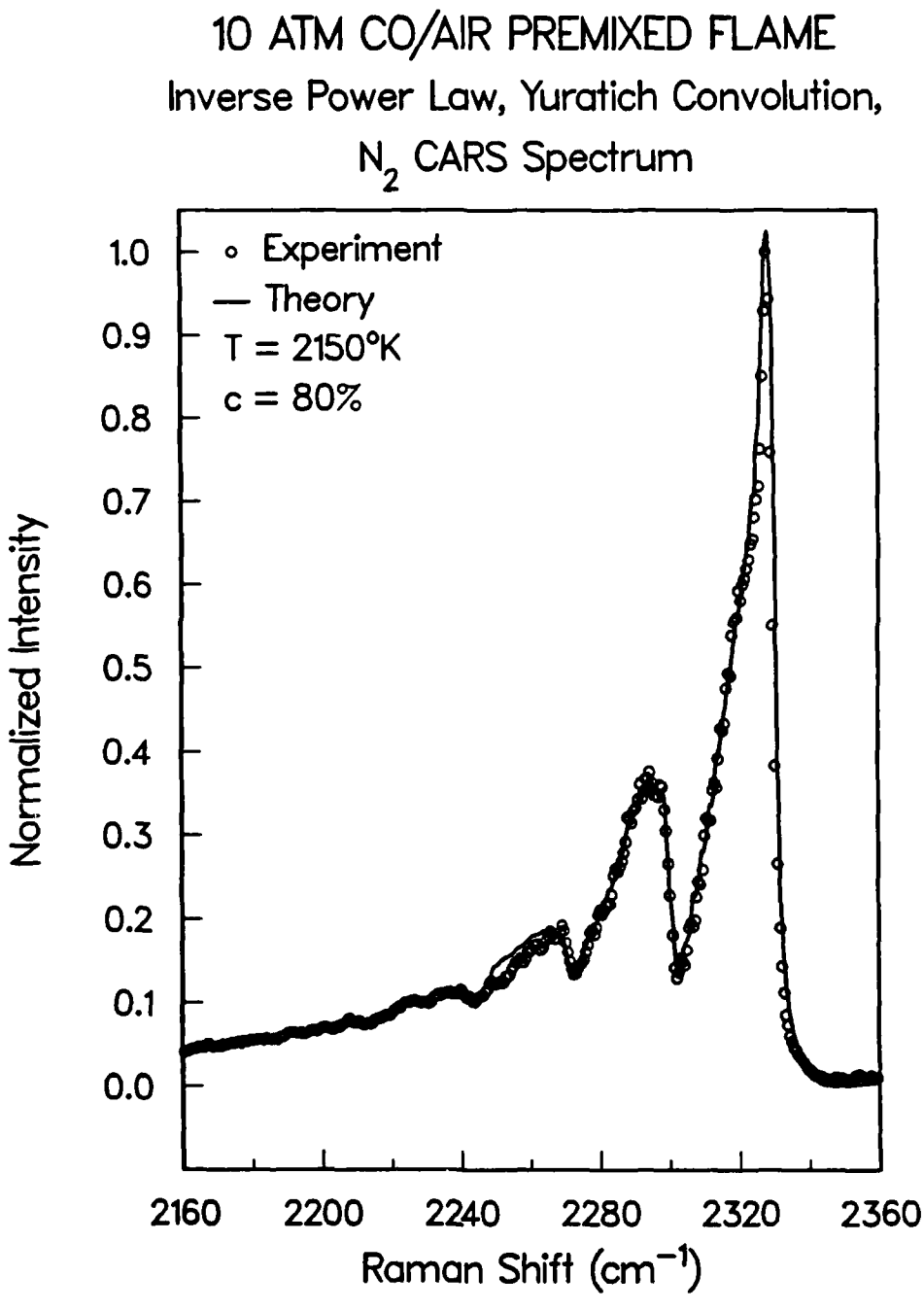
10 ATM CO/AIR PREMIXED FLAME
Inverse Power Law, Yuratich Convolution,
N_2 CARS Spectrum
Experiment
Theory
T = 2150°K
c = 80%
Normalized Intensity
1.0
0.9
0.8
0.7
0.6
0.5
0.4
0.3
0.2
0.1
0.0
2160
2200
2240
2280
2320
2360
Raman Shift (cm^{-1})

The more general approach, and one necessary for the high pressure CO/air premixed flame, addresses the case when the nonresonant contribution to the CARS spectrum cannot be neglected. In this instance the resonant and nonresonant photons need to be separated and individually measured. The technique is called polarization suppression and is fully described in Hall and Eckbreth (1984). The resonant and nonresonant signals have different responses to polarization directions of the laser fields. By adjusting the polarization angles of the pump beams, the resonant and nonresonant signals, which are generated at different polarization angles, can be separated. The purely resonant signal is then monitored, normalized and calibrated to complete the quantitative measurement. The normalization and calibration can be handled in a 'series' or 'parallel' nonresonant cell as described previously but the method is sensitive to alignment errors introduced by refractive index differences between the 'experimental' (flame) path and the path through the calibration cell, normally held at NTP. A more attractive normalization is provided by the 'suppressed' nonresonant signal itself (Farrow, et al., 1982; 1985). By monitoring the purely nonresonant contribution $I_1^2 I_2$ normalization is achieved and an 'in-situ' calibration is provided because the nonresonant signal is proportional to total gas density at exactly the same location as the resonant signal. Scaling of the dispersionless, nonresonant signal to conditions of known density and temperature are accomplished by filling the reaction vessel with a known gas at a known temperature. Being suitably calibrated, the nonresonant signal is then the calibration standard for the resonant signal. Providing that the nonresonant susceptibility for the experimental gas can be calculated (usually a valid assumption), and that the temperature is measured from the resonant species signature, the total gas density of the nonresonant signal provides the calibration for the resonant response.

The polarization suppression techniques are not widely used with broadband approaches because they invoke at least a factor of 16 loss of the resonant signal (Hall and Eckbreth, 1984). However, for high pressure regimes this reduction may be tolerable. The polarization suppression technique was partially implemented in the high pressure premixed flame. Initial experiments were conducted to demonstrate its applicability to the high pressure regime. For this experiment half-wave plates rotated the plane of polarization of each ω_1 pump beam to 60^o relative to the 'P' (0^o) polarization of the ω_2 Stokes laser. This combination of angles maximizes the separation of the resonant and nonresonant parts of the spectrum. A portion of the pure resonant contribution is viewed through an analyzer rotated to 120^o (perpendicular to the nonresonant signal). The result for the 10 atmosphere flame is shown in Fig. 35. The data of Fig. 35 exhibited no pressure or temperature induced depolarization (Farrow, R. L., et al., 1984; Ikawa and

FIG. 35

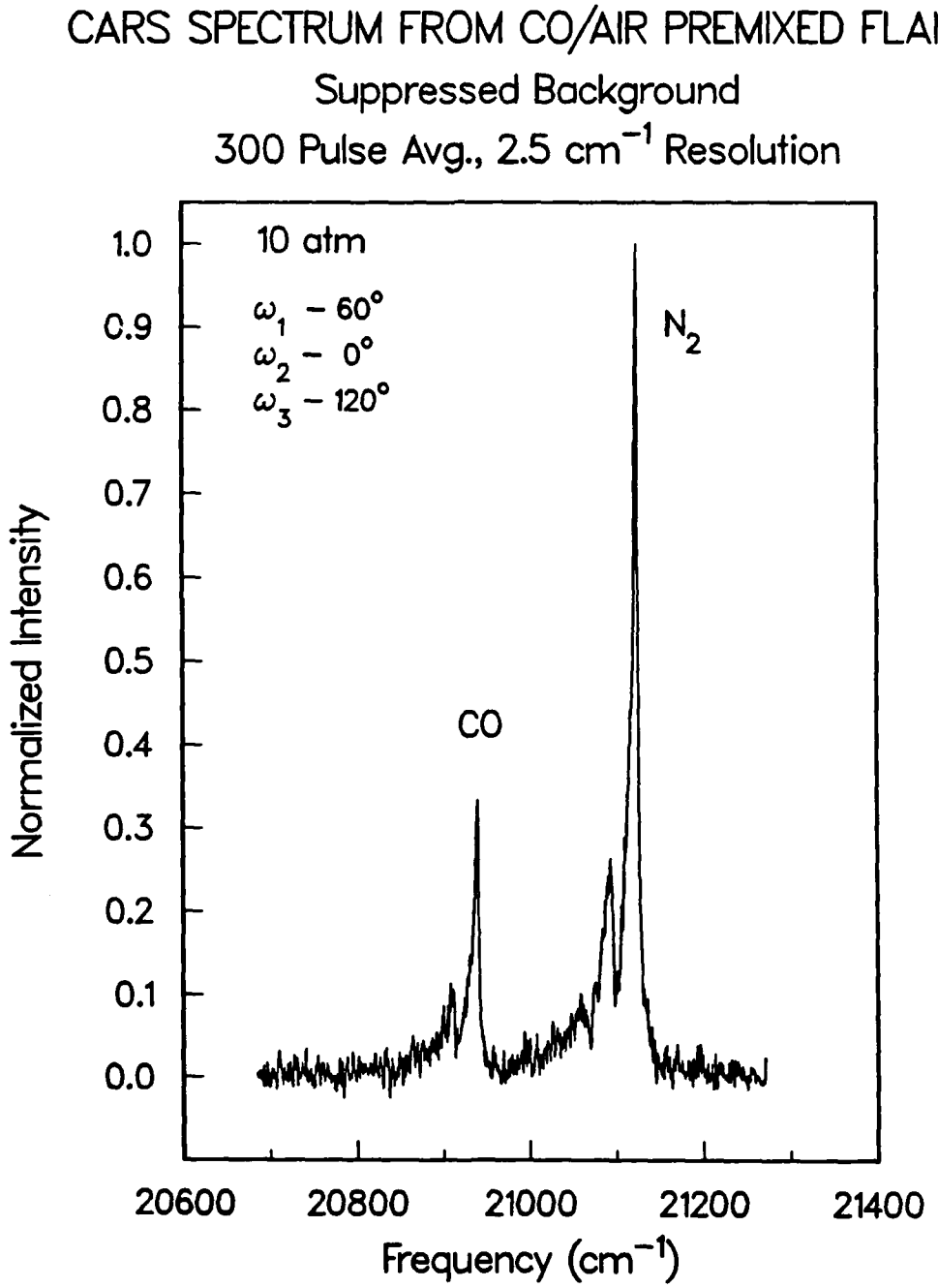
CARS SPECTRUM FROM CO/AIR PREMIXED FLAME
Suppressed Background
300 Pulse Avg., 2.5 cm^{-1} Resolution
10 atm
ω_1 - 60°
ω_2 - 0°
ω_3 - 120°
N$_2$
CO
Normalized Intensity
1.0
0.9
0.8
0.7
0.6
0.5
0.4
0.3
0.2
0.1
0.0
20600
20800
21000
21200
21400
Frequency (cm^{-1})

Whalley, 1984) from the quartz windows of the combustion vessel. The spectrum in Fig. 35 demonstrates very good background suppression, as indicated by the lack of modulation at the bandheads of the two resonant species and the zero-signal baseline (compare with Fig. 27).

By rotating the analyzer to 150° (perpendicular to the resonant contribution) a portion of the nonresonant signal is obtained to provide an 'in situ' normalization for laser power fluctuations and a calibration for concentration measurements of the resonant species. Further work will incorporate separate photomultiplier/gated integrator detector channels for the purely resonant and nonresonant signals and calibration experiments using a gas at known concentration and temperature. Suitable analyses of these signals will produce data for the gas temperature and the total gas and resonant species concentration.

Recommendations

These research investigations at UTRC are continuing and future directions include completion of the partially implemented N_2 concentration measurements and implementation of the polarization suppression technique for concentration measurements of CO_2 as well. The spectroscopy of CO_2 has been studied under previous Army funding (Contract DAAG29-79-C-0008) and the results of the CO_2 investigations appeared in Hall and Stufflebeam, (1984). Although CO_2 is expected to be in low concentration in the high pressure flame the very small spacing of rotational transitions in the CO_2 CARS spectrum results in significant line overlap in each vibrational band, even at 1 atmosphere. The strong overlap is evidenced by a collisionally narrowed spectrum with little or no destructive interference with the nonresonant background (Hall and Eckbreth, 1984). This condition is not amenable to concentration measurements from spectral shapes and so the more complex technique of polarization suppression is warranted.

These initial results are quite encouraging vis-a-vis the ability of CARS to make quantitative measurements in high pressure combustion environments. The directions are clear. The K-T laser convolution needs to be incorporated in the predictive computer codes to improve the accuracy of temperature and concentration predictions. Additional rotational relaxation models (i.e. exponential gap) need to be incorporated for comparative predictions of collisional narrowing and inclusion of the Gordon-McGinnis algorithm should greatly speed-up computer response. These enhancements of the diagnostic ability of CARS should contribute to programs of relevance to the Army.

DUAL BROADBAND CARS

During this contract period, a novel approach to multiple species measurements using vibrational CARS in which only one additional laser beam needs to be introduced was developed at UTRC (Eckbreth and Anderson, 1985, Appendix C of this report). One of the limitations of CARS, as normally implemented, is the inability to interrogate more than one constituent at a time. Except for a few fortuitous instances of closely spaced Raman resonances (i.e. N_2 and CO as evidenced in the previous section of this report), a separate Stokes dye laser is required for each constituent to be measured. Using two separate Stokes lasers, N_2 and O_2 have been simultaneously measured (Jarrett, et al. 1985). In reality, to employ more than two Stokes sources, becomes quite cumbersome and complex.

The dual broadband technique employs two independent broadband Stokes sources in combination with a pump laser in the following manner. Besides the two separate two-color wave-mixing processes between the pump and Stokes lasers, spectrally-resolved CARS is produced in a three-color process from species whose Raman resonances correspond to the frequency differences of the two broadband sources. Particularly serendipitous in hydrocarbon-fueled combustion is the fact that when the Stokes sources are positioned to coincide with CO_2 and H_2O, the major products of combustion, the frequency difference between the two coincides with the Raman resonances of heavy diatomics such as N_2, CO, NO which can then be observed via the three-color process. Yuratich (1979) pointed out that one could perform CARS with high spectral resolution using two broadband sources if the third laser source was narrowband. Since these Raman frequencies are well-defined, spectral smearing does not occur even with broadband excitation. The narrowband laser then scatters off the coherent Raman excitation in the medium resulting in CARS at a spectral resolution characteristic of the narrowband source.

One broadband source covers the 1200-1600 cm^{-1} Stokes spectral region as illustrated in Fig. 36. This source, wavemixing with a frequency-doubled neodymium:YAG laser beam at 532 nm, produces CARS in the normal way from CO_2, O_2 and potentially C-^ bond stretches should such constituents be present. A second broadband dye laser covers the 3000-3700 cm^{-1} region and produces CARS in the normal way from H_2O and C-H stretch Raman modes. The dye to use is DCM which lases over a very wide spectral region around 640 nm. The two broadband dye lasers in turn excite all Raman resonances with shifts in the range from about 1400 cm^{-1} to 2500 cm^{-1} and produce CARS, after wavemixing with 532 nm, from such constituents as N_2, N_2O, CO, HCN, NO and C≡C stretches. Despite the use of two broadband sources in the three color wavemixing, spectral resolution is determined by the pump laser linewidth

FIG. 36

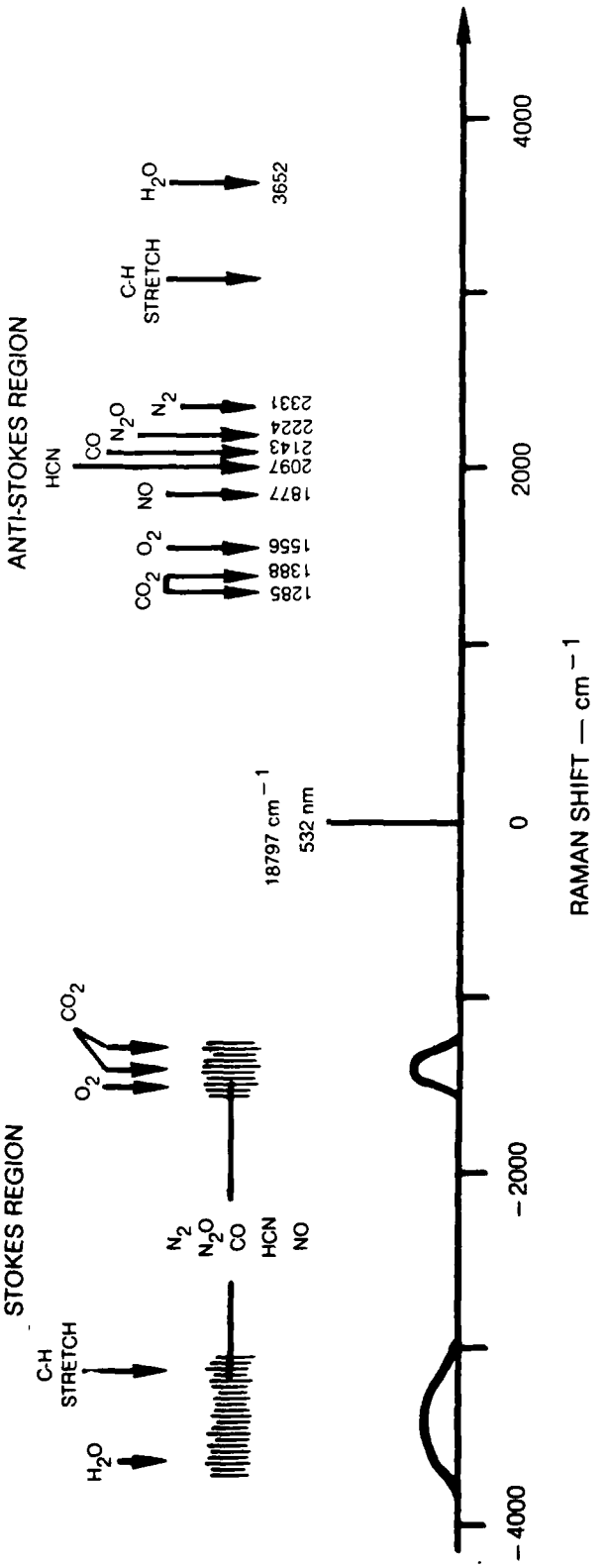
DUAL BROADBAND, MULITPLE SPECIES CARS MEASUREMENT APPROACH
STOKES REGION
ANTI-STOKES REGION
C-H STRETCH
H_2O
N_2
N_2O
CO
HCN
NO
O_2
CO_2
18797 cm^{-1}
532 nm
1285
1388
1556
1877
2097
2143
2224
2331
3652
−4000
−2000
0
2000
4000
RAMAN SHIFT — cm^{-1}
85-11-92-18

and/or spectrometer resolution just as in two color wavemixing. Phase matching is easily achieved via a variety of approaches, e.g. collinear, closely-packed three beam, combined planar BOXCARS or combined planar-folded BOXCARS schemes.

Due to the spectral energy partitioning inherent in the use of two broadband sources, the dual broadband signals are somewhat weaker than would normally pertain in two-color wave mixing. For dynamic measurements, dual broadband CARS might be restricted to elevated pressure combustion applications, e.g. gas turbines, diesels, propellant burning. At elevated pressure, the signal decrease accompanying dual broadband CARS would be compensated by the nominal quadratic scaling of the CARS signal with density. This new technique is currently being implemented in the UTRC High Pressure CARS Facility and will allow simultaneous measurements of all major flame products, N_2, CO and CO_2.

REFERENCES

Aron, K. and Harris, L. E. (1984). CARS Probe of RDX Decomposition. Chemical Physics Letters, Vol. 103, pp. 413-417.

Benedict, W. S. and Kaplan (1959). Calculation of Line Widths in H_2O-N_2 Collisions. Journal of Chemical Physics, Vol. 30, pp. 388-399.

Benedict, W. S. and Kaplan (1964). Calculation of Line Widths in H_2O-H_2O and H_2O-O_2 Collisions. Journal of Quantitative Spectroscopy and Radiative Transfer, Vol. 4, pp. 453-469.

Bribes, J. L., Gaufres, R., Monan, M., Lapp, M. and Penney, C. M. (1976). Detailed Study of the Q-Branch Profile of the ν_1 of Water Molecule from 293 K to 1600 K. in Schmid, E. D. et al., (Eds.), Proceedings of the 5th International Conference on Raman Spectroscopy, Universitat Freiburg, Sept. 2-8, 1976, Hans Ferdinand Schulz Verlag, Freiburg in Breisgau, 1976.

Dexheimer, S. L., Durand, M., Brunner, T. A. and Pritchard, D. E. (1982). Dynamical Constraints on the Transfer of Angular Momentum in Rotationally Inelastic Collisions of $I_2(B^3\pi)$ with He and Xe. Journal of Chemical Physics, Vol. 76, pp. 4996-5004.

Dobbs, G. M., Boedecker, L. R. and Eckbreth, A. C. (1985). Interference to CARS in Highly-Sooting Flames from C_2 Absorption. Proceedings of the 1985 Fall Technical Meeting of the Eastern Section of the Combustion Institute, November 4-6, 1985, Philadelphia. pp. 78-1 to 78-4.

Eckbreth, A. C. and Anderson, T. J. (1985). Dual Broadband CARS for Simultaneous, Multiple Species Measurements. Applied Optics, Vol. 24, pp. 2731-2736.

Eckbreth, A. C., Anderson, T. J. and Dobbs, G. M. (1986). Conditional Sampling for Fuel and Soot in CARS Thermometry. submitted to 21st Symposium (International) on Combustion, Munich, West Germany, August 3-8, 1986.

Eckbreth, A. C., Bonczyk, P. A. and Verdieck, J. F. (1979). Combustion Diagnostics by Laser Raman and Fluorescence Techniques. Progress in Energy and Combustion Science, Vol. 5, pp. 253-322.

Eckbreth, A. C., Dobbs, G. M., Stufflebeam, J. H. and Tellex, P. A. (1984). CARS Temperature and Species Measurements in Augmented Jet Engine Exhausts. Applied Optics, Vol. 23, pp. 1328-1339.

Eckbreth, A. C. and Hall, R. J. (1981). CARS Concentration Sensitivity With and Without Nonresonant Background Suppression. Combustion Science and Technology, Vol. 25, pp. 175-192.

Farrow, R. L., Lucht, R. P., Clark, G. L. and Palmer, R. E. (1985). Species Concentration Measurements using CARS with Nonresonant Susceptibility Normalization. Applied Optics, Vol. 24, pp. 2241-2251.

Farrow, R. L., Lucht, R. P., Flower, W. L. and Palmer, R. E. (1984). Coherent anti-Stokes Raman Spectroscopic Measurements of Temperature and Acetylene Spectra in a Sooting Diffusion Flame. Proceedings of the 20th Symposium (International) on Combustion, The Combustion Institute, Pittsburgh, PA, pp. 1307-1312.

Farrow, R. L., Mattern, P. L. and Rahn, L. A. (1982). Comparison Between CARS and Corrected Thermocouple Temperature Measurements in a Diffusion Flame. Applied Optics, Vol. 21, pp. 3119-3125.

Farrow, R. L. and Rahn, L. A. (1985). Interpreting Coherent anti-Stokes Raman Spectra Measured with Multimode Nd:YAG Pump Lasers. Journal of the Optical Society of America B, Vol.2, pp. 903-907.

Fraser, J. M. and Daniels, F. (1958). The Heterogeneous Decomposition of Nitric Oxide with Oxide Catalysts. Journal of Physical Chemistry, Vol. 62, pp. 215-220.

Gordon, R. G. (1966a). On the Rotational Diffusion of Molecules. Journal of Chemical Physics, Vol. 44, pp. 1830-1836.

Gordon, R. G. (1966b). Semiclassical Theory of Spectra and Relaxation in Molecular Gases. Journal of Chemical Physics, Vol. 45, pp. 1649-1655.

Gordon, R. G. and McGinnis, R. P. (1968). Line Shapes in Molecular Spectra. Journal of Chemical Physics, Vol. 49, pp. 2455-2456.

Gordon, S. and McBride, B. J. (1976). Computer Program for Calculation of Complex Chemical Equilibrium Compositions, Rocket Performance, Incident and Reflected Shocks, and Chapman-Jouquet Detonations. NASA report SP-273.

Greenhalgh, D. A., Hall, R. J., Porter, F. M. and England, W. A. (1984). Applications of the Rotational Diffusion Model to the CARS Spectra of High-Temperature, High-Pressure Water Vapour. Journal of Raman Spectroscopy, Vol. 15, pp. 71-79.

Hall, R. J. (1983). Coherent anti-Stokes Raman Spectroscopic Modeling for Combustion Diagnostics. Optical Engineering Vol 22, pp. 322-329.

Hall, R. J. and Eckbreth, A. C. (1984). Coherent anti-Stokes Raman Spectroscopy (CARS): Application to Combustion Diagnostics, in Ready, J. F. and Erf, R. K. (Eds), Laser Applications, Vol. 5, Academic Press, New York, pp. 213-309.

Hall, R. J. and Greenhalgh, D. G. (1982). Application of the Rotational Diffusion Model to Gaseous N_2 CARS Spectra. Optics Communications, Vol. 40, pp. 417- 420.

Hall, R. J. and Shirley J. A. (1983). Coherent anti-Stokes Raman Spectroscopy of Water Vapor for Combustion Diagnostics. Applied Spectroscopy, Vol. 37, pp. 196-202.

Hall, R. J., Shirley, J. A. and Eckbreth, A. C. (1979). Coherent anti-Stokes Raman Spectroscopy: Spectra of Water Vapor in Flames. Optics Letters, Vol. 4, pp. 87-89.

Hall, R. J. and Stufflebeam, J. H. (1984). Quantitative CARS Spectroscopy of CO_2 and N_2O. Applied Optics, Vol. 23, pp. 4319-4327.

Hall, R. J., Verdieck, J. F. and Eckbreth, A. C. (1980). Pressure-Induced Narrowing of the CARS Spectrum of N_2. Optics Communications, Vol. 35, pp. 69-75.

Hedman, P. O., Eckbreth, A. C. and Stufflebeam, J. H. (1986). Development of Diffusion and Premixed Burners for CARS Measurements in High Pressure Flames. To be submitted for publication.

Ikawa, S. and Whalley, E. (1984). Polarization Scrambling by the Glass Windows of a Raman Cell up to 18 Kbar. Review of Scientific Instruments, Vol. 55, pp. 1273-1279.

Jarrett, O. Jr., Antcliff, R. R. and Rogers, R. C. (1985). CARS System for Simultaneous Measurement of Temperature, Nitrogen and Oxygen Densities in a Turbulent Flame. Presented at the 22nd JANNAF Combustion Meeting, Pasadena, CA.

Kataoka, H., Maeda, S. and Hirose, C. (1982). Effects of Linewidths on the Coherent anti-Stokes Raman Spectroscopy Spectral Profile. Applied Spectroscopy, Vol. 36, pp. 565-569.

Koszykowski, M. L., Farrow, R. L. and Palmer, R. E. (1985). Calculation of Collisionally Narrowed Coherent anti-Stokes Raman Spectroscopy Spectra. Optics Letters, Vol. 10, pp. 478-480.

Laane, J. and Kiefer, W. (1980). Interference Effects in the High Resolution CARS Spectra of Gases. Journal of Raman Spectroscopy, Vol. 9, pp. 353-360.

Lempert, W., Rosasco, G. J. and Hurst, W. S. (1984). Rotational Collisional Narrowing in the NO Fundamental Q Branch, Studied with CW Stimulated Raman Spectroscopy. Journal of Chemical Physics, Vol. 81, pp. 4241-4245.

Mandin, J. -Y., Camy-Peyret, C., Flaud, J. M. and Guelachvili, G. (1982). Measurements and Calculations of Self-Broadening Coefficients of Lines Belonging to the $2\nu_2$, ν_1, and ν_3 Bands of $H_2{}^{16}O^1$. Canadian Journal of Physics, Vol. 60, pp. 94-101.

McCullough, R. W., Kruger, C. H. and Hanson, R. K. (1977). A Flow Tube Reactor Study of Thermal Decomposition Rates of Nitric Oxide. Combustion Science and Technology, Vol. 15, pp. 213-223.

Polyani, J. C. and Woodall, K. B. (1972). Mechanism of rotational relaxation. Journal of Chemical Physics, Vol. 56; pp. 1563-1572.

Rahn, L. A., Farrow, R. L. and Lucht, R. P. (1984). Effects of Laser Field Statistics on Coherent anti-Stokes Raman Spectroscopy Intensities. Optics Letters, Vol. 9, pp. 223-225.

Shirley, J. A., Hall, R. J. and Eckbreth, A. C. (1980). Folded BOXCARS for Rotational Raman Studies. Optics Letters, Vol. 5, pp. 380-382.

Stufflebeam, J. H., Hall, R. J. and Eckbreth, A. C. (1983). Investigation of the CARS Spectrum of Carbon Monoxide at High Pressure and Temperature. UTRC Report R83-956020-F, United Technologies Research Center, East Hartford, CT.

Stufflebeam, J. H., Hall, R. J. and Verdieck, J. F. (1984). CARS Diagnostics of High Pressure and Temperature Gases, in Roux, J. A. and McCay, T. D. (Eds.), Combustion Diagnostics by Nonintrusive Methods, Vol. 92 of Progress in Astronautics and Aeronautics, AIAA, 1984, pp. 3-23.

Teets, R. E. (1984). Accurate Convolutions of Coherent anti-Stokes Raman Spectra. Optics Letters, Vol. 9, pp. 226-228.

Tsao, C. J. and Curnutte, B. (1962). Line-Widths of Pressure-Broadened Spectral Lines. Journal of Quantitative Spetroscopy and Radiative Transfer, Vol. 2, pp. 41-91.

Wise, H. and Frech, M. F. (1952). Kinetics of Decomposition of Nitric Oxide at Elevated Temperatures. I. Rate Measurements in a Quartz Vessel. Journal of Chemical Physics, Vol. 20, pp. 22-24.

Yuan, E. L., Slaughter, J. I., Koerner, W. E. and Daniels, F. (1959). Kinetics of the Decomposition of Nitric Oxide in the Range 700-1800° C. Journal of Physical Chemistry, Vol. 63, pp 952-956.

Yuratich, M. A. (1979). Effects of Laser Linewidth on Coherent Anti-Stokes Raman Spectroscopy. Molecular Physics, Vol. 38, pp. 625-655.

APPENDIX A

PUBLICATIONS/PRESENTATIONS UNDER ARO CONTRACT DAAG29-83-C-0001 CARS DIAGNOSTICS OF HIGH PRESSURE COMBUSTION

1. Stufflebeam, J. H., Hall, R. J. and Verdieck, J. F. (1984). CARS Diagnostics of High Pressure and Temperature Gases, in Roux, J. A. and McCay, T. D. (Eds.), Combustion Diagnostics by Nonintrusive Methods, Vol. 92 of Progress in Astronautics and Aeronautics, AIAA, 1984, pp. 3-23.

2. Hall, R. J. and Stufflebeam, J. H. (1984). Recent CARS Spectroscopic Studies of N_2, CO, N_2O, and CO_2; Theory and Experiment. Presented at the IX^{th} International Conference on Raman Spectroscopy, Tokyo, Japan, August 27-September 1.

3. Hall, R. J. and Stufflebeam, J. H. (1984). Quantitative CARS Spectroscopy of CO_2 and N_2O. Applied Optics, Vol. 23, pp. 4319-4327.

4. Eckbreth, A. C. and Anderson, T. J. (1985). Dual Broadband CARS for Simultaneous, Multiple Species Measurements. Applied Optics, Vol. 24, pp. 2731-2736.

APPENDIX B

PARTICIPATING SCIENTIFIC PERSONNEL AND DEGREES AWARDED DURING THIS CONTRACT

A. C. Eckbreth
R. J. Hall
J. A. Shirley
J. H. Stufflebeam

APPENDIX C

DUAL BROADBAND CARS FOR SIMULTANEOUS, MULTIPLE SPECIES MEASUREMENTS

Reprinted from Applied Optics, Vol. 24, page 2731, August 15, 1985

Dual broadband CARS for simultaneous, multiple species measurements

Alan C. Eckbreth and Torger J. Anderson

An approach to CARS is described and demonstrated which permits CARS to be generated from a multiplicity of species simultaneously. The technique employs two independent broadband Stokes sources in combination with a pump laser. In addition to the two separate two-color wave-mixing processes between the pump and Stokes lasers, spectrally resolved CARS is produced in a three-color process from species whose Raman resonances correspond to the frequency differences of the two broadband sources. CARS is thus derived from a large number of species simultaneously removing the nominal limitation of CARS to interrogate only one constituent at a time.

I. Introduction

CARS (coherent anti-Stokes Raman spectroscopy) is by now a well-established technique for the remote, spatially and temporally resolved probing of instrumentally hostile environments typical of practical combustion and plasma devices.[1-4] A major limitation of CARS, in addition to increased complexity, when compared to spontaneous Raman scattering, is the inability to interrogate more than one molecular species at a time as usually implemented. Different constituents are generally addressed sequentially by switching dye cells within the Stokes oscillator cavity[4] or changing the dye solution. In the fortuitous instances of closely spaced Raman resonances, e.g., N_2 and N_2O,[5] CO_2 and O_2, a single broadband dye laser allows more than a single constituent to be measured at a time. Several constituents can also be measured simultaneously by introducing a separate broadband Stokes source for each species to be measured. Folded BOXCARS phase-matching schemes[6,7] expedite such approaches and have been employed with two Stokes sources to monitor O_2 and N_2 simultaneously.[8] To employ more than two Stokes sources is clearly cumbersome and complex. In this paper we report on a dual broadband Stokes approach to CARS which permits several, i.e., more than just two, constituents to be measured simultaneously.

The authors are with United Technologies Research Center, East Hartford, Connecticut 06108.
Received 8 March 1985.
0003-6935/85/162731-06$02.00/0.

In the next section of the paper, the basic dual broadband CARS concept is outlined. Phase matching all the simultaneous two- and three-color processes is then described in some detail. The paper concludes with a discussion concerning spectral positioning of the Stokes sources and an experimental demonstration of simultaneous CARS generation from postflame N_2, CO_2, and H_2O.

II. Dual Broadband Stokes Approach

The concept, as specifically implemented here, is illustrated in Fig. 1. A narrowband pump laser ($\Delta\omega_1 \lesssim 1\ cm^{-1}$) wave mixes with two separate broadband Stokes sources, ω_2 and ω_2', where $\omega_2 > \omega_2'$. For this discussion and without loss of generality, the pump laser is the widely employed, frequency-doubled Nd:YAG laser at 532 nm. Assuming for the moment that all phase-matching requirements are satisfied, ω_1 wave mixes with ω_2 and ω_2' each separately in normal two-color CARS processes producing CARS at $2\omega_1 - \omega_2$ and $2\omega_1 - \omega_2'$ for Raman resonances corresponding to $\omega_1 - \omega_2$ and $\omega_1 - \omega_2'$, respectively. In addition, there is the three-color CARS process, again assuming phase matching is satisfied, which produces CARS at $\omega_1 + \omega_2 - \omega_2'$ for Raman resonances at $\omega_2 - \omega_2'$. Depending on the bandwidths of the broadband sources, the frequency differences $\omega_2 - \omega_2'$ can span a spectral region of many hundreds of cm^{-1} permitting a multiplicity of constituents to be addressed. Thus CARS is generated from any constituent whose Raman resonances coincide with $\omega_1 - \omega_2$, $\omega_1 - \omega_2'$, or $\omega_2 - \omega_2'$. Besides the three-color process at $\omega_1 + \omega_2 - \omega_2'$ for Raman resonances at $\omega_2 - \omega_2'$, i.e., the dual broadband process, there will also be three-color wave mixing at the same frequency from Raman transitions at $\omega_1 - \omega_2'$. However for the reason detailed below, the latter radiation will not have high

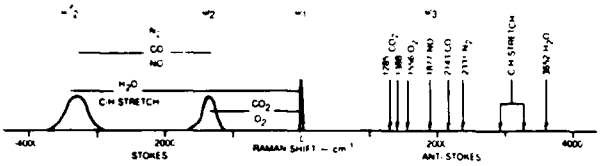

Fig. 1. Dual broadband Stokes approach to simultaneous, multiple species CARS measurements.

resolution but will be spectrally smeared. As such it could contribute to the nonresonant background and complicate species concentration measurements; thus, its presence and importance need to be scrutinized. For thermometry, its effect could be minimized by employing data reduction approaches which employ the nonresonant background as a fitting parameter.[9] In the experiments to be described later, its presence was not readily apparent.

For the two, two-color cases and the one, three-color process with dual broadband excitation, the instrumental spectral resolution is determined by the pump laser linewidth and/or slit function even for the three-color mixing. In the latter, despite the employment of the two broadband sources in the three-color process, high spectral resolution results, because, as pointed out by Yuratich,[10] the broadband sources serve only to excite the vibrational–rotational Raman resonances corresponding to their frequency differences. Since the Raman frequencies are well defined by the constituent molecules, spectral smearing does not occur even with dual broadband excitation. The relatively narrowband pump laser then scatters off the resultant coherent Raman excitation in the medium resulting in CARS at a spectral resolution characteristic of the narrowband source and/or spectrometer employed. On the other hand, the three-color CARS process for Raman resonances at $\omega_1 - \omega_2'$ will result from the broadband ω_2 source scattering from the coherent excitation of those modes and will be spectrally diffuse. That the three-color CARS spectrum with dual broadband excitation of the Raman modes is indeed sharp is experimentally demonstrated in Fig. 2 where the CARS spectrum of ambient N_2 is displayed. The experimental apparatus employed here is similar to and is a laboratory version of the CARS instrument described in Ref. 4. The main difference is the employment of portions of the 532-nm beam to pump two separate oscillator cavities rather than an oscillator/amplifier combination as commonly done. The N_2 signature was generated in a crossed-beam three-color CARS process in which two broadband sources (150–200-cm^{-1} FWHH), centered at ~17471 cm^{-1} (ω_2) and ~15140 cm^{-1} (ω_2'), excited the N_2 vibrational fundamental Q-branch Raman resonances from which the 18,797-cm^{-1} pump scattered. A 300-mm focal length lens was employed with the following beam angles relative to the central lens axis: ω_1, 1.05°, ω_2, 1.13° and ω_2', 1.28°. The moderate spectral resolution displayed (~2.7 cm^{-1}) is the result of inserting the 50-μm diam optical fiber from the CARS receiver directly into the 0.75-m spectrograph fitted

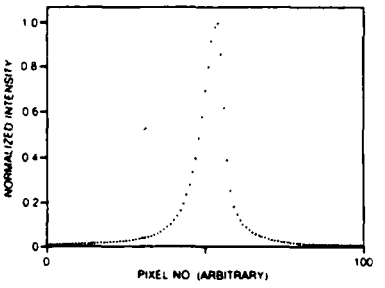

Fig. 2. Dual broadband CARS signature of N_2 in room air generated from the three-color wave mixing of ω_1, ω_2, and ω_2'. Spectral dispersion is 0.53 cm^{-1}/pixel. The spectral resolution is 2.7 cm^{-1}. The FWHH of the N_2 CARS spectrum is 4.5 cm^{-1}.

with a self-scanned optical multichannel detector (PAR model 1420).

III. Phase-Matching Schemes

To this point, all the various frequency mixing combinations have been assumed to be phase matched. This is readily achieved via a variety of approaches. In gases, neglecting dispersion which is generally valid, all the various wave-mixing combinations can be collinearly phase matched employing appropriate dichroic elements for beam juxtaposition and signal separation. For applications where high spatial resolution is required, phase matching is possible with a variety of BOXCARS schemes,[6,7] all planar, all folded, or combined planar–folded. For the initial experimental demonstrations presented here, a combination of planar and folded approaches has been employed as shown in Fig. 3. Figure 3 depicts the laser beam arrangement incident on the focusing field lens (*INPUT*) and the recollimating field lens (*OUTPUT*) viewed against the direction of beam propagation. ω_2 is phase matched with the two ω_1 beams via standard planar BOXCARS, ω_2' with ω_1 by folded BOXCARS, and the dual broadband three-color process by folded BOXCARS. In this arrangement, if the individual two-color processes are phase matched, the dual broadband process is phase matched as well. This can be shown by considering the three phase-matching diagrams shown in Fig. 4. The phase-matching equations for the various wave-mixing combinations are

$\underline{\omega_1,\omega_2}$

$$2k_1 \cos\alpha = k_2 \cos b + k_c \cos c, \tag{1a}$$

$$k_2 \sin b = k_c \sin c; \tag{1b}$$

$\underline{\omega_1,\omega_2'}$

$$2k_1 \cos\alpha = k_2' \cos t + k_h \cos h, \tag{2a}$$

$$k_2' \sin t = k_h \sin h; \tag{2b}$$

$\underline{\omega_1,\omega_2,\omega_2'}$

$$k_1 \cos A + k_2 \cos B = k_2' \cos T + k_n \cos N, \tag{3a}$$

$$k_1 \sin A = k_2 \sin B, \tag{3b}$$

$$k_2' \sin T = k_n \sin N. \tag{3c}$$

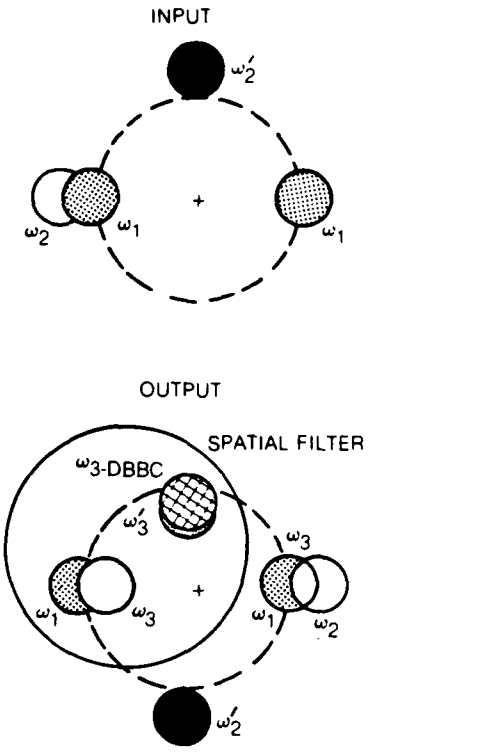

Fig. 3. Laser beam arrangement for the dual broadband CARS experimental demonstrations. The beam geometry is shown just prior to the focusing field lens (*INPUT*) and after the recollimating field lens (*OUTPUT*) viewed against the direction of propagation. ω_1 and ω_2 are mixed via planar BOXCARS, while ω_1,ω_2' and $\omega_1,\omega_2,\omega_2'$ are 3-D phase matched (folded BOXCARS).

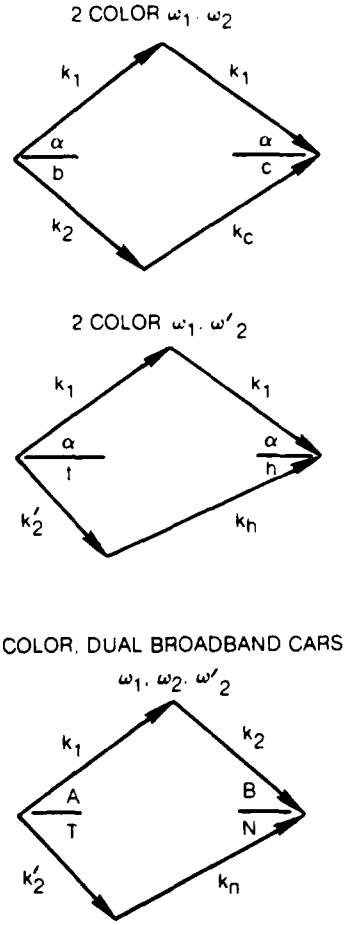

Fig. 4. Phase-matching diagrams for the individual wave-mixing combinations comprising dual broadband CARS.

The photon energy conservation equations may be written, assuming no dispersion, as

$$2k_1 = k_2 + k_c, \tag{4a}$$

$$2k_1 = k_2' + k_h, \tag{4b}$$

$$k_1 + k_2 = k_2' + k_n. \tag{4c}$$

In the small angle approximation, i.e., $\sin\theta \to \theta$, $\cos\theta \to 1 - \theta^2/2$, Eqs. (1)–(4) may be recast, after some manipulation, to

$\underline{\omega_1,\omega_2}$

$$\alpha^2 = bc, \quad \alpha^2 = \frac{k_2}{k_c} b^2, \quad c = \frac{k_2}{k_c} b; \tag{5a,b,c}$$

$\underline{\omega_1,\omega_2'}$

$$\alpha^2 = th, \quad \alpha^2 = \frac{k_2'}{k_h} t^2, \quad h = \frac{k_2'}{k_h} t; \tag{6a,b,c}$$

$\underline{\omega_1,\omega_2,\omega_2'}$

$$AB = NT, \quad k_1 A = k_2 B, \quad \frac{k_1}{k_2} A^2 = \frac{k_2'}{k_n} T^2. \tag{7a,b,c}$$

The small angle approximations are valid for angles at least up to 10°; BOXCARS experiments very seldom exceed these values.

If the CARS and Stokes wave vectors are expressed in terms of the pump wave vector and Raman shift Δ, namely,

$$\begin{aligned} k_c &= k_1 + \Delta_c, \quad k_2 = k_1 - \Delta_c, \\ k_h &= k_1 + \Delta_h, \quad k_2' = k_1 - \Delta_h, \\ k_n &= k_1 + \Delta_n = k_1 + \Delta_h - \Delta_c \end{aligned} \tag{8}$$

it is easily shown for $\Delta^2 \ll k^2$ that

$$k_1^2 = k_2 k_c, \tag{9a}$$

$$k_1^2 = k_2' k_h, \tag{9b}$$

$$k_1 k_2 = k_2' k_n. \tag{9c}$$

To prove that the three-color dual broadband process is phase matched when the individual two-color processes are each separately phase matched, one proceeds as follows. Beginning with $A = \alpha$, one can show that $B = b$ by squaring Eq. (7b), replacing k_1^2 by Eq. (9a), and comparing the resultant expression with Eq. (5b). Similarly $T = t$ can be shown by substituting sequen-

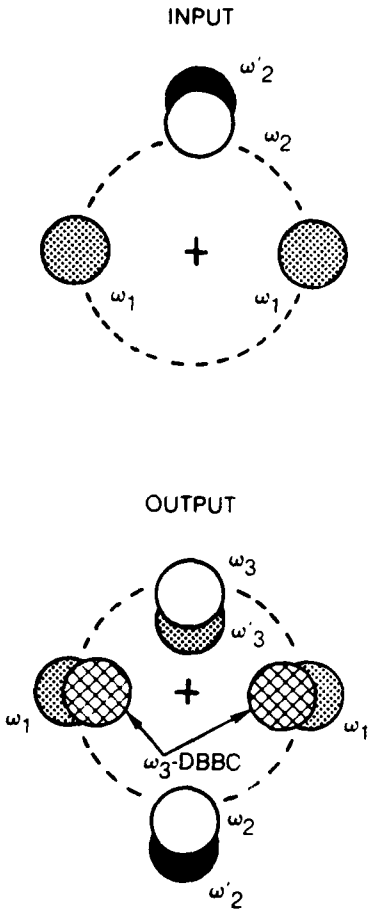

Fig. 5. Laser beam arrangement for dual broadband CARS in which all wave-mixing combinations are 3-D phase matched and each ω_1 component participates in the three-color process.

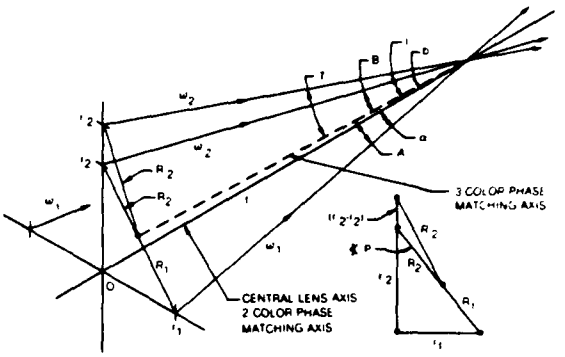

Fig. 6. Phase-matching geometry for the laser beam arrangement of Fig. 5. Two-color processes are phase matched about the central lens axis. The three-color processes are phase matched about the dashed axis residing in a plane inclined to the ω_1 beam crossing plane.

tially Eqs. (9c) and (9b) in Eq. (7c) and comparing with Eq. (6b). Thus, the three-color dual broadband CARS phase-matching angles equal the two-color phase-matching angles for this combination of planar and folded BOXCARS. For very broadband sources, there will be some phase mismatch for frequencies far from line center. This could result in a signal decrease due to lack of perfect phase matching, but, for small angle beam crossings, probably does not result in any spectral distortion within a specific Raman resonance band region.

There are two drawbacks to the phase-matching scheme shown in Fig. 3. First, only one of the ω_1 components participates in the three-color dual broadband process. Second, for high spatial resolution applications, the collinear CARS component generated in the planar BOXCARS process (ω_1,ω_2) needs to be eliminated by spatial filtering. In Fig. 5, what may well be the optimal phase-matching scheme for dual broadband CARS is suggested. In this arrangement, all the major wave-mixing processes are phase matched by folded BOXCARS. Furthermore, each ω_1 component participates separately in the dual broadband CARS process, i.e., each ω_1 component scatters off the coherent Raman excitation established by the nearly collinear ω_2,ω'_2 components. There will also be a weak, spectrally smeared collinear CARS signal at $2\omega_2 - \omega'_2$ residing along the ω_2,ω'_2 beams. This is easily eliminated by trapping and is located spectrally at a smaller anti-Stokes shift from ω_1 than the CARS signal from the ω_1,ω_2 interaction.

It is also possible to prove here, as before, that the three-color dual broadband CARS process is phase matched when the individual two-color CARS processes are phase matched. The proof in this instance is more complicated since the three-color CARS process is no longer phase matched about the central lens axis as in the planar–folded orientation of Fig. 3. The phase-matching axes reside in planes tilted relative to the lens axis as shown in Fig. 6. For this reason, the three-color processes will have a slightly different interaction length, and thus spatial resolution, than the individual two-color combinations. In Fig. 6, only the three-color process for one of the ω_1 pump components is shown; the other process possesses an identical geometry. The location of the dotted phase-matching axis is selected so that angles A and B satisfy the three-color phase-matching relation in Eq. (7b). The proof proceeds by demonstrating that the angle T, solved for geometrically, satisfies phase-matching closure indicated by Eq. (7c). We assume a field lens of focal length f much larger than the displacements of the laser beams from the central lens axis about which the two-color wave-mixing processes are phase matched. The displacements of the beams from the central axis are denoted by r_i and for $r_i \ll f$, generally the case, one may express the beam displacements in terms of the two-color phase-matching angles thusly,

$$r_1 = af, \quad r_2 = bf, \quad r'_2 = tf, \tag{10a,b,c}$$

where the subscripts denote the laser frequencies. The displacements of the beams from the three-color phase-matching axis are denoted by R_i and are related to the three-color phase-matching angles by

$$R_1 = Af, \qquad R_2 = Bf, \qquad R_2' = Tf. \tag{11a,b,c}$$

One should note that the three-color process is not planar but slightly folded. The three-color phase-matching axis is selected to satisfy the Eq. (7b) phase-matching condition. Thus the R_2,R_1 partitioning is given by

$$\frac{R_1}{R_2} = \frac{A}{B} = \frac{k_2}{k_1}, \tag{12}$$

where

$$R_1 + R_2 = \sqrt{r_1^2 + r_2^2}. \tag{13}$$

Applying the law of cosines to the slender, obtuse triangle formed by R_2', R_2 and $(r_2' - r_2)$ one has

$$R_2'^2 = R_2^2 + (r_2' - r_2)^2 - 2R_2(r_2' - r_2)\cos(180 - P), \tag{14}$$

where

$$\cos P = \frac{r_2}{\sqrt{r_1^2 + r_2^2}}. \tag{15}$$

Dividing Eq. (14) by f^2 and substituting from Eqs. (10) and (11) transform Eq. (14) to

$$T^2 = B^2 + (t - b)^2 + \frac{2B(t - b)b}{A + B}. \tag{16}$$

Dividing Eq. (13) by f leads to

$$(A + B)^2 = \alpha^2 + b^2, \tag{17}$$

or to

$$\alpha^2 = \frac{(k_1 + k_2)^2}{2k_1k_2}A^2, \tag{18}$$

after eliminating B and b using Eqs. (5b) and (7b). In Eq. (16) B may be expressed in terms of A, t and b in terms of α, and, thus, of A leading to

$$T^2 = \frac{k_1^2}{k_2^2}A^2 + k_1\left(\frac{1}{k_2'} - \frac{1}{k_2}\right)^2\frac{(k_1 + k_2)^2}{2k_2}A^2 + \frac{k_1^2}{k_2^2}\left(\frac{1}{k_2'} - \frac{1}{k_2}\right)(k_1 + k_2)A^2. \tag{19}$$

Numerical calculations indicate, fortunately, that the second term on the right-hand side of Eq. (19) is quite small and can be neglected; this is equivalent to dropping the second term on the right-hand side of Eq. (14). After considerable manipulation, using Eqs. (9), Eq. (19) simplifies to

$$k_2k_2'T^2 = k_1\left[k_1 + \frac{k_c}{k_n}(k_h - k_c)\right]A^2. \tag{20}$$

For typical values of k_c (20, 123 cm^{-1}) and k_n (21,128 cm^{-1}), the term in brackets is, from Eq. (8), equal to k_n to within 0.5%. Thus Eq. (20) is equivalent to

$$k_2k_2'T^2 = k_1k_nA^2, \tag{21}$$

demonstrating that T does satisfy the phase-matching condition of Eq. (7c). Exact numerical calculations show that the three-color process is indeed phase matched indicative of the validity of the approximations employed.

IV. Dual Stokes Spectral Selection

The spectral positioning of the two broadband dye laser sources clearly depends on the application and species of measurement interest. For the purposes of the following discussion, note that most 2 × Nd:YAG-pumped, broadband dye lasers possess spectral profiles with FWHH of the order of 150–200 cm^{-1} and base-widths approximately twice this value. Binary dye combinations, which we have not yet investigated extensively, can be found which yield even larger lasing bandwidths. For combustion applications, some ω_2,ω_2' combinations come readily to mind. For ω_2', one would certainly like to exploit the broad frequency coverage provided by the dye DCM.[11] Depending on solvent and concentration, this dye, when 2 × Nd:YAG pumped, lases over many hundreds of cm^{-1} and can be used to generate CARS from H_2O and the C–H stretch modes of a variety of hydrocarbons. With DCM dissolved in DMSO, we have experimentally seen Stokes FWHH of the order of 350 cm^{-1}. Assume a base spectral coverage over the 3000–3700-cm^{-1} range. One choice for ω_2 then is the 1200–1600-cm^{-1} region permitting CARS directly from CO_2 and O_2. Dual broadband CARS is then obtained from species with resonances covered by $\omega_2 - \omega_2'$ or the 1400–2500-cm^{-1} range, e.g., N_2, NO, CO, N_2O, C_2, etc. In the flame work to be presented subsequently, we centered ω_2' at H_2O (3657 cm^{-1}) and ω_2 at 1326 cm^{-1} so that maximum dual broadband CARS would be generated from N_2. Another choice for ω_2 would be the 2000–2400-cm^{-1} region to generate CARS directly from N_2, CO, etc., with $\omega_2 - \omega_2'$ covering resonances between 600 and 1700 cm^{-1}, e.g., CO_2, O_2. If ω_2' is set to lase between 3600 and 4200 cm^{-1} corresponding to H_2O and H_2 and ω_2 to 1300–1600 cm^{-1} (O_2,CO_2), dual broadband CARS would be generated from resonances in the 2000–3000-cm^{-1} range.

Due to the spectral energy partitioning inherent in the use of broadband dye sources in wave-mixing experiments, dual broadband CARS may be restricted, particularly for dynamic measurements, to elevated pressure combustion applications, e.g., propellant burning, diesel combustion. At elevated pressures, the signal decrease accompanying the use of dual broadband sources is compensated by the nominal quadratic scaling of $|\chi^{(3)}|^2$ with density.[12] The exact scaling depends on the detailed spectroscopy of the particular species in mind, e.g., transition spacing, Raman linewidth, collisional narrowing effects,[3] etc. The signal for any particular species will also depend on the $\omega_2 - \omega_2'$ overlap integral with the Raman resonances excited. For example, if ω_2 and ω_2' have the same bandwidth and the center frequencies $\omega_2(0)$ and $\omega_2'(0)$ coincide with a particular Raman resonance, all the energy in each laser is available to excite those particular Raman resonances. This is unlike normal broadband CARS with a narrowband pump source in which only a fraction of the broadband dye laser energy participates in the resonant wave mixing. Thus, the signal decrease with dual broadband CARS relative to normal two-color CARS is probably not as large as one might originally antici-

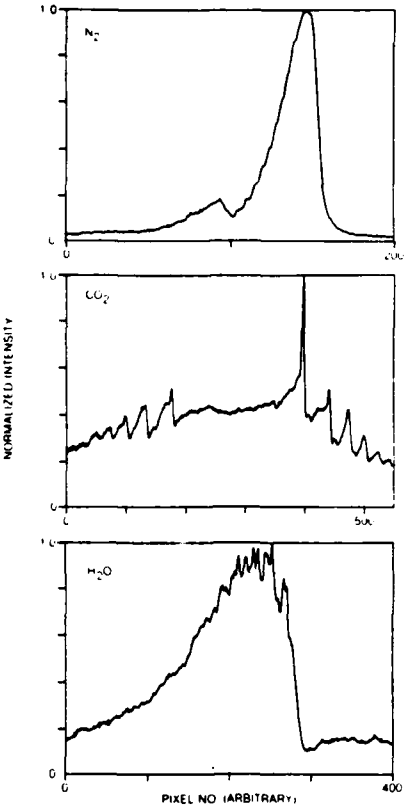

Fig. 7. Simultaneously generated dual broadband CARS signatures from N_2, CO_2, and H_2O in the postflame zone of an ~1700 K premixed CH_4–air flame. The dispersions are ~0.53 cm^{-1}/pixel for N_2, 0.59 cm^{-1}/pixel for H_2O, and 0.47 cm^{-1}/pixel for CO_2. In CO_2 both the ν_1 and $2\nu_2$ bands are displayed.

pate. In our initial experiments, for example, with $\omega_2(0) - \omega_2'(0) = \Delta_{N_2}$, dual broadband CARS from N_2 in the postflame zone of an atmospheric pressure, premixed CH_4–air flame, was readily recorded with time averaging over 600 laser pulses or 30 sec and a spatial resolution of several millimeters as shown in Fig. 7. Also shown there are the postflame CARS spectra from CO_2 and H_2O simultaneously generated with the N_2 CARS signal and sequentially recorded by merely tuning the spectrograph. These of course could be simultaneously recorded employing a spectrograph with less dispersion than used here or, preferably, placing the spectral images at high dispersion on different portions of either a linear or 2-D array detector using various alignment schemes. In practical measurement applications, many of the simultaneously generated CARS signals would be recorded as spectrally integrated photomultiplier outputs.

When the beam crossing angles are small, all the CARS beams generated can be conveniently focused into the spectrograph or receiver optical fiber[4] with a single lens. However, as the beam crossing angles increase, the spatial separation of the CARS beams may lead to incidence angles in excess of that acceptable based on the *f*/No. of the spectrograph or numerical aperture of the fiber. In those instances, separate capture of the individual CARS beams can be employed with subsequent optical repositioning to meet the *f*/No. constraints of the optical detection system.

It is also interesting to speculate on the single pulse quality of dual broadband CARS spectra when detector shot noise is not problematical. Normal two-color single pulse CARS spectra are affected by the amplitude ripple on the broadband Stokes dye laser.[4] This leads to distorted single pulse CARS spectra and a decrease in the accuracy of single shot measurements. For two statistically independent dye sources, where many frequency combinations drive each individual Raman resonance, one might expect dual broadband CARS single pulse quality to be considerably better. This would arise from an averaging in effect over the random amplitude profiles of the two broadband sources which should lead to smoother single pulse spectra. This aspect, as well as others, will be reported as investigations of dual broadband CARS progress.

V. Summary

We have described a readily implemented, dual broadband approach to CARS which permits many molecular species to be monitored simultaneously thus eliminating one of the major drawbacks to CARS diagnostics. The precise range of sensitivity and applicability of the technique will become clearer with further investigations in this regard and engineering developments.

The authors would like to acknowledge the contributions of Gregory M. Dobbs and the capable technical assistance of Normand Gantick. Portions of this research were sponsored by the Chemistry Division of the Army Research Office.

References

1. S. A. J. Druet and J. P. E. Taran, "CARS Spectroscopy," Prog. Quantum Electron. **7**, 1 (1981).
2. J. F. Schooley, Ed., *Temperature, Its Measurement and Control in Science and Industry*, *Vol. 5* (American Institute of Physics, New York, 1982), pp. 575–620.
3. J. F. Ready and R. K. Erf, Eds., *Laser Applications*, *Vol. 5* (Academic, Orlando, 1984), pp. 129–309.
4. A. C. Eckbreth, G. M. Dobbs, J. H. Stufflebeam, and P. A. Tellex, "CARS Temperature and Species Measurements in Augmented Jet Engine Exhausts," Appl. Opt. **23**, 1328 (1984).
5. L. E. Harris, "Broadband N_2 and N_2O CARS Spectra from a CH_4/N_2O Flame," Chem. Phys. Lett. **93**, 335 (1982).
6. Y. Prior, "Three-Dimensional Phase Matching in Four-Wave Mixing," Appl. Opt. **19**, 1741 (1980).
7. J. A. Shirley, R. J. Hall, and A. C. Eckbreth, "Folded BOXCARS for Rotational Raman Studies," Opt. Lett. **5**, 380 (1980).
8. G. L. Switzer *et al.*, "Simultaneous CARS and Luminosity Measurements in a Bluff-Body Combustor," AIAA Paper 83-1481 (1983).
9. R. J. Hall and L. R. Boedeker, "CARS Thermometry in Fuel-Rich Combustion Zones," Appl. Opt. **23**, 1340 (1984).
10. M. A. Yuratich, "Effects of Laser Linewidth on Coherent Anti-Stokes Raman Spectroscopy," Mol. Phys. **38**, 625 (1979).
11. *Laser Dyes Catalog*, Exciton Chemical Company, Inc., Dayton, Oho 45431.
12. W. B. Roh and P. W. Schreiber, "Pressure Dependence of Integrated CARS Power," Appl. Opt. **17**, 1418 (1978).